UNIVERSIDADE ESTADUAL DE MARINGÁ
CENTRO DE TECNOLOGIA
DEPARTAMENTO DE ENGENHARIA QUÍMICA
PROGRAMA DE PÓS-GRADUAÇÃO EM ENGENHARIA QUÍMICA

RENATA MARIANE DE SOUZA PROVENSI

DESENVOLVIMENTO E APLICAÇÃO DE MATERIAIS ADSORVENTES DE FONTE NATURAL E SINTÉTICA PARA REMOÇÃO DE FÁRMACOS

MARINGÁ
2025

RENATA MARIANE DE SOUZA PROVENSI

DESENVOLVIMENTO E APLICAÇÃO DE MATERIAIS ADSORVENTES DE FONTE NATURAL E SINTÉTICA PARA REMOÇÃO DE FÁRMACOS

Tese apresentada ao Programa de Pós-Graduação em Engenharia Química da Universidade Estadual de Maringá (UEM), como requisito parcial para a obtenção do título de Doutora em Engenharia Química.

Orientadora: Profª. Drª Rosângela Bergamasco

MARINGÁ

2025

Dados Internacionais de Catalogação-na-Publicação (CIP)
(Biblioteca Central - UEM, Maringá - PR, Brasil)

P969d

Provensi, Renata Mariane de Souza

Desenvolvimento e aplicação de materiais adsorventes de fonte natural e sintética para remoção de fármacos / Renata Mariane de Souza Provensi. -- Maringá, PR, 2025.

151 f. : figs., tabs.

Orientadora: Profa. Dra. Rosângela Bergamasco.

Tese (doutorado) - Universidade Estadual de Maringá, Centro de Tecnologia, Departamento de Engenharia Química, Programa de Pós-Graduação em Engenharia Química, 2025.

1. Tratamento de água. 2. Adsorção. 3. Fármacos. 4. Nanoparticulas. I. Bergamasco, Rosângela, orient. II. Universidade Estadual de Maringá. Centro de Tecnologia. Departamento de Engenharia Química. Programa de Pós-Graduação em Engenharia Química. III. Título.

CDD 23.ed. 660.284235

Rosana de Souza Costa de Oliveira - 9/1366

UNIVERSIDADE ESTADUAL DE MARINGÁ

CENTRO DE TECNOLOGIA

DEPARTAMENTO DE ENGENHARIA QUÍMICA

PROGRAMA DE PÓS-GRADUAÇÃO EM ENGENHARIA QUÍMICA

Esta é a versão final da Tese de Doutorado apresentada por **Renata Mariane de Souza Provensi** perante a Comissão Julgadora do Programa de Pós-graduação em Engenharia Química em 24 de abril de 2025.

COMISSÃO JULGADORA

Prof.ª Dr.ª Rosângela Bergamasco
Presidente/Orientadora - PEQ/UEM

Prof.ª Dr.ª Aline Takaoka Alves Baptista
Membro - DAAEQ/UTFPR

Prof.ª Drª. Letícia Nishi
Membro - PEQ/UEM

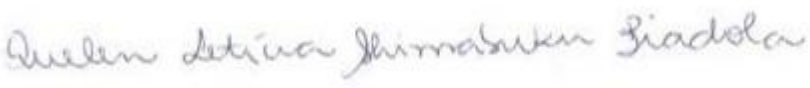

Profª. Drª. Quelen Letícia Shimabuku Biadola
Membro - DEQ/UEM

Profª Drª Márcia Regina Fagundes-Klen
Membro - DEQ/UNIOESTE

AGRADECIMENTOS

Agradeço primeiramente a Deus pela vida, pela saúde e por sempre iluminar meu caminho, especialmente nos momentos mais difíceis. A Nossa Senhora, minha Mãe Santíssima, agradeço por interceder por mim e por sempre levar minhas orações a Deus.

À minha família, por todo o apoio e incentivo ao longo da minha trajetória. Em especial, à minha mãe, que com amor e dedicação me ensinou a ser forte e persistente, sendo minha maior inspiração. Ao meu pai, que sempre me estimulou a estudar e a nunca desistir dos meus sonhos. Aos meus sobrinhos Felipe, Júlia, Laura e Helena, que enchem minha vida de alegria e amor.

Ao meu marido Lucas, meu companheiro de vida, que esteve ao meu lado em todos os momentos, me apoiando e me incentivando a seguir em frente e realizar todos meus sonhos. Sua presença torna cada desafio mais leve, e sou imensamente grata por compartilhar a jornada da vida com você. À família do meu marido, que me acolheu com tanto carinho e me fez sentir parte dela, meus sinceros agradecimentos.

Às minhas amigas Daniella e Heloise, que sempre estiveram ao meu lado e são parte essencial da minha vida. Em especial, minha amiga Helô, com quem compartilho mais de 17 anos de amizade e cumplicidade. Sua amizade é uma força constante, e sou imensamente grata por tê-la comigo em cada etapa dessa caminhada. Também, agradeço à amiga que o laboratório LGCPA colocou em meu caminho e que sei que ficará para sempre, Grace. Seu apoio foi fundamental nesta pesquisa, mas, mais do que isso, sua amizade é um presente que levo para a vida. Sou profundamente grata por sua amizade e generosidade.

Além disso, agradeço aos colegas e amigos do laboratório LGCPA, que compartilharam essa jornada comigo, sempre trocando conhecimentos e oferecendo apoio. Sou grata a todos que, de alguma forma, contribuíram para minha pesquisa, e, em especial, a Jumara, Anna, Gabi, Géssica, Le Nishi, Carol e Luís, cujo auxílio foi essencial, seja na elaboração de trabalhos em conjunto ou na realização de análises e experimentos, seja no esclarecimento de dúvidas ao longo da minha pesquisa, todos eles foram essenciais na minha caminhada. À minha orientadora, professora Rosângela Bergamasco, por esses sete anos de orientação entre TCC e doutorado, por toda sua dedicação e apoio. Sua compreensão, paciência e incentivo foram fundamentais para que eu conseguisse seguir em frente na minha jornada científica. Sou imensamente grata por tudo o que aprendi com você e por toda confiança depositada em mim ao longo desses anos.

Por fim, agradeço à Coordenação de Aperfeiçoamento de Pessoal de Nível Superior (CAPES) pelo apoio financeiro que foi essencial para a realização deste trabalho. A todos que, de alguma forma, contribuíram para essa conquista, meus mais sinceros agradecimentos.

PROVENSI, R. M. de S. Desenvolvimento e aplicação de materiais adsorventes de fonte natural e sintética para remoção de fármacos. [TESE]. Maringá: Programa de Pós Graduação em Engenharia Química, Universidade Estadual de Maringá; 2025.

RESUMO

A contaminação de corpos hídricos por fármacos tem se tornado um desafio ambiental de grande relevância, especialmente devido ao aumento do consumo global de medicamentos, ao uso inadequado de práticas de automedicação pela população e à ineficiência das estações de tratamento de águas residuais (ETARs) em remover completamente esses compostos. Nesta tese, foram desenvolvidos e avaliados materiais adsorventes de origem natural e sintética para a remoção de dois contaminantes emergentes: ivermectina e cloroquina, ambos amplamente utilizados pela população mundial durante a pandemia de COVID-19 em tratamentos precoce da doença. No primeiro estudo, investigou-se o uso da casca da semente de *Moringa oleifera Lam*. funcionalizada com nanopartículas de óxido de ferro para a adsorção de ivermectina. O processo de adsorção atingiu o equilíbrio de adsorção em 400 minutos com capacidade adsortiva de 89,41 $mg\,g^{-1}$, ajustando-se ao modelo cinético de pseudo-primeira ordem. A isoterma de equilíbrio foi melhor descrita pelo modelo de Langmuir, com capacidade máxima de 143,76 $mg\,g^{-1}$. A análise termodinâmica indicou um processo espontâneo, exotérmico e reversível. O material manteve desempenho satisfatório após cinco ciclos de reuso, evidenciando seu potencial para aplicação em sistemas de tratamento de efluentes contendo ivermectina. Já o segundo estudo concentrou-se na síntese, caracterização e aplicação das sílicas mesoporosas MCM-41 e MCM-48 funcionalizadas com nanopartículas de óxido de cobalto para a remoção de cloroquina. Os materiais sintéticos desenvolvidos apresentaram alta cristalinidade, grande área superficial ($S_{BET} > 369\ m^2\,g^{-1}$) e estruturas mesoporosas uniformes. A adsorção foi melhor descrita pelo modelo cinético de Elovich, com capacidades de equilíbrio de 25,30 $mg\,g^{-1}$ (MCM-41-CoO) e 24,04 $mg\,g^{-1}$ (MCM-48-CoO), sendo regida por quimissorção e difusão intrapartícula em múltiplas etapas. As isotermas ajustaram-se melhor ao modelo de Sips, com capacidades máximas de 24,78 $mg\,g^{-1}$ e 24,00 $mg\,g^{-1}$, respectivamente. A análise termodinâmica revelou um processo espontâneo, endotérmico e com baixa aleatoriedade, sugerindo adsorção em monocamada seguida de interações eletrostáticas. Apesar da reutilização limitada, os resultados reforçam o potencial das sílicas modificadas como adsorventes eficientes para contaminantes farmacêuticos. Os achados desta tese contribuem significativamente para o avanço do conhecimento sobre a remoção de fármacos em meio aquoso, demonstrando que materiais alternativos, de baixo custo ou com estrutura controlada, podem ser aplicados de forma eficaz no enfrentamento da poluição por contaminantes emergentes.

Palavras-chave: Tratamento de água; Adsorção; Fármacos, Adsorvente de baixo-custo, Sílicas mesoporosas, Nanopartículas.

PROVENSI, R. M. de S. Development and application of adsorbent materials from natural and synthetic sources for drug removal [thesis]. Maringá: Postgraduate Program in Chemical Engineering, State University of Maringá; 2025.

ABSTRACT

Water contamination by pharmaceuticals has become a highly relevant environmental challenge, especially due to the increase in global drug consumption, the population's inadequate use of self-medication practices, and the inefficiency of wastewater treatment plants (WWTPs) in completely removing these compounds. In this thesis, adsorbent materials of natural and synthetic origin were developed and evaluated to remove two emerging contaminants: ivermectin and chloroquine, both widely used by the world population during the COVID-19 pandemic in early treatment of the disease. The first study investigated the use of *Moringa oleifera Lam*. seed husk functionalized with iron oxide nanoparticles for ivermectin adsorption. The adsorption process reached equilibrium in 400 minutes with an adsorptive capacity of 89.41 mg g^{-1}, fitting the pseudo-first-order kinetic model. The Langmuir model best described the equilibrium isotherm with a maximum capacity of 143.76 mg g^{-1}. Thermodynamic analysis indicated a spontaneous, exothermic and reversible process. The material maintained satisfactory performance after five reuse cycles, evidencing its potential for application in effluent treatment systems containing ivermectin. The second study focused on synthesizing, characterizing, and applying mesoporous silicas MCM-41 and MCM-48 functionalized with cobalt oxide nanoparticles to remove chloroquine. The developed synthetic materials presented high crystallinity, large surface area (S_{BET} > 369 m^2 g^{-1}) and uniform mesoporous structures. The adsorption was best described by the Elovich kinetic model, with equilibrium capacities of 25.30 mg g^{-1} (MCM-41-CoO) and 24.04 mg g^{-1} (MCM-48-CoO), being governed by chemisorption and multistep intraparticle diffusion. The isotherms best fitted the Sips model, with maximum capacities of 24.78 mg g^{-1} and 24.00 mg g^{-1}, respectively. Thermodynamic analysis revealed a spontaneous, endothermic process with low randomness, suggesting monolayer adsorption followed by electrostatic interactions. Despite the limited reusability, the results reinforce the potential of the modified silicas as efficient adsorbents for pharmaceutical contaminants. The findings of this thesis contribute significantly to the advancement of knowledge on the removal of drugs in aqueous media, demonstrating that alternative materials of low cost or with controlled structure can be applied effectively in dealing with pollution by emerging contaminants.

Keywords: Water treatment; Adsorption; Drugs; Low-cost adsorbent; Mesoporous silica; Nanoparticles.

LISTA DE FIGURAS – CAPÍTULO 1

LISTA DE FIGURAS – CAPÍTULO 2

LISTA DE FIGURAS – CAPÍTULO 3

LISTA DE TABELAS – CAPÍTULO 1

LISTA DE TABELAS – CAPÍTULO 2

LISTA DE TABELAS – CAPÍTULO 3

LISTA DE SIGLAS

MSN, Mesoporous Silica Nanoparticles

SM, Silica Mesoporosa

MCM, *Mobil Crystalline Materials ou Mobil Composition of Matter*

MCM-41, Sílica Mesoporosa do tipo 41 (hexagonal).

MCM-48, Sílica Mesoporosa do tipo 48 (cúbica).

CoO, Óxido de Cobalto

MCM-41-CoO, Sílica Mesoporosa do tipo 41, modificada com nanopartículas de óxido de Cobalto.

MCM-48-CoO, Sílica Mesoporosa do tipo 48, modificada com nanopartículas de óxido de Cobalto.

SBA, Santa Barbara Amorphous

MSU, Michigan State University

GO, Óxido de Grafeno

MOF, Metal Organic Framework ou Estruturas Metal-Orgânicas

MO, Casca da Semente de *Moringa Oleifera Lam*.

MNOI-Fe_3O_4, biossorvente funcionalizado com nanopartículas de óxido de Ferro

CQ, Cloroquina

PE, Poluente Emergente

LGCPA, Laboratório de Gestão, Controle e Preservação Ambiental

ETAR, Estação de Tratamento de Águas Residuárias.

DEQ, Departamento de Engenharia Química

BET, Método Brunauer-Emmet-Teller

FTIR, Espectroscopia no infravermelho por transformada de Fourier

MEV ou **SEM**, Microscopia eletrônica de varredura

MET ou **TEM**, Microscopia eletrônica de transmissão

DRX ou **XRD**, Difratometria de Raio-X

m, Massa de adsorvente (g)

FRX, Fluorescência de Raios-X

EDX, Energia Dispersiva de Raios X

CTAB, Brometo de Cetiltrimetil Amônio

TEOS, Ortossilicato de Tetraetila

IUPAC, União Internacional de Química Pura e Aplicada

PPO ou **PFO**, Pseudo-Primeira Ordem

PSO, Pseudo-Segunda Ordem

T, Temperatura (K)

rpm, Rotações por minuto

q_e, Capacidade de adsorção (mg g^{-1})

q_t, Capacidade de adsorção no tempo t (mg g^{-1})

C_0, Concentração inicial da solução (mg L^{-1})

C_f, Concentração final da solução (mg L^{-1})

K_1, Constante de velocidade de adsorção de pseudo-primeira ordem (min^{-1})

K_2, Constante da taxa de pseudo-segunda-ordem (g $mg^{-1}min^{-1}$)

K_{dif}, Constante de velocidade de adsorção ($g/mg^{-1}\,min^{-1/2}$)

C_e, Concentração de equilíbrio de soluto na solução (mg L^{-1})

q_{max}, Capacidade de adsorção máxima (mg g^{-1})

K_L, Constante de Langmuir (L mg^{-1})

K_F, Constante de Freundlich (mg g^{-1})

K_S, Constante de Sips (mg g^{-1})

n_s, Expoente de Sips relacionada à intensidade de adsorção

ΔG°, Energia livre de Gibbs (KJ mol^{-1})

ΔH°, Variação de entalpia (KJ mol^{-1})

ΔS°, Variação de entropia (KJ $mol^{-1}\,K^{-1}$)

R, Constante universal dos gases (8,314 J $mol^{-1}\,K^{-1}$)

χ^2, Teste qui-quadrado

R^2, Coeficiente de determinação

SUMÁRIO

CAPÍTULO 1

1. INTRODUÇÃO À TESE

Com a evolução da medicina, o crescente desenvolvimento de substâncias farmacêuticas e uso irregular de automedicação pela população, promoveu-se um intenso consumo de medicamentos no mundo (GHASEMYANI et al., 2022). Após o consumo, estas substâncias e/ou seus metabólitos atingem os rios e lagos por diferentes rotas, principalmente por meio de carregamento de esgotos doméstico após ineficiente tratamento nas ETARs (QUESADA et al., 2019a). Levando a um desafio ambiental significativo à descontaminação dos corpos hídricos.

Embora os fármacos tenham promovido a melhoria na saúde e qualidade de vida das pessoas, o seu consumo tem se tornado cada vez mais frequente e em quantidades e variedade significativas (GOMES; SILVA; GALVÃO, 2017). Contudo há grandes dificuldades em quantificar o consumo dos medicamentos no mundo, devido ao grande número de substâncias que podem variar de região para região, assim como os hábitos de consumo provocados pela qualidade de vida e facilidade de acesso aos medicamentos (MARQUES et al., 2017; QUESADA et al., 2019a).

Nesse sentido, segundo o Sindicato da Indústria de Produtos Farmacêuticos (SINDUSFarma), o mercado farmacêutico continua em forte expansão com o crescimento de 12,6% em 2024 e 9,3% em 2025, conforme projeções da IQVIA (SINDUSFARMA, 2024). Esse crescimento no consumo reflete na maior circulação de substâncias farmacêuticas podendo potencializar os riscos de contaminação ambiental, especialmente pela liberação de resíduos e metabólitos em corpos hídricos (QUESADA et al., 2019a). Dentre os inúmeros compostos farmacêuticos, destacam-se a Ivermectina e a Cloroquina, amplamente consumidas e utilizadas no tratamento precoce da COVID-19.

A cloroquina tornou-se um dos medicamentos com maior taxa de crescimento de vendas em 2020, quando comparado ao mesmo período de 2019 (FERREIRA; CARVALHO, 2023). Embora seja um medicamento indicado para o tratamento de doenças autoimunes, como lúpus eritematoso sistêmico e artrite reumatoide, além de malária, seu uso foi amplamente difundido, especialmente no Brasil e nos Estados Unidos, para o tratamento da COVID-19 (FOOD AND

DRUG ADMINISTRATION, 2020; TOURET; DE LAMBALLERIE, 2020), sendo relatado um aumento significativo nos níveis de cloroquina em fontes de água (KUMARI; KUMAR, 2021; KURODA et al., 2021), confirmando o transporte da substância.

Assim como a Cloroquina, durante a pandemia da COVID-19, a Ivermectina também passou a ser amplamente utilizada como tratamento precoce da doença do COVID-19, impulsionada por publicações que sugeriam seu potencial efeito antiviral (HEIDARY; GHAREBAGHI, 2020; POPP et al., 2021). No entanto, a Ivermectina é um medicamento de amplo espectro e alta lipossolubilidade, indicado no tratamento de infecções parasitárias, incluindo nematoides, artrópodes e flavivírus, além de ser empregada como inseticida. Também apresenta potenciais aplicações em terapias anticancerígenas (HEIDARY; GHAREBAGHI, 2020; MARTIN; ROBERTSON; CHOUDHARY, 2021).

O uso irregular desse medicamento levou a um aumento expressivo no consumo e, consequentemente, ao maior descarte da substância no meio ambiente, intensificando preocupações sobre seus impactos ecológicos. Estudos indicam que, quando liberada em grandes quantidades, a Ivermectina pode desestabilizar a cadeia alimentar dos ecossistemas, reduzindo significativamente a fertilidade ou até causando a extinção de algumas espécies (OLU-OWOLABI et al., 2021). Além disso, a substância pode infiltrar-se em águas subterrâneas e outras áreas, agravando os riscos ambientais e a contaminação de ecossistemas aquáticos (CUSIOLI et al., 2024).

Para remover esses contaminantes de matrizes aquosas, diversas metodologias, técnicas e tecnologias têm sido desenvolvidas para o tratamento de águas contaminadas por fármacos (AL-SHEHRI et al., 2019; RIVERA-UTRILLA et al., 2013). Dentre esses métodos, a adsorção é amplamente empregada devido à sua alta eficiência na remoção de poluentes, baixo custo de implementação e simplicidade operacional (ALI; ALOTHMAN; AL-WARTHAN, 2016; RIVERA-UTRILLA et al., 2013). Além disso, o processo de adsorção é reconhecido como uma tecnologia de tratamento de água economicamente viável, com custos variando entre US$ 10 e US$ 200 por milhão de litros, em comparação com outras tecnologias que podem atingir US$ 450 e gerar subprodutos perigosos. A adsorção também apresenta vantagens como baixo

consumo de energia, condições operacionais favoráveis e ausência de subprodutos, destacando sua viabilidade econômica e ambiental (GRELA; KUC; BAJDA, 2021).

Existem diversos tipos de materiais adsorventes, originados de fontes naturais ou sintéticas. Por exemplo, os biossorventes que reutilizam resíduos provenientes de fontes naturais (ABDOLALI et al., 2014; AHMAD; DANISH, 2018) e as nanopartículas (TRIPATHY et al., 2024) que são desenvolvidas completamente em laboratório para aprimorar a eficiência do processo de adsorção.

Na agroindústria, grandes quantidades de resíduos são geradas durante o processamento de alimentos (MO et al., 2018; ZHU; FAN; ZHANG, 2008). Para ampliar o aproveitamento desses materiais e reduzir impactos ambientais, alguns subprodutos têm sido investigados como adsorventes de baixo custo (LI et al., 2019; MO et al., 2018; QUESADA et al., 2021), como a *Moringa Oleifera Lam*. Estudos já demonstraram seu potencial na remoção de corantes, íons metálicos, pesticidas e alguns medicamentos, embora ainda haja poucas investigações sobre sua aplicação na remoção de uma grande diversidade de fármacos (GOMES et al., 2022; UEDA YAMAGUCHI et al., 2021).

Entre os adsorventes sintéticos, as sílicas mesoporosas têm se destacado devido às suas propriedades estruturais únicas, como alta área superficial (superior a 1.000 $m^2\ g^{-1}$) e porosidade controlável (BUI; CHOI, 2009; NATARAJAN et al., 2022). O processo de síntese permite modificar sua morfologia e química superficial, tornando-as mais seletivas na remoção de contaminantes específicos (CASHIN et al., 2018; DOU et al., 2011). Contudo, sílicas mesoporosas puras, como a MCM-41, apresentam caráter neutro, o que pode limitar sua aplicação em adsorção (GRELA; KUC; BAJDA, 2021). Para contornar essa limitação, modificações estruturais, como a incorporação de nanopartículas metálicas, têm sido exploradas para aumentar a eficiência do material (ANDRADE et al., 2022; LIU et al., 2019). Estudos apontam a eficiência de sílicas mesoporosas na remoção de fármacos como diclofenaco, carbamazepina, ibuprofeno e tetraciclina (AL-SHEHRI et al., 2019; BUI; CHOI, 2009; GRELA; KUC; BAJDA, 2021). No entanto, ainda há poucas investigações sobre o uso de diferentes tipos de sílicas para a remoção de outros fármacos, como por exemplo, a cloroquina.

Diante desse cenário, torna-se essencial desenvolver e explorar novos materiais adsorventes, tanto de origem natural quanto sintética, para ampliar as alternativas de tratamento de águas contaminadas por fármacos, propondo soluções mais eficientes e sustentáveis, alinhadas às demandas ambientais e tecnológicas atuais.

Nesse sentido, o objetivo desta pesquisa foi desenvolver e avaliar a aplicação de novos materiais adsorventes, tanto de origem natural quanto sintética, para a remoção de contaminantes farmacêuticos, como a cloroquina e ivermectina, em matriz aquosa.

2. OBJETIVOS

2.1. OBJETIVO GERAL

Nesse sentido, o objetivo desta pesquisa foi desenvolver e avaliar a aplicação de novos materiais adsorventes, tanto de origem natural quanto sintética, para a remoção de contaminantes farmacêuticos, como a cloroquina e ivermectina, em matriz aquosa.

2.2. OBJETIVO ESPECÍFICO

Para atingir o objetivo geral, os seguintes objetivos específicos foram desenvolvidos, conforme demonstrado na Figura 1:

- ✓ Realizar a modificação das cascas da semente de *Moringa oleifera Lam*. através do tratamento químico com ácido nítrico e tratamento térmico;
- ✓ Funcionalizar as cascas da semente de *Moringa oleifera Lam.*, modificadas previamente com nanopartículas de óxido de ferro;
- ✓ Sintetizar as sílicas mesoporosas do tipo, MCM-41 e MCM-48.
- ✓ Sintetizar as nanopartículas de óxido de cobalto;
- ✓ Realizar a modificação de ambas sílicas mesoporosas com nanopartículas de óxido de cobalto;

- ✓ Caracterizar todos os adsorventes proveniente de fonte natural e sintética, antes e após modificação, com utilização de análises química, estrutural e textural;
- ✓ Analisar os efeitos de concentração dos adsorventes e o pH para a determinação das melhores condições operacionais do processo de adsorção dos fármacos;
- ✓ Determinar as curvas cinéticas, isotermas de equilíbrio e parâmetros termodinâmicos para os adsorventes de fonte natural e sintética.
- ✓ Avaliar a estabilidade e possibilidade de reuso dos adsorventes de fonte natural e sintética na remoção dos fármacos, ivermectina e cloroquina em ciclos de adsorção.
- ✓ Propor mecanismos para a adsorção da cloroquina em adsorventes a base de sílica mesoporosa funcionalizadas com óxido de cobalto.

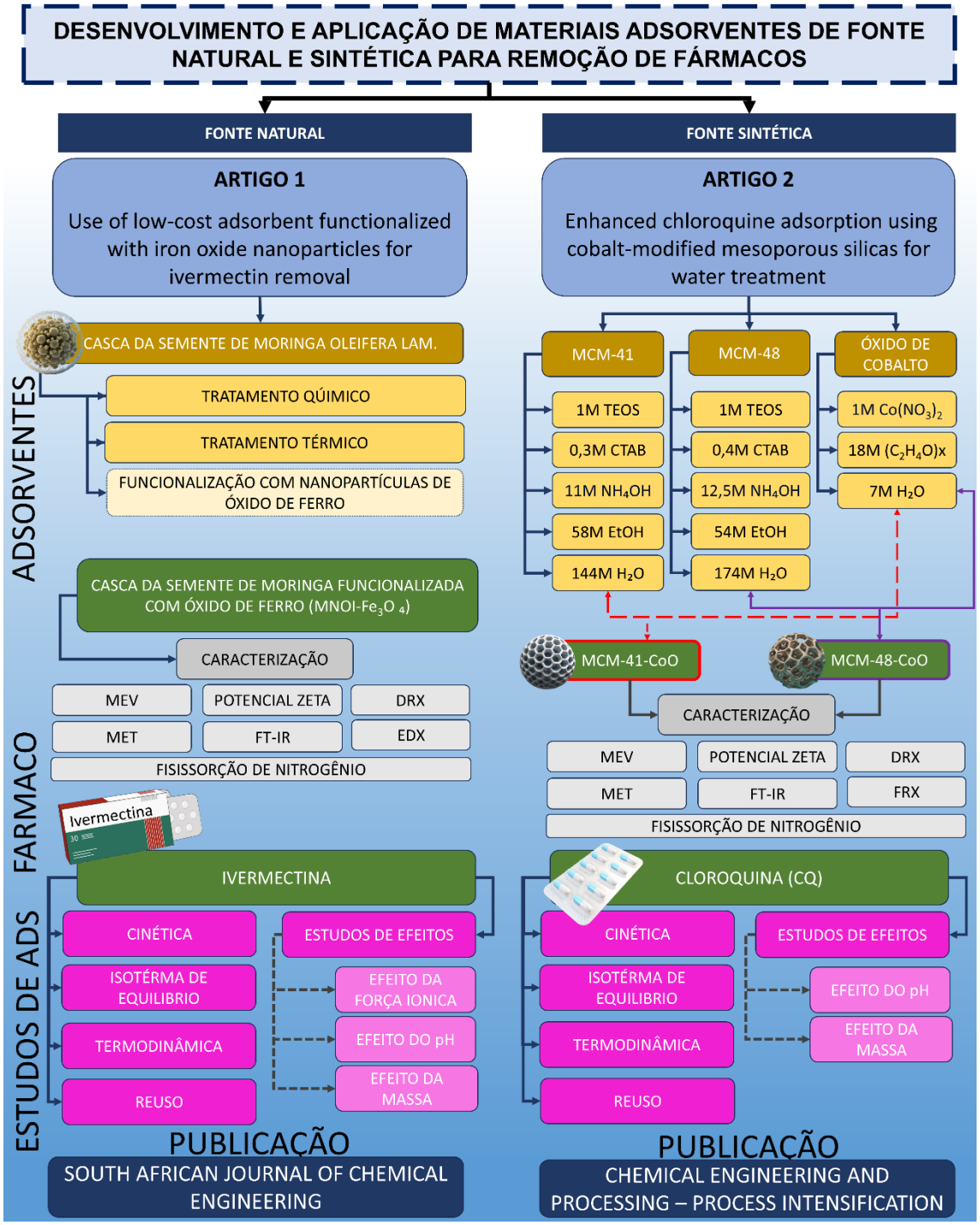

Figura 1. Infográfico sobre uma visão geral da tese: estrutura dos artigos e publicações sobre adsorção de fármacos.

3. REVISÃO BIBLIOGRÁFICA

3.1. POLUENTES EMERGENTES

São considerados poluentes emergentes (PE), compostos que represente pelo menos uma das três características (ÁLVAREZ-RUIZ; PICÓ, 2020):

- Composto novo e/ou desconhecido, até mesmo com poucos relatos;
- Composto conhecido, porém os problemas de contaminação ambiental relativo a estes compostos não são totalmente compreendidos;
- Compostos que podem causar riscos ambientais e à saúde humana.

Entre a grande variedade de compostos denominados como poluentes ou contaminantes emergentes estão os produtos de cuidados pessoais, pesticidas, fármacos e os microplásticos. Os contaminantes emergentes podem ter origem natural, contudo a grande maioria são substâncias sintéticas de origem antrópica (ÁLVAREZ-RUIZ; PICÓ, 2020).

Esses contaminantes são frequentemente presentes em corpos d'águas em baixas concentrações que variam de ng/L a µg/L. Devido à baixa concentração e a grande variedade de substâncias faz com que a detecção, monitoramento e as análises sejam dificultosas, além disso, também torna-se um desafio a sua remoção pelos processos de tratamento de água e efluentes convencionais (LUO et al., 2014).

Além disso, alguns produtos tem característica como a alta persistência no meio ambiente e bioacumulação, causando diversos impactos negativos aos organismos não-alvo (DE SOUZA et al., 2020). De acordo com PETROVIC (2003), alguns compostos são tão frequentemente consumidos no mundo que não necessitam ser persistentes para ser prejudicial ao meio ambiente, pois sua remoção ou decomposição são compensadas por sua continua introdução.

Segundo BOLONG et al. (2009) e QUESADA et al. (2019a), alguns dos grandes problemas relacionados aos contaminantes emergentes são: A inexistência de valores limitantes de descarga dos contaminantes pela

legislação, outra questão é que os avanços industriais e tecnológicos são mais rápidos que as práticas regulatórias. Com isso, nenhuma ou poucas ações de precaução e monitoramento são tomadas para garantir que os compostos não regulamentados ou novas substâncias, não sejam descartados em corpos hídricos. Além disso, há preocupação também com os efeitos desses contaminantes, pois muitos poluentes são considerados desreguladores endócrinos.

Dentre a grande quantidade de produtos químicos incluídos nos contaminantes emergentes os produtos farmacêuticos são considerados uma importante classe devido ao alto consumo em todo o mundo, alta frequência de detecção nos ambientes aquáticos e consequentemente seus impactos negativos (FENT; WESTON; CAMINADA, 2006; QUESADA et al., 2019a).

3.2. FÁRMACOS

Os fármacos são substâncias químicas utilizados para diagnóstico, tratamento, alteração ou prevenção de doenças humana e animal (DAUGHTON, 2003; DAUGHTON; TERNES, 1999). Esses contaminantes emergentes incluem diversos grupos, tais como antibióticos, anti-inflamatórios não esteroides, beta-bloqueadores, hormônios esteroides, antidepressivos, reguladores de lipídios sanguíneo, entre outros (FENT; WESTON; CAMINADA, 2006).

Os medicamentos quando administrados são degradados e absorvidos pelo corpo e atuam de maneira específica, desse modo, alguns desses compostos são persistentes no corpo. Contudo, após a absorção e a ação do fármaco grande parte dos medicamentos são excretados do organismo pela urina e fezes como uma mistura de composto original e metabólitos (FENT; WESTON; CAMINADA, 2006; RIVERA-UTRILLA et al., 2013).

Embora os fármacos tenham promovido a melhoria na saúde e qualidade de vida das pessoas, o seu consumo tem se tornado cada vez mais frequente e em quantidades e variedade significativas (GOMES; SILVA; GALVÃO, 2017). Contudo há grandes dificuldades em quantificar o consumo dos medicamentos no mundo, devido ao grande número de substâncias que variam de região para região, como também os hábitos de consumo provocados pela qualidade de vida

e facilidade de acesso aos fármacos (MARQUES et al., 2017; QUESADA et al., 2019a).

Entretanto, segundo dados fornecidos pela Associação Brasileira de Redes de Farmácia e drogarias (ABRAFARMA), entre os meses de janeiro a setembro de 2021, somente as 26 empresas que integram a ABRAFARMA faturaram R$ 58,85 bilhões neste período, o que representa uma evolução de 17,4% (BRUNO, 2023). Nesse sentido, o expressivo aumento da quantidade de medicamentos consumidos provoca o aumento na descarga desses contaminantes em corpos d'água, consequentemente, a presença mais frequente e em concentrações cada vez mais elevadas das drogas nos ambientes aquáticos.

Assim, a contaminação dos recursos hídricos pelos produtos farmacêuticos, em sua forma parental ou metabólitos, pode ocorrer por diferentes rotas (Figura 2). Sendo a principal rota, à disposição como efluente doméstico após administração do medicamento e metabolismo no corpo humano, seguido pela excreção.

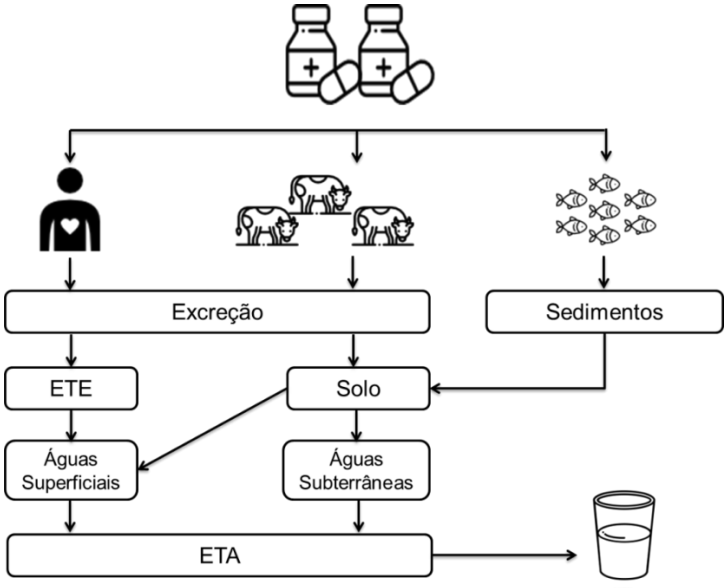

Figura 2. Possíveis rotas dos fármacos no meio ambiente.
Fonte: (QUESADA et al., 2019a)

Dessa maneira, os resíduos dos fármacos são transportados no efluente até atingir as ETARs, podendo ainda sofrer degradações adicionais. Entretanto, há relatos, que muitos destes compostos não são biodegradados e

completamente removidos no tratamento convencional, acabando por serem despejados com o efluente tratado nas águas superficiais (GARCIA-IVARS et al., 2017; PRAVEENA et al., 2018; VERAS et al., 2019). Outra via de contaminação está nos produtos veterinários que podem adentrar no ambiente aquático através do estrume despejado no solo que por meio da precipitação são escoados e atingem rios e lagos. Além disso, também há rota de contaminação através da aplicação direta na aquicultura (piscicultura) (FENT; WESTON; CAMINADA, 2006; QUESADA et al., 2019a; RIVERA-UTRILLA et al., 2013).

A ocorrência desses medicamentos no ambiente aquático e terrestre tem sido associada a uma série de impactos negativos. Ainda que em baixas concentrações esses contaminantes podem causar efeitos crônicos sutis nos organismos não-alvo. Dessa forma, há uma grande dificuldade de avaliação dos efeitos toxicológicos dos fármacos, devido à sua complexidade e a ocorrência de efeitos em longo prazo (FENT; WESTON; CAMINADA, 2006; ZHANG et al., 2014). Embora os efeitos a longo prazo sejam desconhecidos, tem-se o conhecimento dos efeitos adversos que os medicamentos causam sobre o organismo após o consumo.

A cloroquina (CQ) é um medicamento da classe das quinolinas, com propriedades bactericidas, antissépticas e antipiréticas (RAMESH et al., 2018). Embora este fármaco seja indicado para o tratamento de malária, doenças autoimunes, como lúpus eritematoso sistêmico e artrite reumatoide, a droga tem sido estudada em testes in-vitro como antiviral de amplo espectro, inibindo a replicação de vírus respiratórios como influenza A/H5N1, SARS-CoV e coronavírus humano 229E (MURRAY et al., 2010; SAVARINO et al., 2003; VINCENT et al., 2005). Nesse sentido, principalmente no início do período pandêmico, a cloroquina tornou-se um dos medicamentos com maior taxa de crescimento de vendas em 2020, quando comparado ao mesmo período de 2019 (FERREIRA; CARVALHO, 2023). No entanto, sua eficácia para este fim foi amplamente questionada, e diversas pesquisas apontaram sua alta toxicidade para os pacientes (GHAZY et al., 2020; JAMELEDDINE et al., 2020; ROSENBERG et al., 2020; SANDERS et al., 2020; SHUKLA et al., 2020).

Além dos riscos à saúde humana, ao atingir o meio ambiente, a CQ pode provocar diversos impactos a organismos não-alvo, além disso, a substância tende apresentar persistência no meio aquático o que favorece a bioacumulação

em órgãos como rins e fígado, além de influenciar processos metabólicos e enzimáticos de organismos aquáticos (FERREIRA; CARVALHO, 2023).

Assim como a cloroquina, durante a pandemia da COVID-19, a Ivermectina também passou a ser amplamente utilizada como tratamento precoce da doença do COVID-19, impulsionada por publicações que sugeriam seu potencial efeito antiviral (HEIDARY; GHAREBAGHI, 2020; POPP et al., 2021). No entanto, a Ivermectina é um medicamento de amplo espectro e alta lipossolubilidade, indicado no tratamento de infecções parasitárias, incluindo nematoides, artrópodes e flavivírus, além de ser empregada como inseticida. Também apresenta potenciais aplicações em terapias anticancerígenas (HEIDARY; GHAREBAGHI, 2020; MARTIN; ROBERTSON; CHOUDHARY, 2021).

O uso irregular desse medicamento levou a um aumento expressivo no consumo e, consequentemente, ao maior descarte da substância no meio ambiente, intensificando preocupações sobre seus impactos ecológicos. Estudos indicam que, quando liberada em grandes quantidades, a Ivermectina pode desestabilizar a cadeia alimentar dos ecossistemas, reduzindo significativamente a fertilidade ou até causando a extinção de algumas espécies (OLU-OWOLABI et al., 2021). Além disso, a substância pode infiltrar-se em águas subterrâneas e outras áreas, agravando os riscos ambientais e a contaminação de ecossistemas aquáticos (CUSIOLI et al., 2024).

Apesar de ambos os fármacos serem considerados poluentes emergentes, ainda há pouca regulamentação sobre seus limites em efluentes e águas superficiais no Brasil. A legislação ambiental brasileira que inclui a Resolução CONAMA 357/2005 e a Portaria GM/MS Nº 888/2021, não estabelecem padrões específicos para a presença de fármacos na água potável ou nos recursos hídricos (BRASIL, 2021; CONAMA, 2005). Tornando suas presenças neste meio inevitável.

Dependendo do tempo exposição e da dosagem esses contaminantes pode gerar desde alterações bioquímicas e danos celulares até a morte de organismos aquáticos (FERREIRA; CARVALHO, 2023; GUPTA; RANI, 2024). Diante desse cenário, a literatura destaca a importância de estudos voltados para a detecção, remoção e avaliação dos impactos ambientais desses compostos.

3.2.1. IVERMECTINA

A avermectina é um grupo de lactonas macrocíclicas produzidas por actinobactérias do gênero *Streptomyces*, em especial *Streptomyces avermitilis,* que apresentam atividade nematicida, acaricida e inseticida (KWON et al., 2010; LASOTA; DYBAS, 1991). O grupo das avermectinas foi descoberto em 1976, obtidos por meio de caldos de fermentação de culturas no Instituto Kitasato (Japão), durante uma busca por compostos naturais com atividade anti-helmíntica (LASOTA; DYBAS, 1991). Pertence à família das avermectinas as substâncias como: moxidectina, milbemicina oxima, doramectina, selamectina, abamectina e ivermectina, sendo estas duas últimas as mais utilizadas (BAI; OGBOURNE, 2016).

A ivermectina, em especial, tornou-se um “blockbuster” na indústria de saúde animal, com vendas anuais superiores a US$ 1 bilhão durante mais de duas décadas, sendo empregada em larga escala no tratamento de animais de criação em todo o mundo. Além disso, é utilizada de forma *off-label*, ou seja, fora das indicações oficialmente aprovadas, incluindo usos não autorizados, o que amplia ainda mais seu potencial de entrada no meio ambiente e os impactos associados (BAI; OGBOURNE, 2016; CRUMP; OMURA, 2011).

Além dos usos veterinários de forma *off-label*, durante a pandemia da COVID-19, a Ivermectina teve seu uso amplamente disseminado como possível tratamento precoce, devido a hipóteses sobre seu efeito antiviral. No entanto, estudos clínicos não comprovaram sua eficácia contra o SARS-CoV-2. Esse uso indiscriminado levou a um aumento expressivo na produção e descarte do composto, contribuindo para sua presença no meio ambiente (HEIDARY; GHAREBAGHI, 2020; POPP et al., 2021).

A eliminação da Ivermectina ocorre principalmente por excreção fecal, na forma inalterada ou como metabólitos, sendo liberada no solo e corpos hídricos (QUESADA et al., 2019a). A baixa solubilidade em água e a forte afinidade por matéria orgânica fazem com que a substância persista no ambiente, acumulando-se no sedimento e afetando organismos aquáticos (BAI; OGBOURNE, 2016). Estudos indicam que a exposição a concentrações elevadas pode impactar populações de invertebrados, reduzir a fertilidade de

algumas espécies e até causar extinções locais. Além disso, há evidências de que a substância pode infiltrar-se no solo e atingir águas subterrâneas, ampliando os riscos ambientais (BAI; OGBOURNE, 2016; CUSIOLI et al., 2024).

Além disso, o problema ambiental pode ser intensificado, devido a não haver limite máximo regulamentado pela legislação brasileira para a presença desse medicamento em corpos d'água (BRASIL, 2021; CONAMA, 2005). Diante desses fatores, torna-se essencial um controle mais rigoroso sobre o uso da Ivermectina, bem como o desenvolvimento de estratégias para reduzir sua liberação no ambiente, como melhorias nos processos de tratamento de efluentes e o incentivo ao uso racional do fármaco.

3.2.2. CLOROQUINA

A cloroquina (CQ), cujo nome químico é 4-N-(7-chloroquinolin-4-yl)-1-N,1-N-diethylpentane-1,4-diamine, é um medicamento pertencente a classe das quinolinas e possui propriedades bactericidas, antissépticas e antipiréticas (RAMESH et al., 2018). Na tabela 2, apresenta-se as propriedades físico-químicas deste composto.

Tabela 1. Propriedades físico-químicas da Cloroquina.

Cloroquina ($C_{18}H_{26}ClN_3$)		
Estrutura química	**Número CAS**	54-05-7
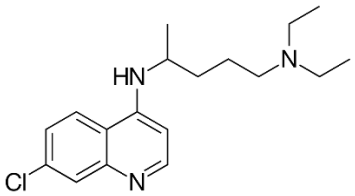	**Peso molecular (g mol^{-1})**	319,9
	Solubilidade em água (mg L^{-1})	Solúvel
	pKa	4 - 8,4 - 10,2

Fonte: Adaptado de (PUBCHEM, 2025) e (MAGALHÃES-GHIOTTO et al., 2023).

A CQ é um fármaco indicado para o tratamento de malária, doenças autoimunes, como lúpus eritematoso sistêmico e artrite reumatoide, entretanto, a droga tem sido estudada em testes in-vitro como antiviral de amplo espectro, inibindo a replicação de vírus respiratórios como influenza A/H5N1, SARS-CoV e coronavírus humano 229E (MURRAY et al., 2010; SAVARINO et al., 2003; VINCENT et al., 2005). Embora, sua eficácia para este fim seja amplamente questionada, e diversas pesquisas apontem que o consumo da droga pode provocar alta toxicidade para os pacientes (GHAZY et al., 2020; JAMELEDDINE

et al., 2020; ROSENBERG et al., 2020; SANDERS et al., 2020; SHUKLA et al., 2020), este medicamento foi amplamente difundido para o tratamento da SARS-CoV (COVID-19), tornando-se um dos medicamentos com maior taxa de crescimento de vendas em 2020, quando comparado ao mesmo período de 2019 (FERREIRA; CARVALHO, 2023).

Estudos relataram um aumento significativo nos níveis de cloroquina e hidroxicloroquina em fontes de água (KUMARI; KUMAR, 2021; KURODA et al., 2021). Por exemplo, durante a pandemia, as concentrações de CQ atingiram quase 50 μg L^{-1} em lodo primário em uma estação de tratamento de águas residuais dos EUA, poucas semanas após a Autorização de Uso Emergencial (NASON et al., 2022). Além disso, epidemiologia baseada em águas residuais também revelou um aumento no uso de CQ de 12 g/dia para 57 g/dia na Grécia durante o mesmo período (GALANI et al., 2021). Outros relatórios incluem concentrações de 1,7 μg L^{-1} na Lombardia, Itália (CAPPELLI et al., 2022), 0,071 μg L^{-1} em Vitoria-Gasteiz, Espanha (DOMINGO-ECHABURU et al., 2022) e 32 ng L^{-1} em águas superficiais durante a pandemia (KURODA et al., 2021). Dados pré-pandêmicos da Nigéria relataram 110 ng L^{-1} em águas superficiais e até 5.000 ng L^{-1} em águas subterrâneas, com concentrações ligadas à incidência de malária (HU et al., 2021; OLATUNDE et al., 2014). Essas descobertas destacam o transporte de cloroquina por esgoto doméstico, levantando preocupações sobre seu impacto ecológico.

Uma pesquisa realizada por BABIĆ; DABIĆ; ĆURKOVIĆ (2017), investigou a estabilidade hidrolítica e fotolítica da CQ. Os resultados indicaram que o fármaco é resistente à degradação hidrolítica e que sua degradação fotolítica ocorre de forma lenta dependendo do pH do meio. A fotodegradação foi mais eficiente em condições alcalinas, com a meia-vida reduzindo de 23,1 horas em pH 4 para apenas 5,5 minutos em pH 9. As características de transporte, persistência e lenta degradação da cloroquina favorecem sua bioacumulação em ecossistemas aquáticos, especialmente diante do aumento expressivo no consumo e descarte desse medicamento durante a pandemia, o que pode representar um risco para organismos.

Segundo FERREIRA; CARVALHO (2023), a poluição por CQ pode causar diversos efeitos aos organismos, desde pequenas alterações bioquímicas, danos a nível celular ou até a morte do indivíduo. Além disso, indiretamente a

poluição por resíduos farmacêuticos no ambiente aquático pode comprometer a resistência dos organismos a patógenos, favorecer a disseminação de doenças e provocar impactos na dinâmica populacional das espécie (BEN ALI et al., 2021; ELLIS et al., 2011; SILVESTRE, 2020).

Em um estudo realizado por BEN ALI et al. (2021), que avalia a toxicidade da CQ em nematoides meiobênticos, constatou uma redução significativa na abundância e diversidade de espécies de nematoides, especialmente nas maiores concentrações testadas, além disso, houve um aumento na prevalência de morfotipos grandes pertencentes ao grupo funcional 2B (onívoros-carnívoros), que são tolerantes à toxicidade e podem bioacumular a CQ. Essas mudanças podem indicar impactos ambientais e riscos para organismos que se alimentam dessa meiofauna, incluindo espécies consumidas por humanos. Em um outro estudo realizado por (RAMESH et al., 2018), que avaliou os efeitos da CQ em peixes (Cyprinus carpio), notou que a CQ causou alterações enzimáticas e danos histológicos nos rins, fígado e brânquias após exposições agudas e subletais. O aumento das atividades enzimáticas de GOT e GPT no plasma sanguíneo e as lesões nos tecidos sugerem toxicidade significativa, mesmo em baixas concentrações, reforçando a necessidade de monitoramento desse fármaco em ecossistemas aquáticos.

Diante da persistência da cloroquina no ambiente aquático e dos impactos ecotoxicológicos associados, torna-se essencial investigar estratégias de remoção eficazes. Nesse contexto, os processos de adsorção surgem como uma alternativa promissora para mitigar a contaminação por fármacos, reduzindo sua biodisponibilidade e minimizando os riscos ambientais.

3.3. PROCESSOS DE ADSORÇÃO

Segundo SING et al. (1985), adsorção é um processo de separação em que um determinado componente da fase fluida (gases ou líquidos) é transferido para a superfície de um sólido. O componente no fluído, geralmente um contaminante, é denominado adsorbato, já o sólido é o adsorvente. Em contrapartida, o processo de transferência inverso é chamado de dessorção, em que o adsorbato é transferido do adsorvente para a fase fluida.

O método de adsorção tem demonstrado ser excelente e promissor no tratamento de água contaminada devido à suas diversas vantagens como o baixo custo de implantação e operação, acessível, excelente desempenho e não gera subprodutos tóxicos (ALI; ASIM; KHAN, 2012; RIVERA-UTRILLA et al., 2013). O processo de adsorção pode ser realizado na forma de batelada ou de fluxo continuo em uma coluna contendo material adsorvente (HO; MCKAY, 1998).

Os adsorventes são materiais porosos que podem ser classificados em duas categorias principais: naturais e sintéticos (FERNÁNDEZ-REYES et al., 2020). Os adsorventes naturais, como por exemplo, carvão de origem mineral, vegetal e animal, cinzas e algumas resinas orgânicas, geralmente possuem menor custo, mas sua área superficial e dimensões de poro são frequentemente limitadas, o que pode restringir sua capacidade adsortiva (BHADRA; SEO; JHUNG, 2016; ELBALKINY et al., 2019; HIEW et al., 2019; QUESADA et al., 2019a). Já os adsorventes sintéticos, como zeólitas sintéticas, estruturas metal-orgânicas (MOFs), sílicas mesoporosas, óxido de grafeno, entre outros, podem apresentar maior eficiência na remoção de contaminantes, porém tendem a ser mais onerosos, dificultando sua aplicação em larga escala (AHMED et al., 2017; GRELA; KUC; BAJDA, 2021; KHAWAJA et al., 2021). Dessa forma, a escolha entre adsorventes naturais e sintéticos depende do objetivo de cada aplicação, disponibilidade e eficiência na remoção de contaminantes. A seguir, serão discutidas em maior detalhe as características de cada uma dessas classes de materiais.

3.3.1. ADSORVENTES DE FONTES NATURAIS

São adsorventes de fontes naturais, aqueles materiais denominados de baixo custo, composto principalmente por subprodutos ou materiais residuais da indústria, os quais seriam destinados ao descarte, como por exemplo: partes de plantas, resíduos de frutas, cascas de grãos entre outros (ABDOLALI et al., 2014; LI et al., 2019; ZOLGHARNEIN; SHAHMORADI; GHASEMI, 2011). Tem-se como vantagens em utilizar os subprodutos e resíduos como materiais adsorventes: a abundante fonte de material, a redução dos custos da aplicação

da técnica de tratamento de água e efluente, além de aumentar o ciclo de vida do material (MO et al., 2018).

No entanto, a capacidade de adsorção dos subprodutos agrícolas in natura é geralmente baixa, por isso, muitas pesquisas que utilizam esses materiais realizam modificações com o objetivo de obter adsorventes com alta capacidade de adsorção e baixo-custo (QUESADA et al., 2019a). Há diversos tipos de modificações, dentre elas, os processos de modificações simplificados como pré-tratamento com lavagem do material, tratamento químico e térmico (AKHTAR et al., 2007).

Os tratamentos químicos são utilizados em biomassas para aprimorar sua capacidade de adsorção dos contaminantes e alterar o comportamento elétrico da superfície. O tratamento químico age quebrando as ligações entre grupos funcionais e a superfície adsorvente, como também na remoção da matéria orgânica e inorgânica contida na superfície do adsorvente. Esta ação do tratamento resulta no aumento do tamanho do poro, bem como interações com outros grupos funcionais do contaminante (AKHTAR et al., 2007; MÓDENES et al., 2017). Os agentes químicos incluem ácidos orgânicos e minerais (HCl, HNO_3, H_2SO_4, CH_3COOH, $C_6H_8O_7$ e CH_2O_2), bases e soluções básicas (NaOH, Na_2CO_3, $Ca(OH)_2$ e $CaCl_2$), agentes oxidantes (H_2O_2 e K_2MnO_4), entre outros compostos (ABDOLALI et al., 2014).

O tratamento térmico é realizado por meio do aquecimento do material em forno e objetiva a degradação da matéria orgânica e o aumento a área superficial do adsorvente, assim, o tratamento melhora a capacidade de adsorção do adsorvente (AKHTAR et al., 2007; COLDEBELLA et al., 2017; QUESADA et al., 2019a).

Para avaliar a capacidade de adsorção dos materiais adsorventes são necessários a realização de estudos de adsorção como o efeito do pH, massa, tempo de contato, temperatura e concentração do contaminante, entre outros. Além disso, análises de caracterização do adsorvente são indicadoras da qualidade da biomassa como adsorvente. Para isso, são comuns as análises de potencial zeta, microscopia eletrônica de varredura (MEV), microscopia eletrônica de transmissão (MET), fisiossorção de nitrogênio, espectroscopia no infravermelho com transformada de Fourier (FTIR), análises de energia

dispersiva de raios X (EDX), Difração de Raios-X (DRX) e de Fluorescência de Raios X (FRX).

3.3.1.1. *MORINGA OLEIFERA* LAM. COMO ADSORVENTE DE FONTE NATURAL

A *Moringa oleífera* Lamarck é uma planta pertencente à família das Moringaceae, originalmente encontrada na Índia e regiões sub-himalaias, contudo, atualmente é cultivada em diversas regiões tropicais e subtropicais, como no continente Norte americano e na América Central (KANSAL; KUMARI, 2014). A *Moringa oleifera Lam.* é uma planta utilizada com fins alimentícios e medicinais, sendo fonte de beta-caroteno, proteínas, vitamina C, cálcio e potássio, além de apresentar atividades farmacológicas atribuídas a compostos com ação antimicrobiana, anti-inflamatória e antioxidante (GOMES et al., 2022).

Além de suas aplicações medicinais, estudos demonstram que as sementes da planta possuem propriedades antimicrobianas e atuam como agentes coagulantes naturais, sendo eficazes na clarificação da água e na redução da carga microbiológica, apresentando aplicabilidade em processos de tratamento de água (KANSAL; KUMARI, 2014). Da mesma forma, todas as partes da *Moringa oleifera Lam.*, como por exemplo: folhas, sementes, vagens, raízes e casca, apresentam características como alta porosidade e área superficial que indicam um potencial promissor para seu uso como biossorventes (AKHTAR et al., 2007; COLDEBELLA et al., 2017; CUSIOLI et al., 2021; QUESADA et al., 2019b). Nesse sentido, pesquisas realizadas demonstram que esses materiais pode ser utilizado para remover metais pesados, corantes, pesticidas e fármacos de soluções aquosas (ABATAL et al., 2021; COLDEBELLA et al., 2017; CUSIOLI et al., 2021; KHALFAOUI et al., 2022).

A casca da *Moringa oleifera Lam.* é um material lignocelulósico rico em celulose, hemicelulose e lignina, contendo grupos funcionais como hidroxilas, carboxilas e carbonilas (COLDEBELLA et al., 2017). Essas características estruturais favorecem a interação com poluentes por meio de diferentes mecanismos de adsorção, incluindo forças eletrostáticas, troca iônica e complexação química (CUSIOLI et al., 2021; QUESADA et al., 2019b).

A modificação química ou térmica da casca pode aumentar sua área superficial e otimizar a distribuição dos sítios ativos, tornando-a ainda mais eficaz na adsorção de contaminantes (AKHTAR et al., 2007; QUESADA et al., 2019b). Além disso, seu uso como adsorvente representa uma alternativa ambientalmente amigável, pois trata-se de um material biodegradável, de baixo custo e abundante em diversas regiões, contribuindo para processos mais sustentáveis de tratamento de águas e efluentes (UEDA YAMAGUCHI et al., 2021).

Assim, no campo ambiental, a *Moringa oleifera Lam.* tem sido explorada como uma alternativa sustentável para o tratamento de águas e efluentes (GOMES et al., 2022; UEDA YAMAGUCHI et al., 2021). Embora, apresente diversos reportes já registrados, a casca da *Moringa oleifera Lam.* ainda é um material relativamente pouco explorado, principalmente quando comparado às sementes, o que abre espaço para investigações mais aprofundadas sobre seu desempenho em diferentes condições experimentais, tipos de modificações e funcionalizações e alvos de descontaminação. Podendo assim, contribuir significativamente para consolidar seu uso como adsorvente de fonte natural em sistemas de tratamento de água e efluentes, especialmente em regiões com recursos limitados.

3.3.2. ADSORVENTES DE FONTES SINTÉTICAS

Os adsorventes de fonte sintética são materiais projetados e fabricados com o objetivo de apresentar propriedades específicas para a remoção de contaminantes em meios aquosos (FERNÁNDEZ-REYES et al., 2020). Diferentemente dos adsorventes naturais, que são derivados de subprodutos ou resíduos, os adsorventes sintéticos são desenvolvidos a partir de processos controlados de síntese química, o que permite a obtenção de materiais com alta área superficial, porosidade, pureza, estrutura interna definida e propriedades ajustáveis (AKHTAR; ALI; ZAMAN, 2024; FERNÁNDEZ-REYES et al., 2020).

Além das características estruturais, os adsorventes sintéticos também apresentam uma versatilidade devido a possibilidade de modificação/funcionalização química de sua superfície tornando o material adsorvente mais seletivo ou coletivo na remoção de contaminantes específicos

(SAHU et al., 2024). Dentre as possibilidades de funcionalização há aplicação de frações de ácido/base, hidrofobicidade, incorporação de metais, grupos iônicos, entretanto a combinação dos funcionalizantes é o mais frequentemente utilizado no tratamento de água (FERNÁNDEZ-REYES et al., 2020).

Devido à ampla diversidade de compostos classificados como contaminantes emergentes, incluindo fármacos, suas distintas estruturas e propriedades físico-químicas, como grupos funcionais, solubilidade, pKa e tamanho molecular, tornam sua remoção um desafio (FERNÁNDEZ-REYES et al., 2020). Para solucionar esse problema, é essencial um design eficiente do adsorvente, desenvolvendo materiais com características específicas, como tamanho de poros, área superficial, funcionalização química e composição estrutural, de modo a otimizar a remoção de contaminantes emergentes e aumentar a seletividade do processo adsortivo (AKHTAR; ALI; ZAMAN, 2024). Nesse contexto, há uma grande diversidade de adsorventes sintéticos porosos desenvolvidos, como zeólitas sintéticas, estruturas metal-orgânicas (MOF), sílicas mesoporosas (SM) e óxidos de grafeno (GO), têm sido amplamente estudados, correlacionando suas propriedades texturais e químicas com seletividade e capacidade adsortiva (BHADRA; JHUNG, 2017; GRELA; KUC; BAJDA, 2021; KHAWAJA et al., 2021; NARAYAN et al., 2018).

Assim, os adsorventes sintéticos, especialmente as sílicas mesoporosas funcionalizadas, representam uma alternativa promissora para a remoção de contaminantes em sistemas de tratamento de água. Sua capacidade de ser projetado e ajustado para aplicações específicas os torna uma ferramenta valiosa no combate à poluição por fármacos e outros contaminantes emergentes. Essa abordagem será explorada em detalhes no próximo tópico, que abordará especificamente o uso de sílicas mesoporosas no tratamento de água.

3.3.2.1. SÍLICAS MESOPOROSAS

Os materiais sólidos porosos têm sido extensivamente estudados para aplicações industriais como catalisadores e adsorventes (UCHÔA, 2011). Um material com alta porosidade e área superficial permite que haja uma maior capacidade de entrada e deposito das moléculas a serem adsorvidas. Tornando-

se um parâmetro frequentemente analisado em estudos de adsorção (QUESADA et al., 2021).

De acordo com a classificação realizada pela União Internacional de Química Pura e Aplicada (IUPAC), os sólidos são divididos pelo tamanho de seus poros, sendo: microporosos com os materiais com diâmetro de poro inferior a 2 nm, mesoporosos para diâmetros que variam entre 2 até 50 nm e macroporosos para materiais com poros de diâmetro superior a 50 nm (WORCH, 2012).

Embora os estudos de síntese de materiais mesoporosos tenham iniciado nos anos de 1970, somente a partir do ano de 1992 que estes materiais ganharam maior interesse no meio cientifico, após pesquisadores da *Mobil Oil Corporation* produzir o primeiro material mesoporoso por meio de géis de alumino-silicato utilizando como mecanismo, o modelo de cristal líquido; tal material foi denominado de *Mobil Crystalline Materials* ou *Mobil Composition of Matter* (MCM), sendo produzido o MCM-41, MCM-48 e MCM-50, os quais apresentavam mesoestrutura do tipo hexagonal, cubica e lamelar, respectivamente (Figura 3) (CECILIA; MORENO TOST; RETUERTO MILLÁN, 2019; NARAYAN et al., 2018).

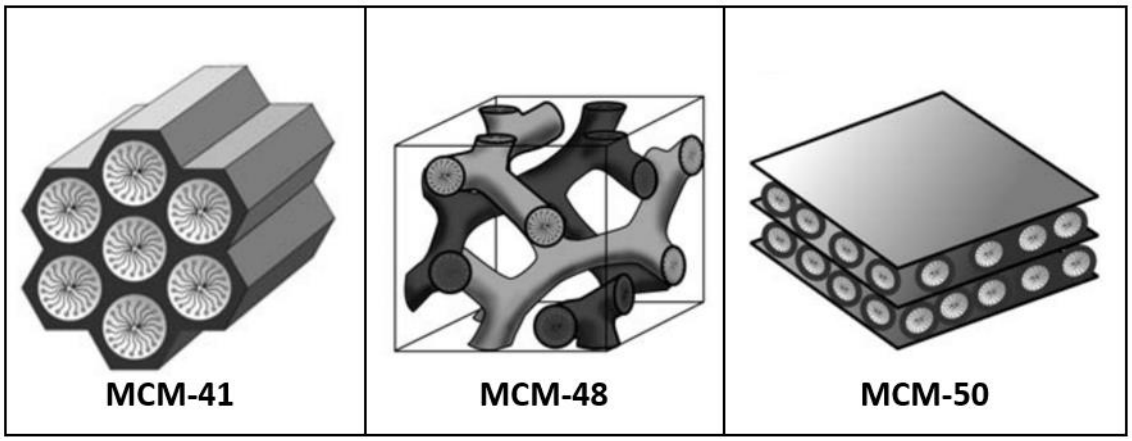

Figura 3. Representação da mesoestrutura dos materiais da família MCM.

Fonte: Adaptado de (HOFFMANN et al., 2006).

O mecanismo de direcionamento via cristal líquido (*Liquid Crystal Templating Mechanism*), consiste na mistura de um tensoativo iônico e uma fonte de silício; o tensoativo (surfactante) atua como um agente direcionador de estrutura, assim, este tem a função de modelar as mesoestruturas, a partir da

organização de suas moléculas, em seguida o reagente como fonte de sílica é atraído pelas moléculas do surfactante e incorporado ao molde, a partir de então, ocorre a condensação e formação da sílica mesoporosa. Após, o surfactante é removido por processo de calcinação, como evidenciado na Figura 4.

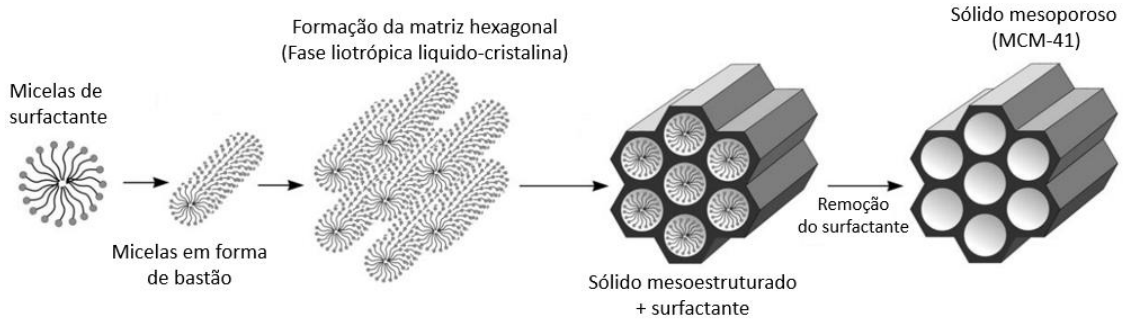

Figura 4. Formação de sílica mesoporosa do tipo MCM-41, por mecanismo de direcionamento via cristal líquido.

Fonte: Adaptado de (HOFFMANN et al., 2006).

A partir de então pesquisadores tem observado que a estrutura dos poros do material podem modificar com a variação de alguns parâmetros, como: o material precursor de sílica, morfologia do surfactante, condições de pH, força iônica, temperatura, entre outros (CECILIA; MORENO TOST; RETUERTO MILLÁN, 2019). Obtendo diferentes tipos de materiais. Dessa forma esta inovação, introduziu uma nova classe de estudos na área de ciências dos materiais através da síntese de *mesoporous sílica nanoparticles* (MSN).

ZHAO et al. (1998), produziram na Universidade da Califórnia, Santa Barbara, sílicas mesoporosas utilizando surfactantes não-iônicos originados de óxido de polipropileno e óxido de polietileno em meios ácidos, produzindo materiais com tamanhos de poros maiores e paredes mais espessas, comparado ao seu antecessor (MCM), proporcionando uma maior rigidez e estabilidade termoquímica. Assim, a sílica mesoporosas produzida pelos autores foi denominada de Santa Barbara Amorphous (SBA), sendo desenvolvida a SBA-15 (estrutura hexagonal) e SBA-16 (estrutura lamelar).

Com metodologia similar ao SBA, porém em meio com pH neutro, pesquisadores da Universidade Estadual do Michigan desenvolveu outro tipo de sílica mesoporosa, nomeada como MSU (*Michigan State University*), as quais

apresentaram grande porosidade e espessura de parede, porém mesoestruturas menos organizadas.

Desde então, as variações dos parâmetros de síntese como as condições experimentais e de seleção de reagentes promove o desenvolvimento de diversas novas composições e estruturas, com grandes áreas superficiais e tamanho de poros ajustáveis, as quais são utilizadas em uma ampla gama de aplicações (CASHIN et al., 2018).

3.3.2.2. MÉTODO DE STÖBER E SEUS EFEITOS

Em 1968, STÖBER; FINK; BOHN (1968), sintetizou as primeiras microesferas de sílica (de tamanhos que variaram de 0,05 a 2µ), utilizando uma mistura de silicato de tetraalquil, álcool (etanol ou metanol), água e amônia, assim, constituindo uma reação do tipo sol-gel em que a amônia possuía a função de catalisador. A metodologia de Stöber foi largamente reconhecida devido a simplicidade da reação, rápido processamento e de excelente controle no desenvolvimento do tamanho das esferas.

De acordo com o modelo de adição de monômero, o desenvolvimento das partículas é realizado em quatro tipos de fases, onde não há o relacionamento das partículas que estão fase de nucleação com as que estão em fase de crescimento. Assim, o modelo descreve que as fases de nucleação e crescimento ocorrem em uma evolução uniforme (GHIMIRE; JARONIEC, 2021), conforme apresentado na Figura 5.

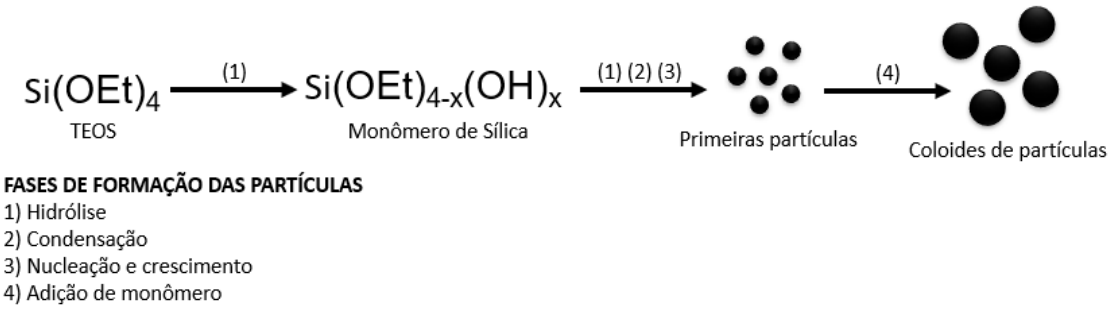

Figura 5. Ilustração do modelo baseado na adição de monômeros para formação das partículas de SM pelo método de Stöber.

Fonte: Adaptado de (GHIMIRE; JARONIEC, 2021).

Embora a sílica mesoporosa do tipo MCM-41, descoberta em 1992, tenha oferecido grandes inovações devido a sua mesoestrutura organizada, seus

grânulos de partículas resultante possuíam diversos tamanhos. A partir disso, em 1997,GRÜN; LAUER; UNGER (1997), introduziu o surfactante brometo de cetiltrimetil amônio (CTAB) no método de Stöber, assim, a modificação do método produziu microesferas de sílicas mesoporosas com estruturas organizadas.

Desde então, pesquisadores realizam modificações nas razões molares dos reagentes utilizado no método de Stöber para produção de sílicas mesoporosas com tamanhos de poros e morfologias personalizadas.

Em um trabalho realizado por WANG et al. (2013), em que houve a variação na proporção de água para produção de SM pelo método de Stöber, resultou na produção de materiais com diferentes morfologias. Os autores identificaram que à medida em que houve o aumento na proporção de água a morfologia das sílicas eram modificadas, variando de esferas para nanobastões.

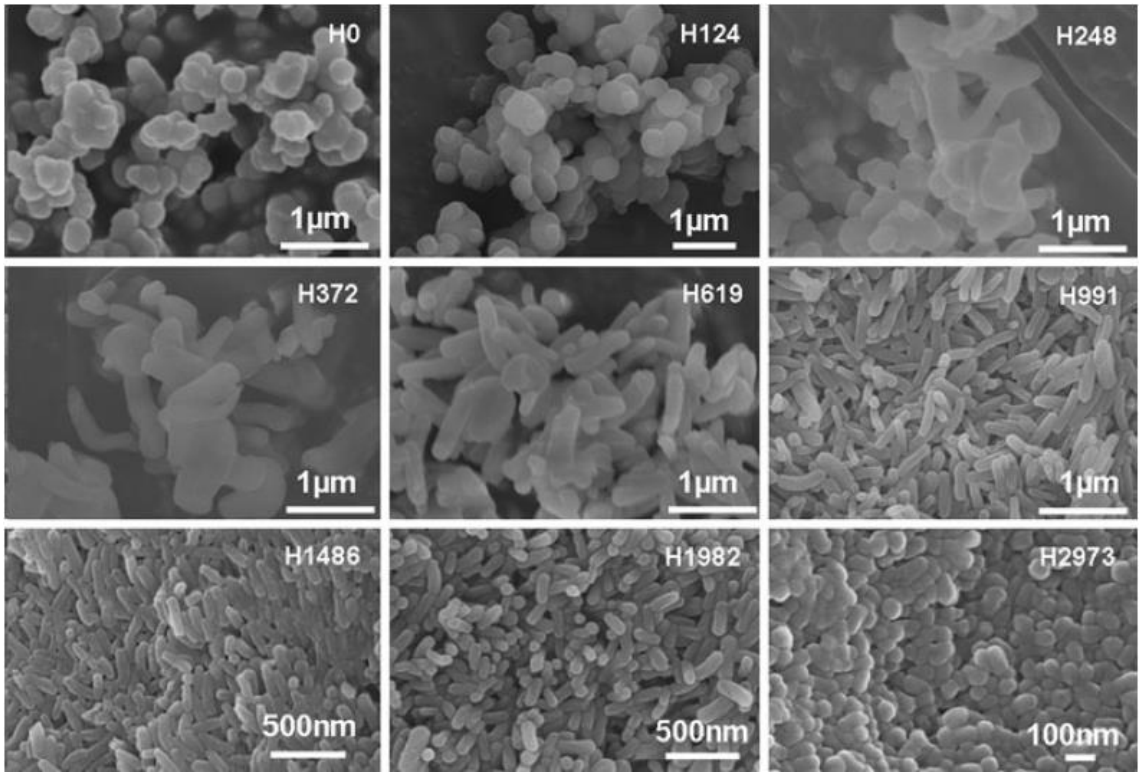

Figura 6. Microeletrônica de varredura de sílicas mesoporosas produzidas em diferentes proporções de água pelo método de Stöber.

Fonte: (WANG et al., 2013)

Já no trabalho desenvolvido por HAN et al. (2017), verificou-se o efeito da variação de concentração da solução do catalisador (amônia) na reação,

obtendo como resultado partículas maiores de SM em alta concentração de NH_3 e partículas menos desenvolvidas em reação com baixa concentração de NH_3, este efeito ocorre, pois o aumento na proporção de catalisador intensifica a fase de polimerização/condensação e aumenta a produção de íons OH^- na solução, assim produz partículas cada vez maiores e aglomerados com cargas superficiais mais negativas. Por outro lado, os autores identificaram que a medida em que as partículas ficam maiores, há uma redução no padrão de homogeneidade de tamanhos das partículas, medida pela polidispersividade. Tal efeito foi similarmente obtido por ZENG et al. (2015), como apresentado na Figura 7.

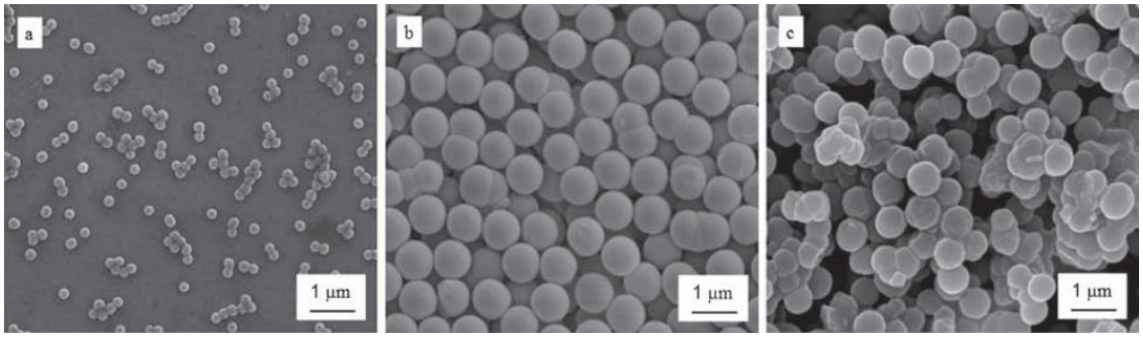

Figura 7. Imagens de MEV das sílicas mesoporosas produzidas em diferentes concentrações de solução de amônia. Sendo a) 0,25 mol/L b) 1,5 mol/L e c) 2 mol/L.

Fonte: (ZENG et al., 2015).

O efeito de produção de partículas maiores também foi observado quando há o aumento na concentração do reagente precursor de sílica (ortossilicato de tetraetila – TEOS), justificado pela grande quantidade de monômeros de ácido ortosilícico hidrolisados produzido que se agregam e formam partículas maiores (WANG et al., 2010).

Alterações nas condições experimentais como, temperatura e pH, também provoca modificações na aglomeração das partículas (GHIMIRE; JARONIEC, 2021). O aumento na temperatura influência na hidrolise da reação aumentando a produção de monômeros de ácido ortosilícico; essa grande quantidade de monômeros diminui o tempo para fase de nucleação e aglomeração, formando partículas menores e mais homogêneas (TAN; BOWEN; EPSTEIN, 1987).

Por fim, o efeito do pH para o desenvolvimento de partículas pelo método de Stöber foi estudado por (MASALOV; SUKHININA; EMEL'CHENKO, 2018), o

qual identificou que somente há formação de partículas homogêneas em meio reacional alcalino. De acordo com ALEXANDER; HESTON; ILER (1954), a solubilidade da sílica amorfa ocorre em soluções de pH superior a 9 à uma temperatura ambiente (20 a 25 ºC). Assim, a síntese de partículas em soluções de pH neutro não ocorre adequadamente, já que os monômeros de sílica até são formados inicialmente, porém são instáveis e formam partículas de tamanhos irregulares. Enquanto que em pH básico as partículas possuem cargas superficiais negativas estáveis que permite o controle da monodispersividade das esferas (GHIMIRE; JARONIEC, 2021).

Desse modo, a partir da definição de parâmetros e concentrações pode-se desenvolver materiais específicos para diferentes tipos de aplicações, como por exemplo na adsorção, conforme discutido no próximo tópico.

3.3.2.3. ADSORVENTE DE SÍLICA MESOPOROSA

As sílicas mesoporosas foram desenvolvidas e são frequentemente aplicadas em processos catalíticos, devido a excelência do material em se adaptar aos diversos tipos de demandas (CECILIA; MORENO TOST; RETUERTO MILLÁN, 2019). Contudo, pesquisas recentes têm demonstrado resultados promissores na aplicação das SM em processos adsortivos para remoção de diversos tipos de contaminantes, tanto em matrizes atmosféricas quanto em soluções aquosas (BUI; CHOI, 2009; DOU et al., 2011; LOU et al., 2020; NATARAJAN et al., 2022).

LOU et al. (2020), desenvolveram uma sílica mesoporosa pelo método de Stöber e funcionalizou sua superfície com amina. Os autores comprovaram a eficiência do material na remoção do poluente, CO_2, atingindo uma capacidade de adsorção de 166 mg g^{-1} em apenas 5 minutos de processo, em 10 min chegou a 180 mg g^{-1} e finalmente o equilíbrio foi atingido com 120 minutos e com uma capacidade de adsorção de 214 mg g^{-1} para uma matriz atmosférica de 100% de CO_2. Além disso, os autores verificaram que o material produzido apresentou uma capacidade de regeneração de 5 ciclos de adsorção/dessorção sem grandes modificações, em que apenas do primeiro para o segundo ciclo, houve uma perda de aproximadamente 18% na capacidade de adsorção e nos

próximos ciclos o material se manteve estável sem prejuízos na sua capacidade de adsorção.

HENAO et al. (2020), também removeram CO_2 em um adsorvente de SM produzida a partir de cascas de arroz como fonte de sílica e funcionalizada com amina, os autores realizaram 3 ciclos de reuso do material com perdas até 10% da capacidade de adsorção.

Já para matriz aquosa, os adsorventes de sílicas mesoporosas também apresentam resultados favoráveis ao reuso. De acordo com um trabalho realizado por HE et al. (2015), utilizando SM do tipo SBA-15 funcionalizada com metal na sua co-condensação, obteve uma capacidade de regeneração de 6 ciclos de adsorção/dessorção de chumbo, ainda, os autores demonstram que após o 6º ciclo de regeneração o adsorvente ainda foi capaz de remover até 93,5% de chumbo em águas residuais ácidas.

Em uma pesquisa realizada por NATARAJAN et al. (2022), o qual desenvolveu uma sílica mesoporosa magnética para adsorção do fármaco acetaminofeno, os autores realizaram até 14 ciclos de reuso do material com perda inferior a 2% a cada ciclo de adsorção/dessorção, obtendo capacidade de adsorção superior a 80% após o 10º ciclo.

Dessa forma, observa-se que a SM apresenta excelente capacidade de regeneração, sendo um importante parâmetro para aplicabilidade do material em grande escala, bem como, aumenta a vida útil do material e consequentemente reduz a geração de resíduos adsorventes. Apesar do reconhecimento do potencial desse material na remoção de contaminantes ambientais, sua aplicação ainda permanece pouco explorada, destacando a necessidade de mais estudos e avanços nessa área.

3.4. ESTUDOS DE ADSORÇÃO

Os estudos de adsorção são desenvolvidos em várias etapas, como por exemplo, o efeito do pH, dosagem do adsorvente, força iônica, cinética, isotermas, termodinâmica e dessorção. Estes estudos objetivam avaliar a aplicabilidade do material adsorvente na remoção de contaminante (TRAN et al., 2017). Para isso, são utilizados dois principais parâmetros: a capacidade de

adsorção e a porcentagem de remoção do contaminante. Os parâmetros são obtidos por meio das Equações 1 e 2.

$$q_e = \frac{(C_0 - C_e) \cdot V}{m} \quad (1)$$

$$\% \text{ remoção} = \frac{(C_0 - C_e) \cdot 100}{C_0} \quad (2)$$

Em que qe é a capacidade de adsorção no equilíbrio (mg g^{-1}), C_0 e C_e são as concentrações inicial e final, respectivamente (mg L^{-1}), V é o volume da solução (L) e m é massa de adsorvente (g).

Dentre os estudos da adsorção, os ensaios cinéticos são essenciais para a determinação do tempo de equilíbrio da reação, como também fornece uma maior compreensão do mecanismo do processo, através de modelos matemáticos (HO, 2006).

3.4.1. CINÉTICA DE ADSORÇÃO

Como descrito anteriormente, a cinética da adsorção descreve, essencialmente a taxa de remoção do contaminante, porém também permite compreender os fatores que a influenciam e fornece um entendimento superficial dos mecanismos do processo (CRINI; BADOT, 2008; HO, 2006; HO; MCKAY, 1998).

O tempo necessário para atingir o equilíbrio da reação é determinado pela resistência a transferência de massa do contaminante em meio aquoso para o interior dos poros do sólido (adsorvente). A transferência de massa ocorre por meio das seguintes etapas (WORCH, 2012) que também representadas na Figura 8:

1ª etapa - Difusão de filme (difusão externa): transporte do contaminante presente na solução para a superfície externa do adsorvente.
2ª etapa - Difusão de poros (difusão intrapartícula): transporte do contaminante da superfície externa do adsorvente para o interior dos poros.
3ª etapa - Reação superficial: fixação do contaminante na superfície interna dos poros do adsorvente.

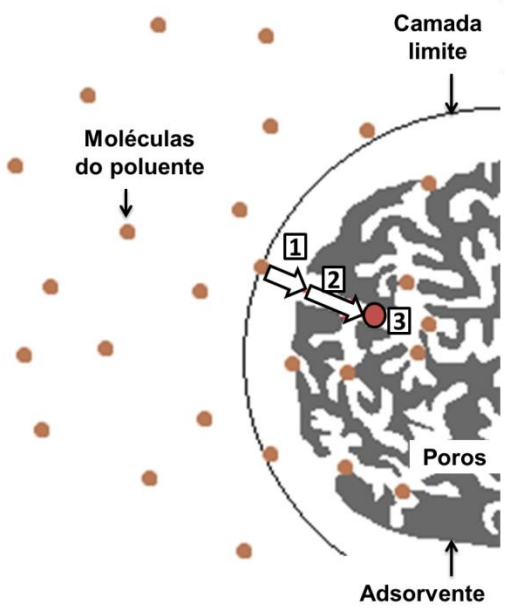

Figura 8. Etapas do processo de transferência de massa na adsorção de contaminante.
Fonte: Autoria própria.

Ainda segundo o autor, a terceira etapa ocorre rapidamente, então a taxa total de adsorção é determinada pela difusão de filme e/ou intrapartícula, sendo esta a etapa mais lenta que caracteriza a adsorção.

Segundo LIU; SHEN (2008), a ordem de uma reação química não está diretamente relacionada com o coeficiente estequiométrico da equação, dessa forma não é possível predizer a lei de velocidade de uma reação sem obtenção de dados experimentais.

Diante disso, os dados cinéticos podem ser analisados por meio de modelos matemáticos, sendo os mais utilizados o pseudo-primeira ordem (PPO) e pseudo-segunda ordem (PSO). Embora, os modelos de Elovich e difusão intrapartícula também têm sido muito aplicados (CRINI; BADOT, 2008; TRAN et al., 2017; VIOTTI et al., 2019).

3.4.1.1. MODELO DE PSEUDO-PRIMEIRA ORDEM

O modelo de pseudo-primeira ordem é também chamado de equação de Lagergren. Ele foi proposto inicialmente para a adsorção de ácido oxálico e malônico em carvão vegetal por Lagergren em 1898. Esse modelo possui o

pressuposto que a velocidade de remoção do adsorbato com o tempo é diretamente proporcional à diferença na concentração de saturação e ao número de sítios ativos de sólido. O modelo é descrito pela Equação 3 (HO; MCKAY, 1998, 1999).

$$q_t = q_e(1 - e^{-K_1 t}) \quad (3)$$

Onde K_1 é constante de velocidade de adsorção (min^{-1}), q_e e q_t são as capacidades de adsorção no equilíbrio e no tempo t, respectivamente ($mg\ g^{-1}$) e t é o tempo de adsorção (min).

3.4.1.2. MODELO DE PSEUDO-SEGUNDA ORDEM

A forma não linear da equação de pseudo-segunda ordem foi inicialmente proposto por BLANCHARD; MAUNAYE; MARTIN (1984) e aplicada por HO; JOHN WASE; FORSTER (1995) e por HO; WASE; FORSTER (1996). Em tal modelo, supõe-se que a capacidade de adsorção é proporcional ao número de sítios ativos ocupados no adsorvente (HO; MCKAY, 1999; TRAN et al., 2017). O modelo de pseudo-segunda ordem é apresentado pela Equação 4.

$$q_t = \frac{k_2 q_e^2 t}{1 + k_2 q_e t} \quad (4)$$

Em que K_2 é a constante de velocidade de adsorção (min^{-1}), q_e e q_t são as capacidades de adsorção no equilíbrio e no tempo t, respectivamente ($mg\ g^{-1}$) e t é o tempo de adsorção (min).

3.4.1.3. MODELO DE ELOVICH

A equação de Elovich foi uma equação empírica primeiramente proposta por ROGINSKY; ZELDOVICH (1934) para a adsorção de monóxido de carbono em dióxido de manganês. A aplicação desse modelo sugere que a quimiossorção é provavelmente o processo controlador da taxa de adsorção (ALLEN; SCAIFE, 1966; CRINI; BADOT, 2008). A Equação 5 demonstra a equação do modelo.

$$q_t = \frac{1}{b} \ln(1 + abt) \quad (5)$$

Em que b é a constante de dessorção (mg/g), q_t é a capacidade de adsorção no tempo t (mg/g), t é o tempo de adsorção (min), 'a' é a constante da taxa inicial ($\frac{dq_t}{dt}$ $\text{quando qt tende a } 0$) (mg/g x min) e b é a constante de dessorção (mg/g).

3.4.1.4. MODELO DE DIFUSÃO INTRAPARTÍCULA

WEBER; MORRIS (1963), propuseram um modelo para o estudo cinético de adsorção, conhecido como modelo de difusão intrapartícula, apresentado pela Equação 6.

$$q_t = K_{dif}\sqrt{t} + C \quad (6)$$

Onde K_{dif} é a constante de velocidade de difusão intrapartícula (mg g^{-1} $min^{-1/2}$), q_t é a capacidade de adsorção no tempo t (mg g^{-1}), t é o tempo de adsorção (min) e C é a constante relacionada com a espessura da camada limite (mg g^{-1}).

3.4.2. EQUILÍBRIO DE ADSORÇÃO

As isotermas são dados experimentais do equilíbrio entre a capacidade de adsorção do adsorvente e a concentração do absorvato em solução à uma temperatura constante. Este dado é de suma importância para melhor compreensão do processo de adsorção (KUMAR, 2007).

Há uma grande variedade de isotermas de equilíbrio para descrever as relações de equilíbrio em um sistema sólido-liquido, sendo os modelos matemáticos mais comuns são: Langmuir, Freundlich, Sips e Temkin. Os parâmetros dessas equações de modelos matemáticos sugerem informações sobre as propriedades da superfície do adsorvente e a afinidade adsorvente/adsorbato que auxiliam na compreensão do mecanismo de adsorção (ANASTOPOULOS; KYZAS, 2016; FOO; HAMEED, 2010).

3.4.2.1. MODELO DE LANGMUIR

O modelo de Langmuir foi apresentado por Irving Langmuir em 1917 para a representação de processos de adsorção de gases em uma superfície sólida, o qual se baseia nas seguintes suposições: existe um número definido de sítios disponíveis no adsorvente e esses têm energias equivalentes e uniformes, a adsorção é irreversível, as moléculas adsorvidas não interagem umas com as outras, a adsorção ocorre em uma monocamada; e cada sítio pode comportar apenas uma molécula adsorvida (ANASTOPOULOS; KYZAS, 2016; FOO; HAMEED, 2010; LIU; LIU, 2008). O modelo de Langmuir é apresentado pela Equação 7 (LANGMUIR, 1918).

$$q_e = \frac{q_{max} K_L C_e}{1 + K_L C_e} \quad (7)$$

Onde q_e e q_{max} são as capacidades de adsorção no equilíbrio e máxima, respectivamente (mg g^{-1}), K_L é a constante de Langmuir de interação adsorbato/adsorvente (L mg^{-1}) e C_e é a concentração do adsorbato no equilíbrio (mg L^{-1}).

3.4.2.2. MODELO DE FREUNDLICH

O modelo proposto por Freundlich em 1907 (FREUNDLICH, 1906), foi um dos primeiros a equacionar a relação entre a quantidade de material adsorvido e sua concentração na solução considerando características empíricas. O modelo é utilizado para superfícies heterogêneas, e, portanto, não traz suposições quanto à capacidade de adsorção de uma monocamada e assume interação entre as moléculas adsorvidas (DIZGE et al., 2008). A equação do modelo de Freundlich está representado na Equação 8.

$$q_e = K_F C_e^{\,1/n_F} \quad (8)$$

Onde q_e é a quantidade adsorvida por grama de adsorvente no equilíbrio (mg g^{-1}), K_F é a constante de Freundlich de interação adsorbato/adsorvente (mg g^{-1})/(mg L^{-1})^n, C_e é a concentração do adsorbato no equilíbrio (mg L^{-1}) e n_F é a constante relacionadas à intensidade de adsorção ou heterogeneidade da superfície.

3.4.2.3. MODELO DE SIPS

Tendo em vista, o problema com o modelo de Freundlich de não apresentar um limite de capacidade máxima de adsorção e assim, não exibir a formação de um platô de equilíbrio, o modelo proposto por Sips (SIPS, 1948) sugere uma equação semelhante à de Freundlich, contudo apresentando um limite finito na capacidade de adsorção em concentrações suficientemente altas (HAMDAOUI; NAFFRECHOUX, 2007; PORTINHO; ZANELLA; FÉRIS, 2017; SIPS, 1948).

Embora o modelo de Langmuir represente de forma mais adequada pontos finais de equilíbrio do sistema, ou seja, propõe um limite finito na capacidade de adsorção, este modelo indica uma superfície do adsorvente homogênea com a formação de uma manocamada. Porém o modelo de Sips, prevê a heterogeneidade da superfície do adsorvente com a formação de platô de equilíbrio (FOO; HAMEED, 2010; PORTINHO; ZANELLA; FÉRIS, 2017).

Assim, modelo proposto por Sips consiste em uma equação mista entre as equações que definem os modelos de Langmuir e Freundlich, sendo representado pela Equação 9.

$$q_{eq} = \frac{Q_{max}(K_S C)^{1/n_S}}{1+(K_S C)^{1/n_S}} \quad (9)$$

Onde q_{eq} é a capacidade de adsorção no equilíbrio (mg g^{-1}), K_s é a constante de Sips de interação adsorbato/adsorvente (mg L^{-1}), C é a concentração do adsorbato (mg L^{-1}) e n_s é a constante relacionadas heterogeneidade da superfície.

3.4.3. TERMODINÂNICA

A termodinâmica é parte das ciências físicas que avalia as variações energéticas relacionada ao movimento da matéria (NASCIMENTO et al., 2014). Por meio do estudo da termodinâmica pode se compreender os mecanismos de adsorção, confirmar a viabilidade, espontaneidade e troca de calor para o processo de adsorção (ZOLGHARNEIN; SHAHMORADI; GHASEMI, 2011).

O estudo termodinâmico pode ser representado por três principais parâmetros: Energia Livre de Gibbs (ΔG°), Entalpia (ΔH°) e Entropia (ΔS°). Tais

parâmetros são afetados por mudanças de temperatura e podem ser calculados utilizando o coeficiente de equilíbrio termodinâmico (K_G) obtido a diferentes temperaturas e concentrações (CRINI; BADOT, 2008). Os parâmetros termodinâmicos podem ser calculados a partir das leis da termodinâmica.

A energia livre de Gibbs é calculada a partir da Equação 10. Este parâmetro relaciona-se com a espontaneidade da reação. Assim, valores negativos indicam que a reação é espontânea e valores positivos indicam que para que a reação prossiga, é necessária entrada de energia (CRINI; BADOT, 2008).

$$\Delta G° = -R\ T\ \ln K_C \quad (10)$$

Onde $\Delta G°$ é a energia livre de Gibbs (KJ mol^{-1}), R é a constante universal dos gases (0,00813 KJ mol^{-1} K^{-1}); T é a temperatura (K) e KC é constante de equilíbrio termodinâmico.

Já os parâmetros de entalpia e entropia são obtidos utilizando a Equação 11 e a partir desta é plotado o gráfico de ln (K_c) Vs. 1/T. Os parâmetros de entalpia e entropia são obtidos, respectivamente, a partir do coeficiente angular e linear do gráfico. Assim, a entalpia indica o calor da reação, em que os valores positivos representam processos de adsorção endotérmicos, ou seja, absorvem calor, e valores negativos representam processos exotérmicos, ou seja, liberam calor. A entropia relaciona-se à aleatoriedade da interação adsorvente/adsorbato; valores positivos são indicativos de aleatoriedade de interação.

$$\ln K_C = \frac{\Delta S}{R} - \frac{\Delta H}{R.T} \quad (11)$$

Onde $\Delta G°$ e $\Delta H°$ são a energia livre de Gibbs e entalpia (KJ mol^{-1}), $\Delta S°$ é a entropia (KJ mol^{-1} K^{-1}), R é a constante dos gases (0,00813 KJ mol^{-1} K^{-1}), T é a temperatura (K) e K_C é constante de equilíbrio termodinâmico.

Nota-se que a estimativa dos parâmetros termodinâmicos é dependente da determinação da constante de equilíbrio (K_C), que é adimensional. Essa constante é obtida através da constante do ajuste aos modelos de isotermas de adsorção, porém com a realização de cálculos adicionais, a fim de transformar a constante do modelo dimensional em adimensional (DOKE; KHAN, 2013; LIU, 2009; TRAN et al., 2017; TRAN; YOU; CHAO, 2016).

4. REFERÊNCIAS BIBLIOGRÁFICAS

ABATAL, M. et al. Comparison of Heavy Metals Removal from Aqueous Solution by Moringa oleifera Leaves and Seeds. **Coatings**, v. 11, n. 5, p. 508, 25 abr. 2021.

ABDOLALI, A. et al. Typical lignocellulosic wastes and by-products for biosorption process in water and wastewater treatment: A critical review. **Bioresource Technology**, v. 160, p. 57–66, maio 2014.

AHMAD, T.; DANISH, M. Prospects of banana waste utilization in wastewater treatment: A review. **Journal of Environmental Management**, v. 206, p. 330–348, jan. 2018.

AHMED, I. et al. Nitrogen-Doped Porous Carbons from Ionic Liquids@MOF: Remarkable Adsorbents for Both Aqueous and Nonaqueous Media. **ACS Applied Materials & Interfaces**, v. 9, n. 11, p. 10276–10285, 22 mar. 2017.

AKHTAR, M. et al. Sorption potential of Moringa oleifera pods for the removal of organic pollutants from aqueous solutions. **Journal of Hazardous Materials**, v. 141, n. 3, p. 546–556, 22 mar. 2007.

AKHTAR, M. S.; ALI, S.; ZAMAN, W. Innovative Adsorbents for Pollutant Removal: Exploring the Latest Research and Applications. **Molecules**, v. 29, n. 18, p. 4317, 11 set. 2024.

ALEXANDER, G. B.; HESTON, W. M.; ILER, R. K. The Solubility of Amorphous Silica in Water. **The Journal of Physical Chemistry**, v. 58, n. 6, p. 453–455, jun. 1954.

ALI, I.; ALOTHMAN, Z. A.; AL-WARTHAN, A. Sorption, kinetics and thermodynamics studies of atrazine herbicide removal from water using iron nano-composite material. **International Journal of Environmental Science and Technology**, v. 13, n. 2, p. 733–742, fev. 2016.

ALI, I.; ASIM, MOHD.; KHAN, T. A. Low cost adsorbents for the removal of organic pollutants from wastewater. **Journal of Environmental Management**, v. 113, p. 170–183, dez. 2012.

ALLEN, J.; SCAIFE, P. The Elovich equation and chemisorption kinetics. **Australian Journal of Chemistry**, v. 19, n. 11, p. 2015, 1966.

AL-SHEHRI, B. M. et al. A review: the utilization of mesoporous materials in wastewater treatment. **Materials Research Express**, v. 6, n. 12, p. 122002, 12 nov. 2019.

ÁLVAREZ-RUIZ, R.; PICÓ, Y. Analysis of emerging and related pollutants in aquatic biota. **Trends in Environmental Analytical Chemistry**, v. 25, p. e00082, mar. 2020.

ANASTOPOULOS, I.; KYZAS, G. Z. Are the thermodynamic parameters correctly estimated in liquid-phase adsorption phenomena? **Journal of Molecular Liquids**, v. 218, p. 174–185, jun. 2016.

ANDRADE, M. B. et al. Evaluation of magnetic nano adsorbent produced from graphene oxide with iron and cobalt nanoparticles for caffeine removal from aqueous medium. **Chemical Engineering and Processing - Process Intensification**, v. 170, p. 108694, jan. 2022.

BABIĆ, S.; DABIĆ, D.; ĆURKOVIĆ, L. **Fate of hydroxychloroquine in the aquatic environment**. 15th International Conference on Environmental Science and Technology. **Anais**... Em: CONFERENCE ON ENVIRONMENTAL SCIENCE AND TECHNOLOGY. Greece: CEST, 2 set. 2017. Disponível em: <https://cest2017.gnest.org/sites/default/files/presentation_file_list/cest2017_00817_poster_paper.pdf>. Acesso em: 7 mar. 2025

BAI, S. H.; OGBOURNE, S. Eco-toxicological effects of the avermectin family with a focus on abamectin and ivermectin. **Chemosphere**, v. 154, p. 204–214, jul. 2016.

BEN ALI, M. et al. Toxicity of hydroxychloroquine, a potential treatment for COVID-19, on free-living marine nematodes. **Marine Pollution Bulletin**, v. 167, p. 112361, jun. 2021.

BHADRA, B. N.; JHUNG, S. H. A remarkable adsorbent for removal of contaminants of emerging concern from water: Porous carbon derived from metal azolate framework-6. **Journal of Hazardous Materials**, v. 340, p. 179–188, out. 2017.

BHADRA, B. N.; SEO, P. W.; JHUNG, S. H. Adsorption of diclofenac sodium from water using oxidized activated carbon. **Chemical Engineering Journal**, v. 301, p. 27–34, out. 2016.

BLANCHARD, G.; MAUNAYE, M.; MARTIN, G. Removal of heavy metals from waters by means of natural zeolites. **Water Research**, v. 18, n. 12, p. 1501–1507, jan. 1984.

BOLONG, N. et al. A review of the effects of emerging contaminants in wastewater and options for their removal. **Desalination**, v. 239, n. 1–3, p. 229–246, abr. 2009.

BRASIL. GM/MS Nº 888. PORTARIA GM/MS Nº 888, DE 4 DE MAIO DE 2021. . 2021.

BRUNO, A. Um setor maduro e em crescimento. **ABRAFARMA**, 2 mar. 2023.

BUI, T. X.; CHOI, H. Adsorptive removal of selected pharmaceuticals by mesoporous silica SBA-15. **Journal of Hazardous Materials**, v. 168, n. 2–3, p. 602–608, set. 2009.

CAPPELLI, F. et al. Suspect screening of wastewaters to trace anti-COVID-19 drugs: Potential adverse effects on aquatic environment. **Science of The Total Environment**, v. 824, p. 153756, jun. 2022.

CASHIN, V. B. et al. Surface functionalization and manipulation of mesoporous silica adsorbents for improved removal of pollutants: a review. **Environmental Science: Water Research & Technology**, v. 4, n. 2, p. 110–128, 2018.

CAUDA, V.; SCHLOSSBAUER, A.; BEIN, T. Bio-degradation study of colloidal mesoporous silica nanoparticles: Effect of surface functionalization with organo-silanes and poly(ethylene glycol). **Microporous and Mesoporous Materials**, v. 132, n. 1–2, p. 60–71, jul. 2010.

CECILIA, J. A.; MORENO TOST, R.; RETUERTO MILLÁN, M. Mesoporous Materials: From Synthesis to Applications. **International Journal of Molecular Sciences**, v. 20, n. 13, p. 3213, 30 jun. 2019.

CHEN, L. et al. Recent developments of mesoporous silica nanoparticles in biomedicine. **Emergent Materials**, v. 3, n. 3, p. 381–405, 1 jun. 2020.

COLDEBELLA, P. F. et al. Potential effect of chemical and thermal treatment on the Kinetics, equilibrium, and thermodynamic studies for atrazine biosorption by the *Moringa oleifera* pods. **The Canadian Journal of Chemical Engineering**, v. 95, n. 5, p. 961–973, maio 2017.

CONAMA. CONAMA N° 357/2005. RESOLUÇÃO CONAMA N° 357, DE 17 DE MARÇO DE 2005. . 2005.

CRINI, G.; BADOT, P.-M. Application of chitosan, a natural aminopolysaccharide, for dye removal from aqueous solutions by adsorption processes using batch studies: A review of recent literature. **Progress in Polymer Science**, v. 33, n. 4, p. 399–447, abr. 2008.

CRUMP, A.; OMURA, S. Ivermectin, “Wonder drug” from Japan: the human use perspective. **Proceedings of the Japan Academy, Series B**, v. 87, n. 2, p. 13–28, 2011.

CUSIOLI, L. F. et al. Modified *Moringa oleifera* Lam. Seed husks as low-cost biosorbent for atrazine removal. **Environmental Technology**, v. 42, n. 7, p. 1092–1103, 21 mar. 2021.

CUSIOLI, L. F. et al. Use of low-cost adsorbent functionalized with iron oxide nanoparticles for ivermectin removal. **South African Journal of Chemical Engineering**, v. 47, p. 142–149, 2024.

DAUGHTON, C. G. Cradle-to-cradle stewardship of drugs for minimizing their environmental disposition while promoting human health. I. Rationale for and avenues toward a green pharmacy. **Environmental Health Perspectives**, v. 111, n. 5, p. 757–774, maio 2003.

DAUGHTON, C. G.; TERNES, T. A. Pharmaceuticals and Personal Care Products in the Environment: Agents of Subtle Change? **Environmental Health Perspectives**, v. 107, 1999.

DE SOUZA, R. M. et al. Occurrence, impacts and general aspects of pesticides in surface water: A review. **Process Safety and Environmental Protection**, v. 135, p. 22–37, mar. 2020.

DIZGE, N. et al. Adsorption of reactive dyes from aqueous solutions by fly ash: Kinetic and equilibrium studies. **Journal of Hazardous Materials**, v. 150, n. 3, p. 737–746, fev. 2008.

DOKE, K. M.; KHAN, E. M. Adsorption thermodynamics to clean up wastewater; critical review. **Reviews in Environmental Science and Bio/Technology**, v. 12, n. 1, p. 25–44, mar. 2013.

DOMINGO-ECHABURU, S. et al. Drugs used during the COVID-19 first wave in Vitoria-Gasteiz (Spain) and their presence in the environment. **Science of The Total Environment**, v. 820, p. 153122, maio 2022.

DOU, B. et al. Adsorption performance of VOCs in ordered mesoporous silicas with different pore structures and surface chemistry. **Journal of Hazardous Materials**, v. 186, n. 2–3, p. 1615–1624, fev. 2011.

ELBALKINY, H. T. et al. Potentiometric diclofenac detection in wastewater using functionalized nanoparticles. **Microchemical Journal**, v. 145, p. 90–95, mar. 2019.

ELLIS, R. P. et al. Immunological function in marine invertebrates: Responses to environmental perturbation. **Fish & Shellfish Immunology**, v. 30, n. 6, p. 1209–1222, jun. 2011.

FENT, K.; WESTON, A.; CAMINADA, D. Ecotoxicology of human pharmaceuticals. **Aquatic Toxicology**, v. 76, n. 2, p. 122–159, 10 fev. 2006.

FERNÁNDEZ-REYES, B. et al. Engineered adsorbents for the removal of contaminants of emerging concern from water. Em: **Contaminants of Emerging Concern in Water and Wastewater**. [s.l.] Elsevier, 2020. p. 3–45.

FERREIRA, M. T.; CARVALHO, C. D. S. Chloroquine and hydroxychloroquine in the environment and aquatic organisms: a review. **Ambiente e Agua - An Interdisciplinary Journal of Applied Science**, v. 18, p. 1–24, 17 mar. 2023.

FOO, K. Y.; HAMEED, B. H. Insights into the modeling of adsorption isotherm systems. **Chemical Engineering Journal**, v. 156, n. 1, p. 2–10, 1 jan. 2010.

FOOD AND DRUG ADMINISTRATION. **EUA Chloroquine Phosphate Health Care Provider Fact Sheet**. FDA, , 27 abr. 2020. Disponível em: <https://www.fda.gov/media/136535/download>. Acesso em: 6 nov. 2023

FREUNDLICH, H. M. F. Over the adsorption in solution. **The Journal of Physical Chemistry**, v. 57, n. 385471, p. 1100–1107, 1906.

GALANI, A. et al. Patterns of pharmaceuticals use during the first wave of COVID-19 pandemic in Athens, Greece as revealed by wastewater-based epidemiology. **Science of The Total Environment**, v. 798, p. 149014, dez. 2021.

GARCIA-IVARS, J. et al. Nanofiltration as tertiary treatment method for removing trace pharmaceutically active compounds in wastewater from wastewater treatment plants. **Water Research**, v. 125, p. 360–373, nov. 2017.

GHASEMYANI, S. et al. Global, WHO Regional, and Continental Prevalence of Self-medication from 2000 to 2018: A Systematic Review and Meta-analysis. **Annals of Public Health**, v. 1, 2022.

GHAZY, R. M. et al. A systematic review and meta-analysis on chloroquine and hydroxychloroquine as monotherapy or combined with azithromycin in COVID-19 treatment. **Scientific Reports**, v. 10, n. 1, p. 22139, 17 dez. 2020.

GHIMIRE, P. P.; JARONIEC, M. Renaissance of Stöber method for synthesis of colloidal particles: New developments and opportunities. **Journal of Colloid and Interface Science**, v. 584, p. 838–865, fev. 2021.

GOMES, H. D. O. et al. Removal of contaminants from water using Moringa oleifera Lam. as biosorbent: An overview of the last decade. **Journal of Water Process Engineering**, v. 46, p. 102576, abr. 2022.

GOMES, V. P.; SILVA, M. T.; GALVÃO, T. F. Prevalência do consumo de medicamentos em adultos brasileiros: uma revisão sistemática. **Ciência & Saúde Coletiva**, v. 22, n. 8, p. 2615–2626, ago. 2017.

GRELA, A.; KUC, J.; BAJDA, T. A Review on the Application of Zeolites and Mesoporous Silica Materials in the Removal of Non-Steroidal Anti-Inflammatory Drugs and Antibiotics from Water. **Materials**, v. 14, n. 17, p. 4994, 1 set. 2021.

GRÜN, M.; LAUER, I.; UNGER, K. K. The synthesis of micrometer- and submicrometer-size spheres of ordered mesoporous oxide MCM-41. **Advanced Materials**, v. 9, n. 3, p. 254–257, mar. 1997.

GUPTA, P.; RANI, V. A Comprehensive Assessment of Environmental Implications, Ecotoxicity and Bioaccumulation Potential of Repurposed Drug Hydroxychloroquine: From Challenges to Sustainability. **Reviews of Environmental Contamination and Toxicology**, v. 262, n. 10, 10 maio 2024.

HAMDAOUI, O.; NAFFRECHOUX, E. Modeling of adsorption isotherms of phenol and chlorophenols onto granular activated carbonPart II. Models with more than two parameters. **Journal of Hazardous Materials**, v. 147, n. 1–2, p. 401–411, 17 ago. 2007.

HAN, Y. et al. Unraveling the Growth Mechanism of Silica Particles in the Stöber Method: In Situ Seeded Growth Model. **Langmuir**, v. 33, n. 23, p. 5879–5890, 13 jun. 2017.

HE, R. et al. Efficient removal of lead from highly acidic wastewater by periodic ion imprinted mesoporous SBA-15 organosilica combining metal coordination

and co-condensation. **Journal of Materials Chemistry A**, v. 3, n. 18, p. 9789–9798, 2015.

HEIDARY, F.; GHAREBAGHI, R. Ivermectin: a systematic review from antiviral effects to COVID-19 complementary regimen. **The Journal of Antibiotics**, v. 73, n. 9, p. 593–602, set. 2020.

HENAO, W. et al. Insights into the CO2 capture over amine-functionalized mesoporous silica adsorbents derived from rice husk ash. **Journal of Environmental Chemical Engineering**, v. 8, n. 5, p. 104362, out. 2020.

HIEW, B. Y. Z. et al. Adsorptive removal of diclofenac by graphene oxide: Optimization, equilibrium, kinetic and thermodynamic studies. **Journal of the Taiwan Institute of Chemical Engineers**, v. 98, p. 150–162, maio 2019.

HO, Y. Review of second-order models for adsorption systems. **Journal of Hazardous Materials**, v. 136, n. 3, p. 681–689, 25 ago. 2006.

HO, Y. S.; JOHN WASE, D. A.; FORSTER, C. F. Batch nickel removal from aqueous solution by sphagnum moss peat. **Water Research**, v. 29, n. 5, p. 1327–1332, maio 1995.

HO, Y. S.; MCKAY, G. A Comparison of Chemisorption Kinetic Models Applied to Pollutant Removal on Various Sorbents. **Process Safety and Environmental Protection**, v. 76, n. 4, p. 332–340, nov. 1998.

HO, Y. S.; MCKAY, G. Pseudo-second order model for sorption processes. **Process Biochemistry**, v. 34, n. 5, p. 451–465, jul. 1999.

HO, Y. S.; WASE, D. A. J.; FORSTER, C. F. Kinetic Studies of Competitive Heavy Metal Adsorption by Sphagnum Moss Peat. **Environmental Technology**, v. 17, n. 1, p. 71–77, jan. 1996.

HOFFMANN, F. et al. Silica-Based Mesoporous Organic–Inorganic Hybrid Materials. **Angewandte Chemie International Edition**, v. 45, n. 20, p. 3216–3251, 12 maio 2006.

HU, L.-X. et al. What is in Nigerian waters? Target and non-target screening analysis for organic chemicals. **Chemosphere**, v. 284, p. 131546, dez. 2021.

JAMELEDDINE, M. et al. PIN3 Chloroquine and Hydroxychloroquine in COVID-19 with or without Azithromycin: A Systematic Review of in Vitro and Clinical Studies. **Value in Health**, v. 23, p. S545, dez. 2020.

KANSAL, S. K.; KUMARI, A. Potential of *M. oleifera* for the Treatment of Water and Wastewater. **Chemical Reviews**, v. 114, n. 9, p. 4993–5010, 14 maio 2014.

KHALFAOUI, A. et al. Uptake of Methyl Red dye from aqueous solution using activated carbons prepared from Moringa Oleifera shells. **Cleaner Chemical Engineering**, v. 4, p. 100069, dez. 2022.

KHAWAJA, H. et al. Synthesis and Application of Covalently Grafted Magnetic Graphene Oxide Carboxymethyl Cellulose Nanocomposite for the Removal of Atrazine From an Aqueous Phase. **Journal of Macromolecular Science, Part B**, v. 60, n. 12, p. 1025–1044, 2 dez. 2021.

KUMAR, K. V. Optimum sorption isotherm by linear and non-linear methods for malachite green onto lemon peel. **Dyes and Pigments**, v. 74, n. 3, p. 595–597, jan. 2007.

KUMARI, M.; KUMAR, A. Can pharmaceutical drugs used to treat Covid-19 infection leads to human health risk? A hypothetical study to identify potential risk. **Science of The Total Environment**, v. 778, p. 146303, jul. 2021.

KURODA, K. et al. Predicted occurrence, ecotoxicological risk and environmentally acquired resistance of antiviral drugs associated with COVID-19 in environmental waters. **Science of The Total Environment**, v. 776, p. 145740, jul. 2021.

KWON, D. H. et al. A point mutation in a glutamate-gated chloride channel confers abamectin resistance in the two-spotted spider mite, *Tetranychus urticae* Koch. **Insect Molecular Biology**, v. 19, n. 4, p. 583–591, ago. 2010.

LANGMUIR, I. THE ADSORPTION OF GASES ON PLANE SURFACES OF GLASS, MICA AND PLATINUM. **Journal of the American Chemical Society**, v. 40, n. 9, p. 1361–1403, set. 1918.

LASOTA, J. A.; DYBAS, R. A. Avermectins, A Novel Class of Compounds: Implications for Use in Arthropod Pest Control. **Annual Review of Entomology**, v. 36, p. 91–117, jan. 1991.

LI, Y. et al. Utilizing low-cost natural waste for the removal of pharmaceuticals from water: Mechanisms, isotherms and kinetics at low concentrations. **Journal of Cleaner Production**, v. 227, p. 88–97, ago. 2019.

LIU, J. et al. Adsorption of Congo red dye on FexCo3-xO4 nanoparticles. **Journal of Environmental Management**, v. 238, p. 473–483, maio 2019.

LIU, Y. Is the Free Energy Change of Adsorption Correctly Calculated? **Journal of Chemical & Engineering Data**, v. 54, n. 7, p. 1981–1985, 9 jul. 2009.

LIU, Y.; LIU, Y.-J. Biosorption isotherms, kinetics and thermodynamics. **Separation and Purification Technology**, v. 61, n. 3, p. 229–242, 15 jul. 2008.

LIU, Y.; SHEN, L. A general rate law equation for biosorption. **Biochemical Engineering Journal**, v. 38, n. 3, p. 390–394, mar. 2008.

LOU, F. et al. Enhanced kinetics for CO2 sorption in amine-functionalized mesoporous silica nanosphere with inverted cone-shaped pore structure. **Applied Energy**, v. 264, p. 114637, abr. 2020.

LUO, Y. et al. A review on the occurrence of micropollutants in the aquatic environment and their fate and removal during wastewater treatment. **Science of The Total Environment**, v. 473–474, p. 619–641, mar. 2014.

MAGALHÃES-GHIOTTO, G. A. V. et al. Composite hydrogel based on chemically modified gelatin and PVA containing graphene oxide nanoparticles (CHGP-GOn). **Environmental Nanotechnology, Monitoring & Management**, v. 20, p. 100877, dez. 2023.

MAMAEVA, V.; SAHLGREN, C.; LINDÉN, M. Mesoporous silica nanoparticles in medicine—Recent advances. **Advanced Drug Delivery Reviews**, v. 65, n. 5, p. 689–702, maio 2013.

MARQUES, S. C. R. et al. Pharmaceuticals removal by activated carbons: Role of morphology on cyclic thermal regeneration. **Chemical Engineering Journal**, v. 321, p. 233–244, ago. 2017.

MARTIN, R. J.; ROBERTSON, A. P.; CHOUDHARY, S. Ivermectin: An Anthelmintic, an Insecticide, and Much More. **Trends in Parasitology**, v. 37, n. 1, p. 48–64, jan. 2021.

MASALOV, V. M.; SUKHININA, N. S.; EMEL'CHENKO, G. A. Synthesis of Monodisperse Silica Nanoparticles via Heterogeneous Tetraethoxysilane Hydrolysis Using L-Arginine as a Catalyst. **Inorganic Materials**, v. 54, n. 2, p. 156–162, fev. 2018.

MO, J. et al. A review on agro-industrial waste (AIW) derived adsorbents for water and wastewater treatment. **Journal of Environmental Management**, v. 227, p. 395–405, dez. 2018.

MÓDENES, A. N. et al. Potential of *Salvinia auriculata* biomass as biosorbent of the Cr(III): directed chemical treatment, modeling and sorption mechanism study. **Environmental Technology**, v. 38, n. 12, p. 1474–1488, 18 jun. 2017.

MURRAY, S. M. et al. Reduction of Immune Activation with Chloroquine Therapy during Chronic HIV Infection. **Journal of Virology**, v. 84, n. 22, p. 12082–12086, 15 nov. 2010.

NARAYAN, R. et al. Mesoporous Silica Nanoparticles: A Comprehensive Review on Synthesis and Recent Advances. **Pharmaceutics**, v. 10, n. 3, p. 118, 6 ago. 2018.

NASCIMENTO, R. F. et al. **Adsorção: aspectos teóricos e aplicações ambientais**. Fortaleza: Imprensa Universitária, 2014.

NASON, S. L. et al. Changes in Sewage Sludge Chemical Signatures During a COVID-19 Community Lockdown, Part 1: Traffic, Drugs, Mental Health, and Disinfectants. **Environmental Toxicology and Chemistry**, v. 41, n. 5, p. 1179–1192, maio 2022.

NATARAJAN, R. et al. Adsorption performance of magnetic mesoporous silica microsphere support toward the remediation of acetaminophen from aqueous solution. **Journal of Water Process Engineering**, v. 48, p. 102835, ago. 2022.

OLATUNDE, J. O. et al. Determination of pharmaceutical compounds in surface and underground water by solid phase extraction-liquid chromatography. **Journal of Environmental Chemistry and Ecotoxicology**, v. 6, n. 3, p. 20–26, 30 jun. 2014.

OLU-OWOLABI, B. I. et al. Utilizing eco-friendly kaolinite-biochar composite adsorbent for removal of ivermectin in aqueous media. **Journal of Environmental Management**, v. 279, p. 111619, fev. 2021.

PETROVIC, M. Analysis and removal of emerging contaminants in wastewater and drinking water. **TrAC Trends in Analytical Chemistry**, v. 22, n. 10, p. 685–696, nov. 2003.

POPP, M. et al. Ivermectin for preventing and treating COVID-19. **Cochrane Database of Systematic Reviews**, v. 2021, n. 10, 28 jul. 2021.

PORTINHO, R.; ZANELLA, O.; FÉRIS, L. A. Grape stalk application for caffeine removal through adsorption. **Journal of Environmental Management**, v. 202, p. 178–187, nov. 2017.

PRAVEENA, S. M. et al. Pharmaceuticals residues in selected tropical surface water bodies from Selangor (Malaysia): Occurrence and potential risk assessments. **Science of The Total Environment**, v. 642, p. 230–240, nov. 2018.

PUBCHEM. **Chloroquine**. **Pub Chem National Center for Biotechnology Information**, 2025. Disponível em: <https://pubchem.ncbi.nlm.nih.gov/>. Acesso em: 7 mar. 2025

QUESADA, H. B. et al. Surface water pollution by pharmaceuticals and an alternative of removal by low-cost adsorbents: A review. **Chemosphere**, v. 222, p. 766–780, maio 2019a.

QUESADA, H. B. et al. Acetaminophen adsorption using a low-cost adsorbent prepared from modified residues of *Moringa oleifera* Lam. seed husks. **Journal of Chemical Technology & Biotechnology**, v. 94, n. 10, p. 3147–3157, out. 2019b.

QUESADA, H. B. et al. Evaluation of novel activated carbons from chichá-do-cerrado (Sterculia striata St. Hil. et Naud) fruit shells on metformin adsorption and treatment of a synthetic mixture. **Journal of Environmental Chemical Engineering**, v. 9, n. 1, p. 104914, fev. 2021.

RAMESH, M. et al. Evaluation of acute and sublethal effects of chloroquine (C18H26CIN3) on certain enzymological and histopathological biomarker responses of a freshwater fish Cyprinus carpio. **Toxicology Reports**, v. 5, p. 18–27, 2018.

RIVERA-UTRILLA, J. et al. Pharmaceuticals as emerging contaminants and their removal from water. A review. **Chemosphere**, v. 93, n. 7, p. 1268–1287, out. 2013.

ROGINSKY, S. Z.; ZELDOVICH, J. **Acta physicochim**. [s.l.] USSR, 1934. v. 1

ROSENBERG, E. S. et al. Association of Treatment With Hydroxychloroquine or Azithromycin With In-Hospital Mortality in Patients With COVID-19 in New York State. **JAMA**, v. 323, n. 24, p. 2493, 23 jun. 2020.

SAHU, D. et al. Applications of different adsorbent materials for the removal of organic and inorganic contaminants from water and wastewater – A review. **Desalination and Water Treatment**, v. 317, p. 100253, jan. 2024.

SANDERS, J. M. et al. Pharmacologic Treatments for Coronavirus Disease 2019 (COVID-19): A Review. **JAMA**, 13 abr. 2020.

SAVARINO, A. et al. Effects of chloroquine on viral infections: an old drug against today's diseases. **The Lancet Infectious Diseases**, v. 3, n. 11, p. 722–727, nov. 2003.

SHUKLA, A. et al. Azithromycin and Hydroxychloroquine combination: The future pharmacotherapy of COVID-19. **Journal of Biomedical Sciences**, v. 7, n. 2, p. 54–57, 31 dez. 2020.

SILVESTRE, F. Signaling pathways of oxidative stress in aquatic organisms exposed to xenobiotics. **Journal of Experimental Zoology Part A: Ecological and Integrative Physiology**, v. 333, n. 6, p. 436–448, jul. 2020.

SINDUSFARMA. Indústria farmacêutica projeta crescimento de 12% este ano e 9% no próximo. **Sindicato da Indústria de Produtos Farmacêuticos**, 12 jun. 2024.

SING, K. S. W. et al. Reporting physisorption data for gas/solid systems with special reference to the determination of surface area and porosity. **Pure and Applied Chemistry**, v. 57, n. 4, p. 603–619, 1985.

SIPS, R. On the Structure of a Catalyst Surface. **The Journal of Chemical Physics**, v. 16, n. 5, p. 490–495, maio 1948.

STÖBER, W.; FINK, A.; BOHN, E. Controlled growth of monodisperse silica spheres in the micron size range. **Journal of Colloid and Interface Science**, v. 26, n. 1, p. 62–69, jan. 1968.

TAN, C. G.; BOWEN, B. D.; EPSTEIN, N. Production of monodisperse colloidal silica spheres: Effect of temperature. **Journal of Colloid and Interface Science**, v. 118, n. 1, p. 290–293, jul. 1987.

TOURET, F.; DE LAMBALLERIE, X. Of chloroquine and COVID-19. **Antiviral Research**, v. 177, p. 104762, maio 2020.

TRAN, H. N. et al. Mistakes and inconsistencies regarding adsorption of contaminants from aqueous solutions: A critical review. **Water Research**, v. 120, p. 88–116, set. 2017.

TRAN, H. N.; YOU, S.-J.; CHAO, H.-P. Thermodynamic parameters of cadmium adsorption onto orange peel calculated from various methods: A comparison study. **Journal of Environmental Chemical Engineering**, v. 4, n. 3, p. 2671–2682, set. 2016.

TRIPATHY, J. et al. Advances in Nanoparticles and Nanocomposites for Water and Wastewater Treatment: A Review. **Water**, v. 16, n. 11, p. 1481, 23 maio 2024.

UCHÔA, A. F. J. UNIVERSIDADE FEDERAL DO CEARÁ CENTRO DE CIÊNCIAS DEPARTAMENTO DE QUÍMICA ORGÂNICA E INORGÂNICA PROGRAMA DE PÓS-GRADUAÇÃO EM QUÍMICA. p. 94, 2011.

UEDA YAMAGUCHI, N. et al. A review of Moringa oleifera seeds in water treatment: Trends and future challenges. **Process Safety and Environmental Protection**, v. 147, p. 405–420, mar. 2021.

VERAS, T. B. et al. Analysis of the presence of anti-inflammatories drugs in surface water: A case study in Beberibe river - PE, Brazil. **Chemosphere**, v. 222, p. 961–969, maio 2019.

VINCENT, M. J. et al. Chloroquine is a potent inhibitor of SARS coronavirus infection and spread. **Virology Journal**, v. 2, n. 1, p. 69, dez. 2005.

VIOTTI, P. V. et al. Diclofenac removal from water by adsorption on Moringa oleifera pods and activated carbon: Mechanism, kinetic and equilibrium study. **Journal of Cleaner Production**, v. 219, p. 809–817, maio 2019.

WANG, H. et al. A simple room-temperature synthesis of mesoporous silica rods with tunable size and porosity. **Journal of Nanoparticle Research**, v. 15, n. 3, p. 1501, mar. 2013.

WANG, X.-D. et al. Preparation of spherical silica particles by St?ber process with high concentration of tetra-ethyl-orthosilicate. **Journal of Colloid and Interface Science**, v. 341, n. 1, p. 23–29, jan. 2010.

WEBER, W. J.; MORRIS, J. C. Kinetics of Adsorption on Carbon from Solution. **Journal of the Sanitary Engineering Division**, v. 89, n. 2, p. 31–59, 1 abr. 1963.

WORCH, E. **Adsorption technology in water treatment: fundamentals, processes, and modeling**. Berlin ; Boston: De Gruyter, 2012.

ZENG, D. et al. Effect of Ammonia Concentration on Silica Spheres Morphology and Solution Hydroxyl Concentration in Stober Process. **Journal of Nanoscience and Nanotechnology**, v. 15, n. 9, p. 7407–7411, 1 set. 2015.

ZHANG, D. et al. Removal of pharmaceuticals and personal care products in aquatic plant-based systems: A review. **Environmental Pollution**, v. 184, p. 620–639, jan. 2014.

ZHAO, D. et al. Triblock Copolymer Syntheses of Mesoporous Silica with Periodic 50 to 300 Angstrom Pores. **Science**, v. 279, n. 5350, p. 548–552, 23 jan. 1998.

ZHU, B.; FAN, T.; ZHANG, D. Adsorption of copper ions from aqueous solution by citric acid modified soybean straw. **Journal of Hazardous Materials**, v. 153, n. 1–2, p. 300–308, maio 2008.

ZOLGHARNEIN, J.; SHAHMORADI, A.; GHASEMI, J. Pesticides Removal Using Conventional and Low-Cost Adsorbents: A Review. **CLEAN – Soil, Air, Water**, v. 39, n. 12, p. 1105–1119, dez. 2011.

CAPÍTULO 2

ARTIGO 1: USE OF LOW-COST ADSORBENT FUNCTIONALIZED WITH IRON OXIDE NANOPARTICLES FOR IVERMECTIN REMOVAL

De acordo com as normas do Programa de Pós-graduação em Engenharia Química (Resolução nº 142/2023/CTC, Art. 63º), o primeiro artigo foi elaborado e formatado conforme as normas para publicação científica do periódico: *South African Journal of Chemical Engineering.*

A revista *South African Journal of Chemical Engineering* apresenta uma classificação A1, segundo a plataforma Sucupira-CAPES, possuí o de CiteScore 8.4.

DOI: 10.1016/j.sajce.2023.11.005

Use of low-cost adsorbent functionalized with iron oxide nanoparticles for ivermectin removal

Luís Fernando Cusioli[1*], Renata Mariane de Souza [2], Laiza Bergamasco Beltran[3], Rosângela Bergamasco[4].

[1] State University of Maringa, Department of Chemical Engineering, Maringa 87020-900, Parana, Brazil. Tel: 55-44-3011-4782, e-mail: luiscusioli@gmail.com.

[2] State University of Maringa, Department of Chemical Engineering, Maringa 87020-900, Parana, Brazil. Tel: 55-44-3011-4782, e-mail: renatamarianee@gmail.com

[3] State University of Maringa, Department of Food Engineering, Maringa 87020-900, Parana, Brazil. Tel: 55-44-3011-4531, e-mail: laizabeltran@hotmail.com

[4] State University of Maringa, Department of Chemical Engineering, Maringa 87020-900, Parana, Brazil. Tel: 55-44-3011-4782, e-mail: rbergamasco@uem.br.

*Corresponding author:
Luís Fernando Cusioli
State University of Maringa, Department of Chemical Engineering, Maringa 87020-900, Parana, Brazil. Tel: 55-44-3011-4782, e-mail: luiscusioli@gmail.com

ABSTRACT

Ivermectin is a commonly used anti-parasitic drug that has been linked to environmental problems. It has been known to cause neurological and reproductive effects on birds, fish, and other wildlife exposed to it. The overuse of ivermectin can lead to a loss of biodiversity, adding to the global environmental crisis. Thus, the present study aimed to evaluate and investigate the adsorption of ivermectin, using *Moringa oleifera Lam.* seed husks functionalized with iron oxide nanoparticles. In view of the kinetic study, the equilibrium occurred in 400 min with an adsorptive capacity of 89.41 mg g^{-1}, the experimental data fit better with the pseudo-first order model and the Langmuir model, obtaining a maximum capacity value of 143.76 mg g^{-1}. Given the values of the thermodynamic parameters, it was determined that the process occurred spontaneously, exothermic and reversible. The material was reused in five cycles, indicating that the material has great potential for removing emerging contaminants.

Keywords: Ivermectin, Emerging contaminants, Emerging contaminants, Agroindustrial residue, Iron oxide nanoparticles.

5. INTRODUÇÃO

Emerging compounds found in the environment, including pharmaceuticals, pose a serious threat to aquatic species and other wildlife. They are detected in the water, air, soil, and even inside living organisms. Emerging contaminants, especially pharmaceuticals, can be difficult to detect because of their low concentrations requiring sensitive analytical techniques (BUNTING et al., 2021). It is important to identify emerging compounds to develop an accurate understanding of their source, fate, and transport, as well as their potential ecological and human health risks (LOFRANO et al., 2012). The use, production, and disposal of pharmaceuticals can lead to contamination of surface and ground waters, contributing to the contamination of aquatic ecosystems. Research has indicated that pharmaceutical contamination can adversely affect reproduction, development, and behavior of aquatic species (HUCKELE; TRACK, 2013; LOFRANO et al., 2012). To reduce ecological risks associated with pharmaceuticals, proper regulatory measures need to be implemented and monitored. Education on the importance of proper disposal and use of pharmaceuticals is also essential. By increasing our knowledge of emerging contaminants, like pharmaceuticals, we can work to protect and preserve the environment (MATTHEWS; WILBY; MURPHY, 2019).

Ivermectin is a drug used to treat a variety of diseases and infections. It has a variety of uses, including insecticide, anti-parasitic and anti-cancer therapy (MARTIN; ROBERTSON; CHOUDHARY, 2021). However, due to its broad use, ivermectin has been known to contaminate the environment as a result of its production, manufacturing, and application processes (KINOBE; OWENS, 2021). This contamination can lead to potential health risks for humans, animals, and the surrounding ecosystem. If released in large quantities, ivermectin has the potential to disrupt the ecosystem's food chain, leading to significantly decreased fertility or extinction in some species (OLU-OWOLABI et al., 2021). Additionally, ivermectin has been known to leach into groundwater and other areas, further threatening the environment. Various methods have been proposed in order to reduce environmental ivermectin contamination, such as smothering it in soil or placing it in bio-degradable bags (CORREA et al., 2022). Ultimately, it is

important to reduce our collective ivermectin input and help to protect the environment and its inhabitants (DIAGBOYA et al., 2022).

Conventional water treatments are largely inefficient in terms of energy and cost. Treating contaminated water using conventional methods often requires a complex step of processes and infrastructure which affects the cost of the treatment itself (RAMO et al., 2017). Moreover, such methods tend to be energy-intensive, which further increases the cost of the process and contributes to negative environmental impacts (CUSIOLI et al., 2021; QUESADA et al., 2019b). Another major issue is the high sludge generation resulting from conventional water treatments, which can pose additional cost, transportation, disposal and treatment costs. Finally, conventional treatments are usually unable to effectively remove emerging contaminants like pharmaceuticals and synthetic hormones, which remain present in water supplies. Therefore, conventional water treatments are not optimal in terms of efficiency and they do not provide the full extent of water safety and security that is desired (MARSON et al., 2022).

Moringa oleifera Lam. is a native tree from South Asia, often referred to as the "Miracle Tree" because of its many uses in health and nutrition (NDABIGENGESERE; NARASIAH; TALBOT, 1995; UEDA YAMAGUCHI et al., 2021). It has been used as a medicinal plant for thousands of years to treat a variety of ailments (BAPTISTA et al., 2017). In the modern world, it is becoming increasingly popular as a dietary supplement and natural health product. It is also known for its ability to be used as a natural water purifier, due to its purifying properties, especially when combined with clay and sand (BEZERRA et al., 2018; QUESADA et al., 2019b). *Moringa oleifera Lam.* has been studied in numerous countries as an effective way to decrease waterborne diseases, particularly in poorer countries with limited access to clean drinking water. Its properties allow it to remove bacteria, parasites and other particles from water, making it an inexpensive and natural way to treat water (RECK et al., 2018; WERNKE et al., 2020).

Iron oxide nanoparticles are a highly effective tool for water treatment. These ultra-fine particles are capable of removing impurities from water and increasing its quality (ATTIA et al., 2022). They are effective at a wide range of pH levels and can reduce the presence of heavy metals, organic pollutants, and suspended particles. Furthermore, they can improve water clarity by increasing

the filtration capacity of the water (FERNÁNDEZ-BARAHONA et al., 2020). Nanoparticles can also be engineered to have a specific size range to maximize their effectiveness. These particles offer the potential to improve water quality without the need for expensive chemicals or high-pressure systems (FERNÁNDEZ-BARAHONA et al., 2020). Additionally, iron oxide nanoparticles are safe, inexpensive, and easily biodegradable. This makes them an attractive option for water treatment in many industries around the world (MAHDAVINIA; ETEMADI, 2019) (NAWI et al., 2022).

Thus, the present work aimed to verify the adsorption capacity of the adsorbent from the seed bark of *Moringa oleifera Lam.*, functionalized with iron oxide nanoparticles, to remove ivermectin.

6. MATERIALS AND METHODS

The ivermectin used in this study was from Sigma-Aldrich (99% pure), *Moringa oleifera Lam.* seeds were collected from the experimental farm at the State University of Maringá. And the compounds used in this study were from Synth and Merck (purities > 95%).

6.1. ADSORBENT PREPARATION

The seed hulls were washed in ultrapure water at a temperature of 70 ± 10º C and subsequently dried in ovens at 105º for 24 h. With the material without moisture, chemical treatment was performed using methyl alcohol (CH_3OH) 0.1 M and then with nitric acid (HNO_3) 0.1 M, both treatments were 1:5 (m/v), in which it was A wash was performed with ultrapure water to remove excess reagents from the material. The thermal treatment was carried out in a muffle furnace (Jung 10.012) at 300º C for 1 h (AKHTAR et al., 2007).

Then the biosorbent was inserted 2.8 g of ferrous sulfate ($(FeSO_4).7H_2O$) and 1.1g of iron nitrate ($Fe(NO_3)3.9H_2O$) both dissolved in 20 mL of deionized water, soon after adding the biosorbent with the prepared solutions, in a single flask in agitation for 1 h (IQBAL et al., 2017). At the end of the established time, the coprecipitation process occurred, in which the pH was changed to 11, with the aid of a pH meter (Thermo Scientific), where the material with iron oxide

nanoparticles called MNOI-Fe_3O_4 (CUSIOLI et al., 2020). After that, the material was characterized with some techniques, such as transmittance electron microscopy (TEM) (JOEL JEM-1250) of 120 k (TEM). Scanning electron microscopy (SEM) (Quanta 250 FEI) equipped with EDX software. X-ray diffraction (XRD) (D8 Advence, Bruker) Kα 1.5406 Å was performed at a voltage of 40 Kv at 30 mA. Infrared spectroscopy with Fourier transform. (FTIR) was in Vertex 70 v (Bruker), the surface charges were analyzed in the zeta potential with the help of the particle analyzer DelsaTMNanoC (Beckman Coulter) and the Brunauer– Emmett–Teller (BET) method using adsorption/desorption isotherms.

6.2. EFFECT OF MASS AND PH

The mass effect of the material developed was using 0.01 to 0.05 grams of the material. The pH effect was carried out at acid, neutral and alkaline pH (4, 7 and 10). Both effects were used MNOI-Fe_3O_4 and ivermectin solution at 30 mg L^{-1} under constant rotation of 150 rpm at 25º C for 24 h.

6.3. KINETIC AND EQUILIBRIUM STUDY

Kinetic and equilibrium studies were performed after obtaining the best conditions for the effect of mass and pH, using 0.01 g of MNOI-Fe_3O_4 in 30 mL of ivermectin solution 30 mg L^{-1} at 150 rpm, pH 7 to temperature of 25º C, removing aliquots established in specific times from 1 to 1440 min. With the withdrawal of each aliquot, filtration was performed on a 0.45 µm cellulose acetate membrane (Unifil). Readings were obtained in a spectrophotometer at 260 nm. In which the tests were performed in triplicate. Once the final concentration of the aliquot was obtained, the adsorption capacity (q_e) in mg g^{-1} was calculated according to Equation 1.

$$q_e = \frac{(C_i - C_f)V}{m} \quad (1)$$

C_i and C_f are the concentrations for both initial and final, V represents the volume of ivermectin solution (L) and m is the mass of the material (g). The experimental data were applied to pseudo-first order (PFO) and pseudo-second

order (PSO) models. The PFO model is (Lagergren, 1898) according to Equation 2.

$$q_t = q_e(1 - e^{-K_1 t}) \quad (2)$$

The q_t and q_e determine the adsorption capacities at time t and at equilibrium (mg g^{-1}), k_1 is the PFO adsorption rate constant (min^{-1}), and t is the contact time (min). The PSO was proposed by (HO; MCKAY, 1998) presented in Equation 3. Where k2 is a constant PSO adsorption rate.

$$q_t = \frac{k_2 q_e^2 t}{1 + k_2 q_e t} \quad (3)$$

6.4. ADSORPTION ISOTHERMS

The adsorption isotherms were carried out at four different temperatures 15, 25, 35 and 45º C in which 30 mL of ivermectin solution ranging from 2 to 300 mg L^{-1} was used in contact with 0.01 g of MNOI-Fe_3O_4 at pH natural (6.4) stirring at 150 rpm for 600 min. With that the calculations of the adsorption capacity, in which the most classic models, Langmuir and Freundlich.

The Langmuir isotherm is entitled by the assumption that there is a set number of active sites and there is no competition between them, in which I assumed that adsorption occurs at an individual site for the active sites already occupied (LANGMUIR, 1918), and presented in Equation 5.

$$q_{eq} = \frac{q_m b_L C_e}{1 + b_L C_e} \quad (5)$$

Where b_L is the Langmuir isotherm (L mg^{-1}) constant. The Freundlich model applies to models that have heterogeneous surfaces and do not provide the assumptions regarding their monolayer adsorption capacity, assuming that there is interaction between their adsorbed molecules (FREUNDLICH, 1906) and presented in Equation 6.

$$q_{eq} = K_F C_e^{1/n} \quad (6)$$

Where k_F is the Freundlich isotherm constant (mg L^{-1}) (L g^{-1})$^{1/n}$. Then, the isotherm models for adsorption were applied, where the established equilibrium data were used to calculate thermodynamic parameters such as: enthalpy (ΔH), entropy (ΔS), equilibrium constant K_c and Gibbs free energy (ΔG).

6.5. EFFECT OF IONIC STRENGTH

The ionic strength study was carried out to determine a common salt that may be present in water and its respective ions, to observe whether there is influence on the adsorption of ivermectin at 30 mg L^{-1}. Different salts were used, such as: sodium chloride (NaCl), potassium chloride (KCl), calcium chloride ($CaCl_2$) and magnesium chloride ($MgCl_2$) in dissociated ions of 0.1, and 0.3 M of free ions, in contact with 24 hours at 25°C.

6.6. REGENERATION STUDY

The regeneration of the material developed has the intention of extending the reuse of the biosorbent, in which eluents were used to determine which is the best to be worked on, with this, the following were used: 1M hydrochloric acid, 1M sodium hydroxide, pure ethyl alcohol, ethyl alcohol in the proportion 50% (v/v), pure methyl alcohol and methyl alcohol in the proportion 50% (v/v). And consequently, the adsorption and desorption cycles were evaluated and calculated according to Equation 7.

$$q_{ds} = \frac{C_{ds}V}{m_{ad}} \quad (7)$$

Where C_{ds} is the concentration after the adsorption of ivermectin (mg L^{-1}), v is the volume of the solution (L), and mad is the mass of MNOI-Fe_3O_4 in (g).

7. RESULTS AND DISCUSSION

7.1. CHARACTERIZATION OF MNOI-FE_3O_4

Figure 1 shows the X-ray diffractograms of the pure biosorbent (MO) and the MNOI-Fe_3O_4.

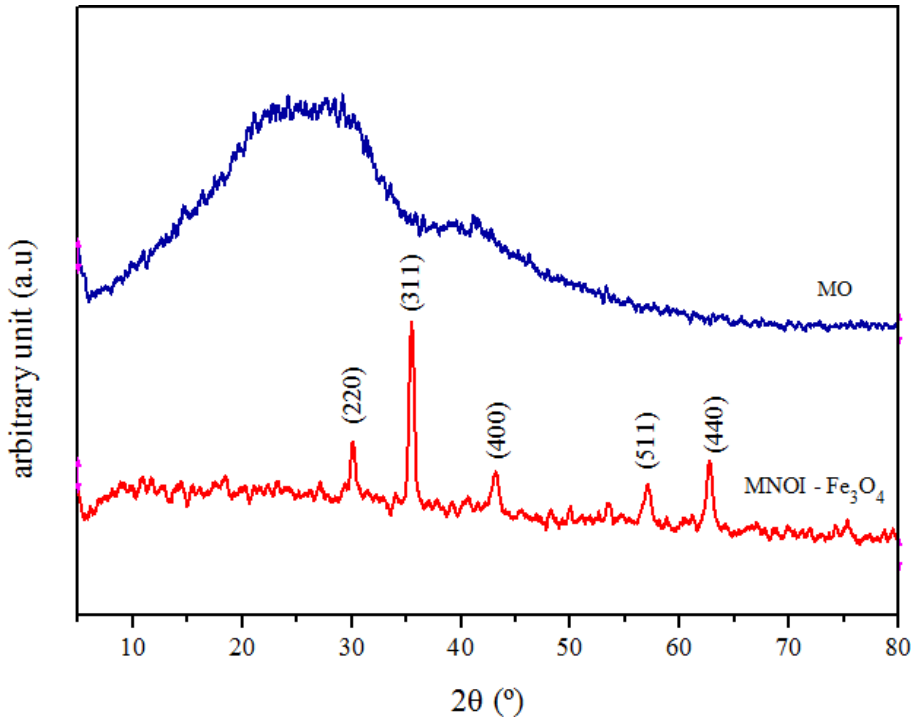

Figure 1. X-ray diffraction of MO and MNOI-Fe_3O_4.

The MO XRD is observed in the upper part of the image, where the peaks are not visible in the region 2Θ = 15.2 to 32.4º, where the predominance of amorphous material is verified (NAYAK; SINGH, 2007; PATIDAR; JAIN, 2017). On the other hand, the XRD of the MNOI-Fe_3O_4, the region demonstrates in the same region of the MO, an amorphous material 2Θ = 15.2 to 32.4º, this fact can be caused by the intensity that the peaks of the iron oxide nanoparticles acted (JAIN et al., 2018). And the iron oxide nanoparticles obtained peaks defined at 2Θ = 29.9º, 34.8º, 42.9º, 57.4º and 62.2º, indicating diffraction planes for magnetite (220), (311), (400), (511) and (440) respectively. Because these peaks are characteristic of magnetite with crystalline structure with cubic shape (RĂCUCIU; OANCEA, 2021; ZAMBRI et al., 2019).

The materials were analyzed at SEM and TEM, verifying their morphological structure. SEM images are shown in Figure 2.

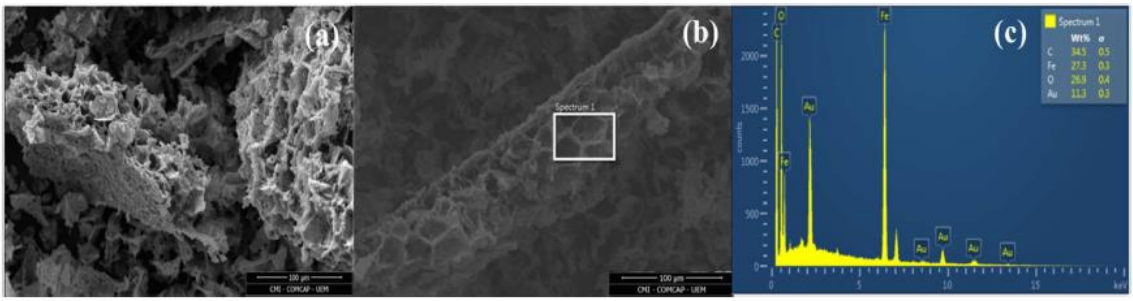

Figure 2. (a) Morphological structure of MNOI-Fe_3O_4. (b) Spectrum for obtaining the EDX. (c) EDX of the elements.

It is observed in Figure 2(a), a high number of porous, heterogeneous cavities that help the adsorption capacity of MNOI-Fe_3O_4 (QUESADA et al., 2019a). The modifications carried out in the MO are possibly promising for the adsorption process in types of metallic chemical species and emerging contaminants. The presence of agglomerated particles must be related to α-Fe_2O_3 (CUSIOLI et al., 2020). With that, the seed husks of *Moringa oleifera Lam* functionalized with iron oxide, confirm that the material was adhered to the surface. The EDX analysis was performed shown in Figure 2(b). Figure 2(c), determines the composition of the MNOI-Fe_3O_4 material, with the presence of carbon (C), oxygen (O), iron (Fe) and gold (Au) the gold found in the sample is due to the coating of the sample, which had 34.5, 27.3, 26.9 and 11.3% respectively (CUSIOLI et al., 2021). Verification of MNOI-Fe_3O_4 iron oxide nanoparticles were determined at TEM, shown in Figure 3.

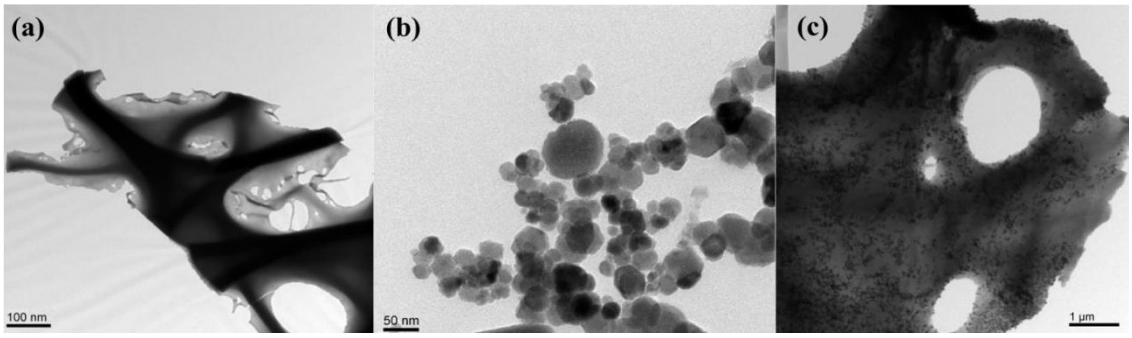

Figure 3. Transmittance electron microscopy micrographs (a) MO (b) iron oxide nanoparticles (c) MNOI-Fe_3O_4.

Figure 3(a) demonstrates the structure of the material in which there are heterogeneous cavities that favor the adsorption process (KALAISELVI et al., 2018). Figure 3(b), are the iron oxide nanoparticles with an average size of 14.3 nm obtained by the Scherrer method and cubic format (MOODLEY et al., 2018).

Figure 3(c) shows the superimposition of iron oxide nanoparticles on the MO, correlating an excellent interaction and helping to form MNOI-Fe_3O_4 (RAVIKUMAR; UDAYAKUMAR, 2021).

The FTIR analysis determined which functional groups were present in the MONI material to verify whether the functionalization as occurred with iron oxide nanoparticles remained on the surface of the MNOI-Fe_3O_4, as shown in Figure 4.

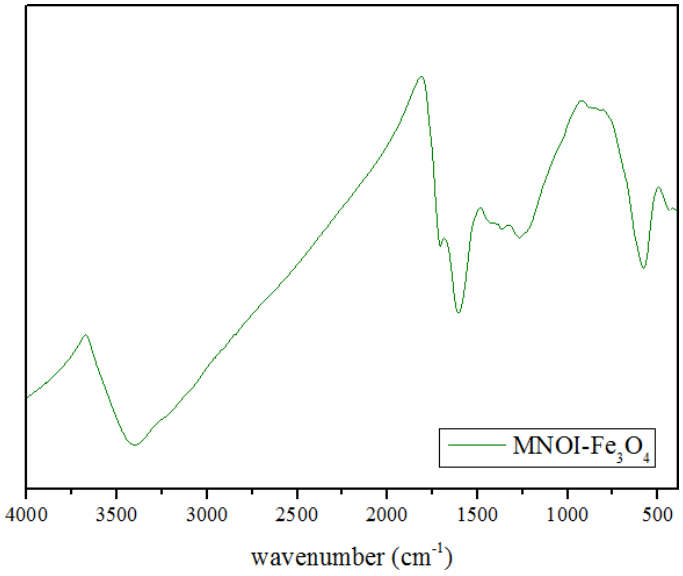

Figure 4. FTIR spectra MNOI-Fe_3O_4.

In the FTIR analysis there is a broad band at 3712-3642 cm^{-1}, demonstrating hydrogen bonds. The peak at 2911 cm^{-1} determines the presence of methylcellulose as there is asymmetric elongation for the C−H bond of the CH_2 group. The peak at 2824 cm^{-1} is the symmetrical elongation of the C−H bonds of the CH_3 group (M et al., 2021). At 1683 cm^{-1}, there is a variation of increasing relative area, shifting to the peak of 1653 cm^{-1}. Such a change is related to the elongation of COO^- and its partial N−H deformations of secondary amines (FATIQIN; AMRULLOH; SIMANJUNTAK, 2021). The peak at 933 cm^{-1} is characteristic of C−O, in which it associates with lignin, cellulose and hemicellulose. Iron oxide is determined in the region of 602–549 cm^{-1}, corresponding to the Fe−O bond. The vibrational bands between 591 and 648 cm^{-1} are expressly characteristic of magnetite, where Fe^{2+} – O_2 bonds and symmetric deformation at octahedral sites are associated (KHALID et al., 2023).

Since the adsorption is initiated, BET analysis was performed to evaluate the porosity of the studied material. The large specific area contributes to the adsorption of ivermectin in the pores of. Table 1 shows the values obtained.

Table 1. Texture properties of MNOI-Fe_3O_4.

Parameters	MNOI-Fe_3O_4
BET Specific surface area ($m^2\ g^{-1}$)	5.68
Average pore diameter (Å)	17.21
Total pore volume ($cm^3\ g^{-1}$)	0.0850
Micropore volume ($cm^3\ g^{-1}$)	0.0247
Mesopore volume ($cm^3\ g^{-1}$)	0.0603

Mesopores and micropores are types of nano-scale pores found in various materials. Mesopores are classified as having a pore size of 2 − 50 nanometers (nm), while micropores are classified as having a pore size of 0.7 – 2 nm. Verified in the study by (MORALES-PAREDES; RODRÍGUEZ-DÍAZ; BOLUDA-BOTELLA, 2022) who evaluated the use cattle dung for ivermectin removal, obtaining small pore volume.

Check the Figure 5 for the zeta potential at different pH MNOI-Fe_3O_4 (2 – 12). It was observed that in most values, the zeta potential was negative (BAPTISTA et al., 2017). In particular, the isoelectric point occurred at approximately pH 3, confirming a positive charge at pH less than 3, and a negative charge at pH greater than 3 (QUESADA et al., 2019b).

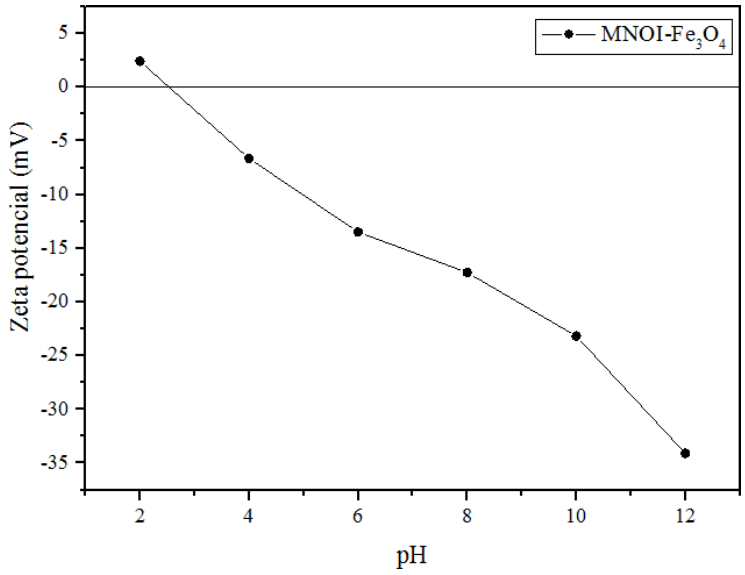

Figure 5. Zeta potential of MNOI-Fe_3O_4.

7.2. ADSORPTION STUDIES

7.2.1. EFFECT OF MASS AND PH

To verify the effect of the concentration of MNOI-Fe_3O_4 and pH, a graph was constructed considering the adsorption capacity and the percentage of removal, as shown in Figure 6.

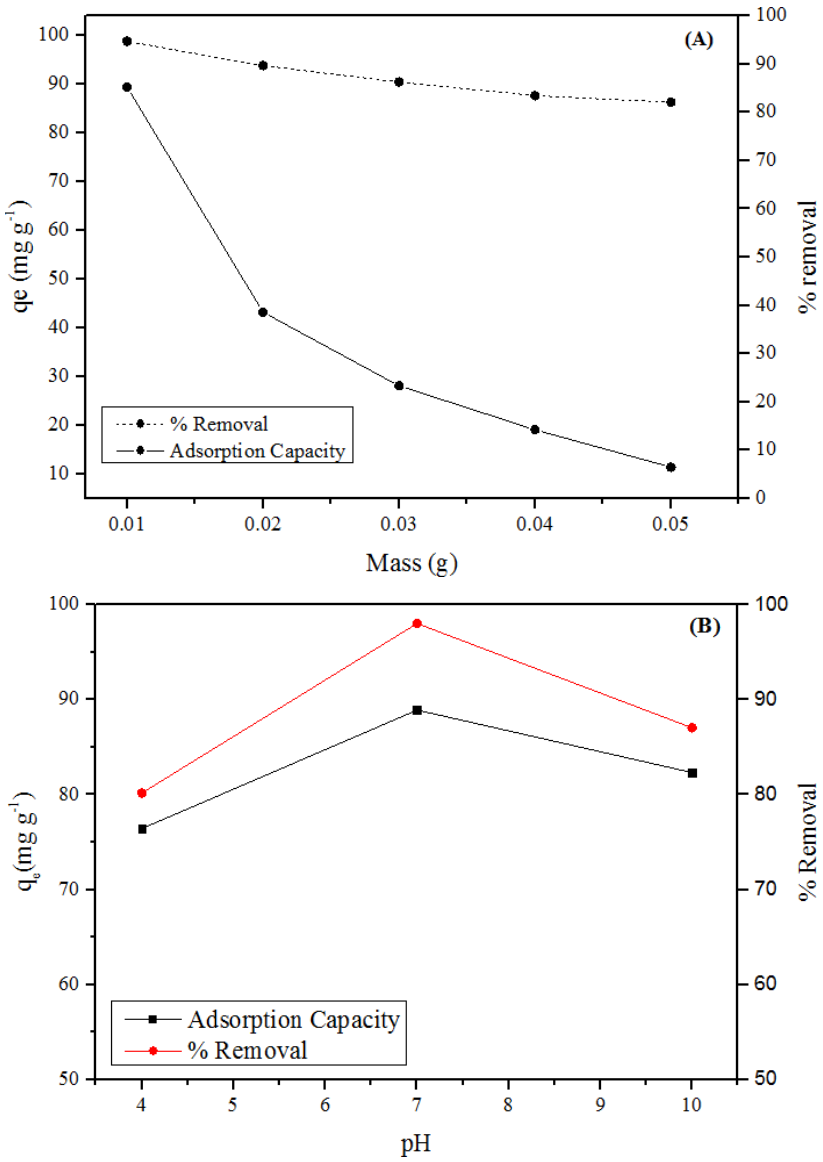

Figure 6. (A) Effect of concentration of MNOI-Fe_3O_4 (B) Effect of pH.

Figure 6(A) is established with variations of the biosorbent masses 0.01, 0.02, 0.03, 0.04 and 0.05 with the following adsorptive capacities, 89.41, 43.2, 28.1, 19.07, 11.38 mg g^{-1}, with the following removals 98.77, 93.79, 90.29, 87.63

and 86.26% respectively. This means that due to the decrease in the amount of mass, the availability of active sites increases the interaction with the contaminant, in the case of this study ivermectin (DIAGBOYA et al., 2021). In Figure 6(B), there was a pH variation at 4, 7 and 10 obtaining qe 76.43, 88.91 and 82.33 mg g^{-1} and the removal percentage of 80.17, 98.03 and 87.03%, respectively.

7.2.2. KINETIC STUDY FOR IVERMECTIN REMOVAL

The study of equilibrium and kinetics for the adsorption process assists in analyzing the capacity of adsorption with respect to time (KABBASHI et al., 2009). Reportedly, the kinetic study is significant in the adsorption process, as it assesses the adsorption capacity of the adsorbent and the removal of the contaminant over time. The graphs of the pseudo-first-order and pseudo-second-order models are shown in Figure 7.

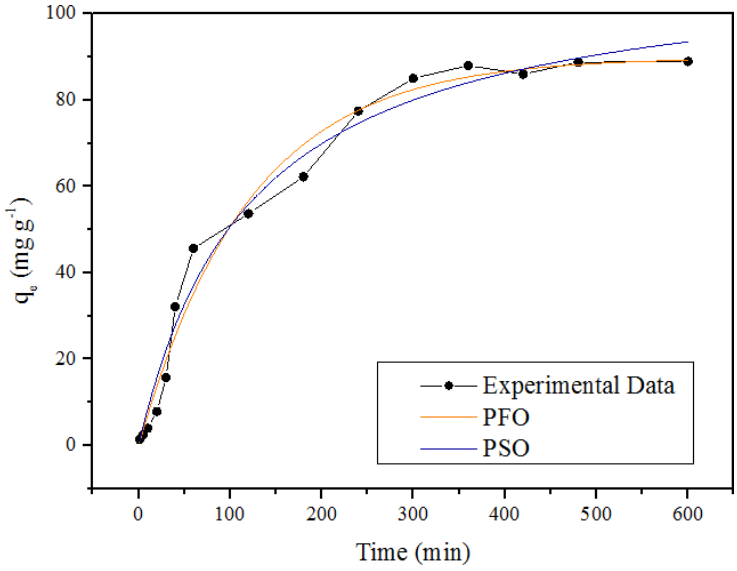

Figure 7. Kinetics of ivermectin adsorption using of MNOI-Fe_3O_4.

In Figure 7 it is determined that the adsorption of ivermectin in the initial phase is fast, proving the possible availability of free active sites. Over time, ivermectin is removed in smaller amounts until it reaches removal stability in approximately 400 min, as there was no significant variation with longer times, that is, the steady state was reached. Because the number of free sites was decreasing, which hindered the adsorption of ivermectin where it made it

impossible to remove other molecules (KROGH et al., 2009; LI; ZHOU; ZHANG, 2015). Achieving stability, a maximum q_e of 89.41 mg g^{-1} of the biosorbent and a removal percentage of 98.03% of ivermectin were obtained, where the kinetic parameters were estimated.

Given the results of the q_e and percentage of removal by time, the experimental data were applied to the PFO and PSO models as shown in Table 2.

Table 2. Kinetic models for ivermectin biosorption from MNOI-Fe3O4.

Models	Parameters	MNOI-Fe_3O_4
Pseudo-first-order	qe (mg g^{-1})	89.86
	k_1 (min^{-1})	0.003
	R^2	0.990
	χ^2	0.022
Pseudo-second-order	qe (mg g^{-1})	112.46
	k_2 (g mg^{-1} min^{-1})	0.007
	R^2	0.919
	χ^2	0.368

It is observed that the correlation coefficients (R^2) for the PFO and PSO models were R^2 = 0.990 and 0.919. And the chi-square (χ^2) value for PFO was 0.022. Thus, the PFO model was the best applied for ivermectin removal, which occurs directly proportionally to the number of MNOI-Fe_3O_4 active sites (HO; MCKAY, 1999).

7.3. ADSORPTION ISOTHERMS

The experiments were conducted at four temperatures 283, 298, 308 and 318 K in which it was evaluated based on the results of the kinetic data. The experimental data were applied to the classical models of Langmuir and Freundlich. Figure 8 shows the temperatures studied.

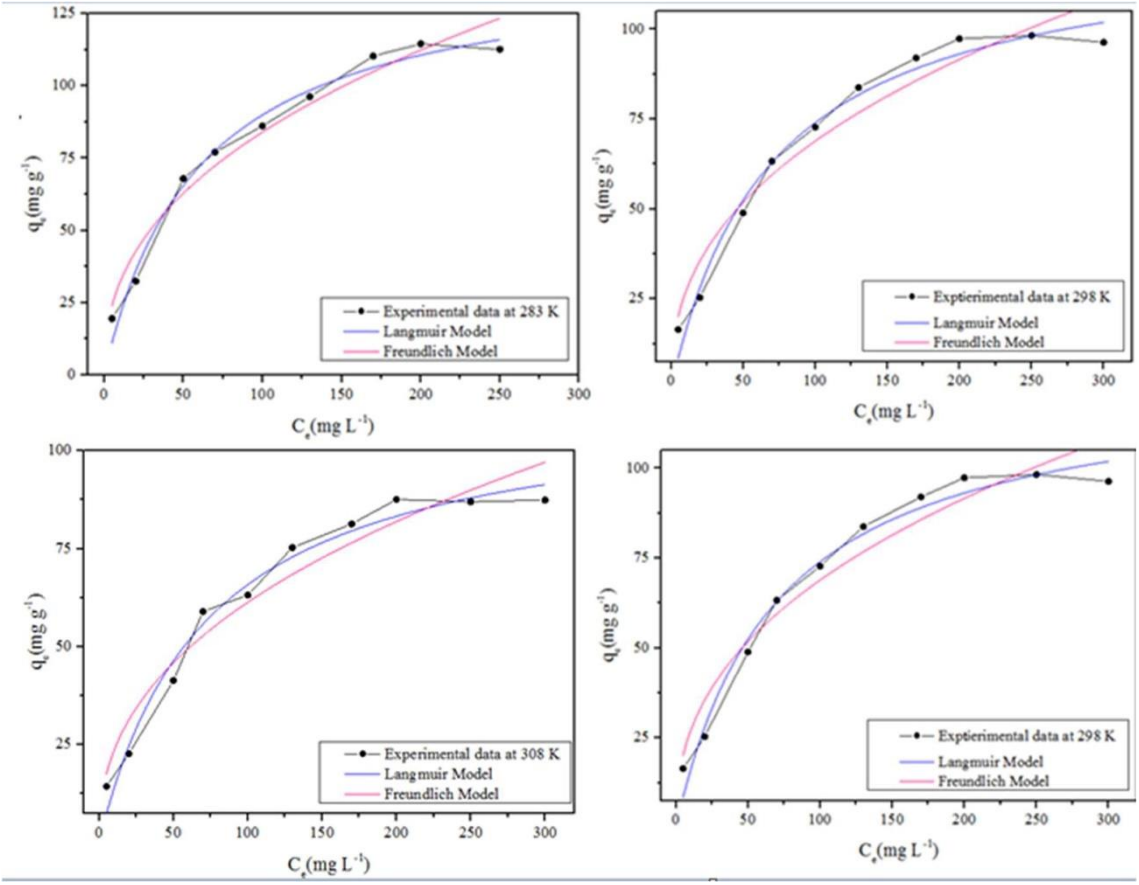

Figure 8. Adjustment of the Freundlich and Langmuir isotherm models to the experimental data.

Determines Figure 8, it is observed that the four temperatures studied have an equilibrium determining the maximum q_e. It is notorious that with the increase in temperature there was a detrimental effect on the adsorption process.

The Langmuir and Freundlich models are the most classic models in the literature and describe the solid-liquid interface. Thus, the results obtained for both models are shown in Table 3.

Table 3. Parameters of equilibrium isotherms models representing equilibrium adsorption data for ivermectin with MNOI-Fe_3O_4.

Models	Parameters	283K	298K	308K	318K
Langmuir	Qmáx (mg g^{-1})	143.76	125.54	109.88	83.24
	K_L (L mg^{-1})	0.167	0.115	0.083	0.041
	R^2	0.989	0.979	0.966	0.958
Freundlich	Qmáx (mg g^{-1})/(mg L^{-1})^{n_F}	12.17	10.36	9.35	8.94
	n_F	2.38	2.25	2.12	2.01
	R^2	0.860	0.843	0.831	0.807

The results in table 3 show the (R^2) values obtained by the Langmuir model at 0.989, 0.979, 0.966 and 0.958 for temperatures of 283, 298, 308 and 318 K respectively. As for the Freundlich model, the (q_{max}) were 12.17, 10.36, 9.35 and 8.94 mg g^{-1}, sequentially, at different temperatures 283, 298, 308 and 318 K, so we can say that the experimental data were adjusted to the model of Langmuir.

7.4. THERMODYNAMIC PARAMETERS

To calculate the thermodynamic parameters, it is necessary to understand the adsorption mechanism, and several factors that can make the process viable (ZOLGHARNEIN; SHAHMORADI; GHASEMI, 2011). Once the constant K_c was determined, it was applied to thermodynamic equations, where K_L in its dimensionless form was stipulated for the determination of thermodynamic parameters (BERGMANN; MACHADO, 2015). The Gibbs free energy (ΔG), enthalpy (ΔH) and entropy (ΔS) values were calculated and presented in Table 4.

Table 4. Thermodynamic parameters of ivermectin biosorption using MNOI-Fe_3O_4.

T (ºC)	T (K)	(ΔG) (KJ mol^{-1})	(ΔH) (KJ mol^{-1})	(ΔS) (KJ mol^{-1})
25	298	-32.54		
35	308	-34.69	-20.33	0.09
45	318	-37.72		

The three temperature variations studied obtained negative ΔG values (-32.54, - 34.69 and -37.72 KJ mol^{-1}), determining that the process was favorable and spontaneous (ELLIOTT; VANDERMEULEN, 2017). The negative value of ΔH determines that the process is exothermic, having disadvantages when there is an increase in temperature, where its value -20.33 KJ mol^{-1} can establish that the mechanism occurs by chemisorption (HAYWARD; TRAPNELL, 1964). The small and positive values of ΔS = 0.09 KJ mol^{-1} report that the interaction between ivermectin and MNOI-Fe_3O_4 occurred through the solid-liquid interface (CRINI, 2006).

7.5. STUDY OF IONIC STRENGTH

The effects of NaCl, KCl, $CaCl_2$ and $MgCl_2$ salts were evaluated at concentrations of 0.1 and 0.3 M. Because in aqueous matrices, there will never be exclusively one compound, but several other inorganic, organic and other compounds that will be dissolved (BERNAL; GIRALDO; MORENO-PIRAJÁN, 2020). Figure 9 demonstrates such ion competition.

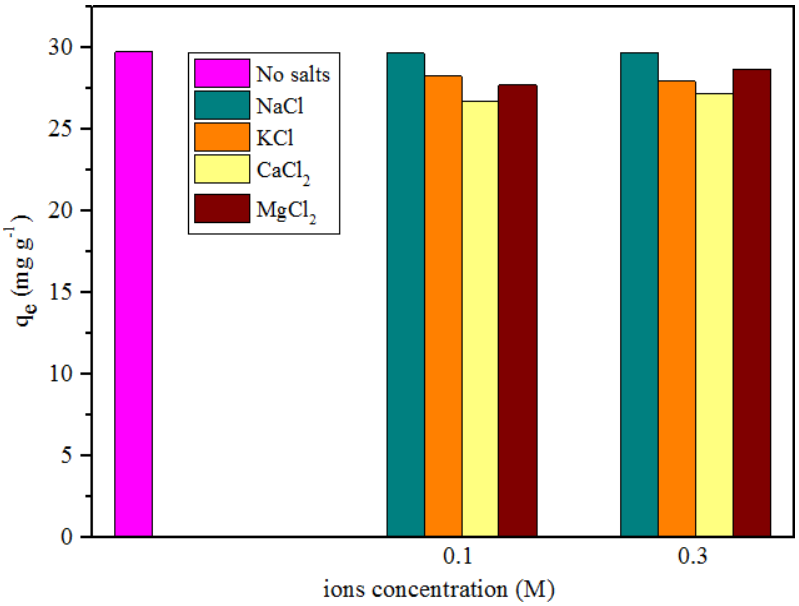

Figure 9. Effect of ionic strength on ivermectin adsorption by MNOI-Fe_3O_4.

The presence of 0.1 and 0.3 M salts did not compromise the adsorption of ivermectin. At the 0.1 M concentration there was a q_e from 0.02 to 3.17 mg g^{-1} and for 0.3 M it was from 0.04 to 2.61 mg g^{-1}. Thus, these values did not influence the removal of ivermectin.

7.6. STUDY OF REGENERATION

The reuse of the MNOI-Fe_3O_4 for ivermectin occurred in five cycles, as shown in Figure 10.

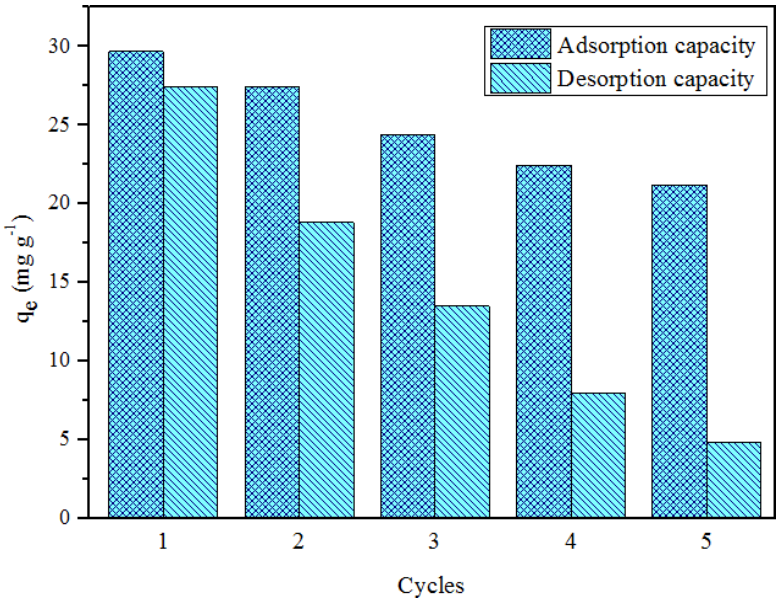

Figure 10. Regeneration of MNOI-Fe_3O_4 for adsorption of ivermectin from water.

At Figure 10 shows that the q_e of the first cycle from 29.59 to 21.45 mg g^{-1} until the fifth cycle, with a variation of 30% of loss. The desorption capacity in the first cycle was from 27.13 to 4.59 mg g^{-1} and in the fifth cycle, there was a variation of 83.5%, this fact is acceptable because biosorbents are fragile materials.

8. CONCLUSIONS

In this study, the removal of ivermectin by the adsorption process using MNOI-Fe_3O_4 was evaluated. The highest q_e was 143.76 at 283 K. The experimental data fit the models and PFO and Langmuir. Thermodynamic data reported that the adsorption process was exothermic, that is, at higher temperatures, the adsorption process is disadvantageous. And that the material has the possibility of high potential for removal of emerging contaminants.

9. REFERENCES

ABATAL, M. et al. Comparison of Heavy Metals Removal from Aqueous Solution by Moringa oleifera Leaves and Seeds. **Coatings**, v. 11, n. 5, p. 508, 25 abr. 2021.

ABDOLALI, A. et al. Typical lignocellulosic wastes and by-products for biosorption process in water and wastewater treatment: A critical review. **Bioresource Technology**, v. 160, p. 57–66, maio 2014.

AHMAD, T.; DANISH, M. Prospects of banana waste utilization in wastewater treatment: A review. **Journal of Environmental Management**, v. 206, p. 330–348, jan. 2018.

AHMED, I. et al. Nitrogen-Doped Porous Carbons from Ionic Liquids@MOF: Remarkable Adsorbents for Both Aqueous and Nonaqueous Media. **ACS Applied Materials & Interfaces**, v. 9, n. 11, p. 10276–10285, 22 mar. 2017.

AKHTAR, M. et al. Sorption potential of Moringa oleifera pods for the removal of organic pollutants from aqueous solutions. **Journal of Hazardous Materials**, v. 141, n. 3, p. 546–556, 22 mar. 2007.

AKHTAR, M. S.; ALI, S.; ZAMAN, W. Innovative Adsorbents for Pollutant Removal: Exploring the Latest Research and Applications. **Molecules**, v. 29, n. 18, p. 4317, 11 set. 2024.

ALEXANDER, G. B.; HESTON, W. M.; ILER, R. K. The Solubility of Amorphous Silica in Water. **The Journal of Physical Chemistry**, v. 58, n. 6, p. 453–455, jun. 1954.

ALI, I.; ALOTHMAN, Z. A.; AL-WARTHAN, A. Sorption, kinetics and thermodynamics studies of atrazine herbicide removal from water using iron nano-composite material. **International Journal of Environmental Science and Technology**, v. 13, n. 2, p. 733–742, fev. 2016.

ALI, I.; ASIM, MOHD.; KHAN, T. A. Low cost adsorbents for the removal of organic pollutants from wastewater. **Journal of Environmental Management**, v. 113, p. 170–183, dez. 2012.

ALLEN, J.; SCAIFE, P. The Elovich equation and chemisorption kinetics. **Australian Journal of Chemistry**, v. 19, n. 11, p. 2015, 1966.

AL-SHEHRI, B. M. et al. A review: the utilization of mesoporous materials in wastewater treatment. **Materials Research Express**, v. 6, n. 12, p. 122002, 12 nov. 2019.

ÁLVAREZ-RUIZ, R.; PICÓ, Y. Analysis of emerging and related pollutants in aquatic biota. **Trends in Environmental Analytical Chemistry**, v. 25, p. e00082, mar. 2020.

ANASTOPOULOS, I.; KYZAS, G. Z. Are the thermodynamic parameters correctly estimated in liquid-phase adsorption phenomena? **Journal of Molecular Liquids**, v. 218, p. 174–185, jun. 2016.

ANDRADE, M. B. et al. Evaluation of magnetic nano adsorbent produced from graphene oxide with iron and cobalt nanoparticles for caffeine removal from aqueous medium. **Chemical Engineering and Processing - Process Intensification**, v. 170, p. 108694, jan. 2022.

ATTIA, N. F. et al. Iron oxide nanoparticles and their pharmaceutical applications. **Applied Surface Science Advances**, v. 11, p. 100284, out. 2022.

BABIĆ, S.; DABIĆ, D.; ĆURKOVIĆ, L. **Fate of hydroxychloroquine in the aquatic environment**. 15th International Conference on Environmental Science and Technology. **Anais**... Em: CONFERENCE ON ENVIRONMENTAL SCIENCE AND TECHNOLOGY. Greece: CEST, 2 set. 2017. Disponível em: <https://cest2017.gnest.org/sites/default/files/presentation_file_list/cest2017_00817_poster_paper.pdf>. Acesso em: 7 mar. 2025

BAI, S. H.; OGBOURNE, S. Eco-toxicological effects of the avermectin family with a focus on abamectin and ivermectin. **Chemosphere**, v. 154, p. 204–214, jul. 2016.

BAPTISTA, A. T. A. et al. Protein fractionation of seeds of Moringa oleifera lam and its application in superficial water treatment. **Separation and Purification Technology**, v. 180, p. 114–124, jun. 2017.

BEN ALI, M. et al. Toxicity of hydroxychloroquine, a potential treatment for COVID-19, on free-living marine nematodes. **Marine Pollution Bulletin**, v. 167, p. 112361, jun. 2021.

BERGMANN, C. P.; MACHADO, F. M. (EDS.). **Carbon Nanomaterials as Adsorbents for Environmental and Biological Applications**. Cham: Springer International Publishing, 2015.

BERNAL, V.; GIRALDO, L.; MORENO-PIRAJÁN, J. C. Thermodynamic analysis of acetaminophen and salicylic acid adsorption onto granular activated carbon: Importance of chemical surface and effect of ionic strength. **Thermochimica Acta**, v. 683, p. 178467, jan. 2020.

BEZERRA, C. D. O. et al. Assessment of the use of *Moringa oleifera* seed husks for removal of pesticide diuron from contaminated water. **Environmental Technology**, v. 41, n. 2, p. 191–201, 10 jul. 2018.

BHADRA, B. N.; JHUNG, S. H. A remarkable adsorbent for removal of contaminants of emerging concern from water: Porous carbon derived from metal azolate framework-6. **Journal of Hazardous Materials**, v. 340, p. 179–188, out. 2017.

BHADRA, B. N.; SEO, P. W.; JHUNG, S. H. Adsorption of diclofenac sodium from water using oxidized activated carbon. **Chemical Engineering Journal**, v. 301, p. 27–34, out. 2016.

BLANCHARD, G.; MAUNAYE, M.; MARTIN, G. Removal of heavy metals from waters by means of natural zeolites. **Water Research**, v. 18, n. 12, p. 1501–1507, jan. 1984.

BOLONG, N. et al. A review of the effects of emerging contaminants in wastewater and options for their removal. **Desalination**, v. 239, n. 1–3, p. 229–246, abr. 2009.

BRASIL. GM/MS Nº 888. PORTARIA GM/MS Nº 888, DE 4 DE MAIO DE 2021. . 2021.

BRUNO, A. Um setor maduro e em crescimento. **ABRAFARMA**, 2 mar. 2023.

BUI, T. X.; CHOI, H. Adsorptive removal of selected pharmaceuticals by mesoporous silica SBA-15. **Journal of Hazardous Materials**, v. 168, n. 2–3, p. 602–608, set. 2009.

BUNTING, S. Y. et al. Emerging organic compounds in European groundwater. **Environmental Pollution**, v. 269, p. 115945, jan. 2021.

CAPPELLI, F. et al. Suspect screening of wastewaters to trace anti-COVID-19 drugs: Potential adverse effects on aquatic environment. **Science of The Total Environment**, v. 824, p. 153756, jun. 2022.

CASHIN, V. B. et al. Surface functionalization and manipulation of mesoporous silica adsorbents for improved removal of pollutants: a review. **Environmental Science: Water Research & Technology**, v. 4, n. 2, p. 110–128, 2018.

CAUDA, V.; SCHLOSSBAUER, A.; BEIN, T. Bio-degradation study of colloidal mesoporous silica nanoparticles: Effect of surface functionalization with organo-silanes and poly(ethylene glycol). **Microporous and Mesoporous Materials**, v. 132, n. 1–2, p. 60–71, jul. 2010.

CECILIA, J. A.; MORENO TOST, R.; RETUERTO MILLÁN, M. Mesoporous Materials: From Synthesis to Applications. **International Journal of Molecular Sciences**, v. 20, n. 13, p. 3213, 30 jun. 2019.

CHEN, L. et al. Recent developments of mesoporous silica nanoparticles in biomedicine. **Emergent Materials**, v. 3, n. 3, p. 381–405, 1 jun. 2020.

COLDEBELLA, P. F. et al. Potential effect of chemical and thermal treatment on the Kinetics, equilibrium, and thermodynamic studies for atrazine biosorption by the *Moringa oleifera* pods. **The Canadian Journal of Chemical Engineering**, v. 95, n. 5, p. 961–973, maio 2017.

CONAMA. CONAMA N° 357/2005. RESOLUÇÃO CONAMA N° 357, DE 17 DE MARÇO DE 2005. . 2005.

CORREA, C. M. A. et al. Ivermectin impacts on dung beetle diversity and their ecological functions in two distinct Brazilian ecosystems. **Ecological Entomology**, v. 47, n. 5, p. 736–748, out. 2022.

CRINI, G. Non-conventional low-cost adsorbents for dye removal: A review. **Bioresource Technology**, v. 97, n. 9, p. 1061–1085, jun. 2006.

CRINI, G.; BADOT, P.-M. Application of chitosan, a natural aminopolysaccharide, for dye removal from aqueous solutions by adsorption processes using batch studies: A review of recent literature. **Progress in Polymer Science**, v. 33, n. 4, p. 399–447, abr. 2008.

CRUMP, A.; OMURA, S. Ivermectin, “Wonder drug” from Japan: the human use perspective. **Proceedings of the Japan Academy, Series B**, v. 87, n. 2, p. 13–28, 2011.

CUSIOLI, L. F. et al. Development of a new low-cost adsorbent functionalized with iron nanoparticles for removal of metformin from contaminated water. **Chemosphere**, v. 247, p. 125852, maio 2020.

CUSIOLI, L. F. et al. Modified *Moringa oleifera* Lam. Seed husks as low-cost biosorbent for atrazine removal. **Environmental Technology**, v. 42, n. 7, p. 1092–1103, 21 mar. 2021.

CUSIOLI, L. F. et al. Adsorption of Covid-19-related drug from contaminated water using activated carbon. **Desalination and Water Treatment**, v. 277, p. 85–89, nov. 2022.

CUSIOLI, L. F. et al. Use of low-cost adsorbent functionalized with iron oxide nanoparticles for ivermectin removal. **South African Journal of Chemical Engineering**, v. 47, p. 142–149, 2024.

DAUGHTON, C. G. Cradle-to-cradle stewardship of drugs for minimizing their environmental disposition while promoting human health. I. Rationale for and avenues toward a green pharmacy. **Environmental Health Perspectives**, v. 111, n. 5, p. 757–774, maio 2003.

DAUGHTON, C. G.; TERNES, T. A. Pharmaceuticals and Personal Care Products in the Environment: Agents of Subtle Change? **Environmental Health Perspectives**, v. 107, 1999.

DE SOUZA, R. M. et al. Occurrence, impacts and general aspects of pesticides in surface water: A review. **Process Safety and Environmental Protection**, v. 135, p. 22–37, mar. 2020.

DIAGBOYA, P. N. et al. Empirical Assessment and Reusability of an Eco-Friendly Amine-Functionalized SBA-15 Adsorbent for Aqueous Ivermectin. **Industrial & Engineering Chemistry Research**, v. 60, n. 6, p. 2365–2373, 17 fev. 2021.

DIAGBOYA, P. N. et al. Comparative empirical evaluation of the aqueous adsorptive sequestration potential of low-cost feldspar-biochar composites for ivermectin. **Colloids and Surfaces A: Physicochemical and Engineering Aspects**, v. 634, p. 127930, fev. 2022.

DIZGE, N. et al. Adsorption of reactive dyes from aqueous solutions by fly ash: Kinetic and equilibrium studies. **Journal of Hazardous Materials**, v. 150, n. 3, p. 737–746, fev. 2008.

DOKE, K. M.; KHAN, E. M. Adsorption thermodynamics to clean up wastewater; critical review. **Reviews in Environmental Science and Bio/Technology**, v. 12, n. 1, p. 25–44, mar. 2013.

DOMINGO-ECHABURU, S. et al. Drugs used during the COVID-19 first wave in Vitoria-Gasteiz (Spain) and their presence in the environment. **Science of The Total Environment**, v. 820, p. 153122, maio 2022.

DOU, B. et al. Adsorption performance of VOCs in ordered mesoporous silicas with different pore structures and surface chemistry. **Journal of Hazardous Materials**, v. 186, n. 2–3, p. 1615–1624, fev. 2011.

ELBALKINY, H. T. et al. Potentiometric diclofenac detection in wastewater using functionalized nanoparticles. **Microchemical Journal**, v. 145, p. 90–95, mar. 2019.

ELLIOTT, S. M.; VANDERMEULEN, D. D. A regional assessment of chemicals of concern in surface waters of four Midwestern United States national parks. **Science of The Total Environment**, v. 579, p. 1726–1735, fev. 2017.

ELLIS, R. P. et al. Immunological function in marine invertebrates: Responses to environmental perturbation. **Fish & Shellfish Immunology**, v. 30, n. 6, p. 1209–1222, jun. 2011.

FATIQIN, A.; AMRULLOH, H.; SIMANJUNTAK, W. Green synthesis of MgO nanoparticles using Moringa oleifera leaf aqueous extract for antibacterial activity. **Bulletin of the Chemical Society of Ethiopia**, v. 35, n. 1, p. 161–170, 7 maio 2021.

FENT, K.; WESTON, A.; CAMINADA, D. Ecotoxicology of human pharmaceuticals. **Aquatic Toxicology**, v. 76, n. 2, p. 122–159, 10 fev. 2006.

FERNÁNDEZ-BARAHONA, I. et al. Iron Oxide Nanoparticles: An Alternative for Positive Contrast in Magnetic Resonance Imaging. **Inorganics**, v. 8, n. 4, p. 28, 10 abr. 2020.

FERNÁNDEZ-REYES, B. et al. Engineered adsorbents for the removal of contaminants of emerging concern from water. Em: **Contaminants of Emerging Concern in Water and Wastewater**. [s.l.] Elsevier, 2020. p. 3–45.

FERREIRA, M. T.; CARVALHO, C. D. S. Chloroquine and hydroxychloroquine in the environment and aquatic organisms: a review. **Ambiente e Agua - An Interdisciplinary Journal of Applied Science**, v. 18, p. 1–24, 17 mar. 2023.

FOO, K. Y.; HAMEED, B. H. Insights into the modeling of adsorption isotherm systems. **Chemical Engineering Journal**, v. 156, n. 1, p. 2–10, 1 jan. 2010.

FOOD AND DRUG ADMINISTRATION. **EUA Chloroquine Phosphate Health Care Provider Fact Sheet**. FDA, , 27 abr. 2020. Disponível em: <https://www.fda.gov/media/136535/download>. Acesso em: 6 nov. 2023

FREUNDLICH, H. M. F. Over the adsorption in solution. **The Journal of Physical Chemistry**, v. 57, n. 385471, p. 1100–1107, 1906.

GALANI, A. et al. Patterns of pharmaceuticals use during the first wave of COVID-19 pandemic in Athens, Greece as revealed by wastewater-based epidemiology. **Science of The Total Environment**, v. 798, p. 149014, dez. 2021.

GARCIA-IVARS, J. et al. Nanofiltration as tertiary treatment method for removing trace pharmaceutically active compounds in wastewater from wastewater treatment plants. **Water Research**, v. 125, p. 360–373, nov. 2017.

GHASEMYANI, S. et al. Global, WHO Regional, and Continental Prevalence of Self-medication from 2000 to 2018: A Systematic Review and Meta-analysis. **Annals of Public Health**, v. 1, 2022.

GHAZY, R. M. et al. A systematic review and meta-analysis on chloroquine and hydroxychloroquine as monotherapy or combined with azithromycin in COVID-19 treatment. **Scientific Reports**, v. 10, n. 1, p. 22139, 17 dez. 2020.

GHIMIRE, P. P.; JARONIEC, M. Renaissance of Stöber method for synthesis of colloidal particles: New developments and opportunities. **Journal of Colloid and Interface Science**, v. 584, p. 838–865, fev. 2021.

GOMES, H. D. O. et al. Removal of contaminants from water using Moringa oleifera Lam. as biosorbent: An overview of the last decade. **Journal of Water Process Engineering**, v. 46, p. 102576, abr. 2022.

GOMES, V. P.; SILVA, M. T.; GALVÃO, T. F. Prevalência do consumo de medicamentos em adultos brasileiros: uma revisão sistemática. **Ciência & Saúde Coletiva**, v. 22, n. 8, p. 2615–2626, ago. 2017.

GRELA, A.; KUC, J.; BAJDA, T. A Review on the Application of Zeolites and Mesoporous Silica Materials in the Removal of Non-Steroidal Anti-Inflammatory Drugs and Antibiotics from Water. **Materials**, v. 14, n. 17, p. 4994, 1 set. 2021.

GRÜN, M.; LAUER, I.; UNGER, K. K. The synthesis of micrometer- and submicrometer-size spheres of ordered mesoporous oxide MCM-41. **Advanced Materials**, v. 9, n. 3, p. 254–257, mar. 1997.

GUPTA, P.; RANI, V. A Comprehensive Assessment of Environmental Implications, Ecotoxicity and Bioaccumulation Potential of Repurposed Drug Hydroxychloroquine: From Challenges to Sustainability. **Reviews of Environmental Contamination and Toxicology**, v. 262, n. 10, 10 maio 2024.

HAMDAOUI, O.; NAFFRECHOUX, E. Modeling of adsorption isotherms of phenol and chlorophenols onto granular activated carbonPart II. Models with more than two parameters. **Journal of Hazardous Materials**, v. 147, n. 1–2, p. 401–411, 17 ago. 2007.

HAN, Y. et al. Unraveling the Growth Mechanism of Silica Particles in the Stöber Method: In Situ Seeded Growth Model. **Langmuir**, v. 33, n. 23, p. 5879–5890, 13 jun. 2017.

HAYWARD, D. O.; TRAPNELL, B. M. W. **Chemisorption**. Londres: Butterworth, 1964.

HE, R. et al. Efficient removal of lead from highly acidic wastewater by periodic ion imprinted mesoporous SBA-15 organosilica combining metal coordination and co-condensation. **Journal of Materials Chemistry A**, v. 3, n. 18, p. 9789–9798, 2015.

HEIDARY, F.; GHAREBAGHI, R. Ivermectin: a systematic review from antiviral effects to COVID-19 complementary regimen. **The Journal of Antibiotics**, v. 73, n. 9, p. 593–602, set. 2020.

HENAO, W. et al. Insights into the CO2 capture over amine-functionalized mesoporous silica adsorbents derived from rice husk ash. **Journal of Environmental Chemical Engineering**, v. 8, n. 5, p. 104362, out. 2020.

HIEW, B. Y. Z. et al. Adsorptive removal of diclofenac by graphene oxide: Optimization, equilibrium, kinetic and thermodynamic studies. **Journal of the Taiwan Institute of Chemical Engineers**, v. 98, p. 150–162, maio 2019.

HO, Y. Review of second-order models for adsorption systems. **Journal of Hazardous Materials**, v. 136, n. 3, p. 681–689, 25 ago. 2006.

HO, Y. S.; JOHN WASE, D. A.; FORSTER, C. F. Batch nickel removal from aqueous solution by sphagnum moss peat. **Water Research**, v. 29, n. 5, p. 1327–1332, maio 1995.

HO, Y. S.; MCKAY, G. A Comparison of Chemisorption Kinetic Models Applied to Pollutant Removal on Various Sorbents. **Process Safety and Environmental Protection**, v. 76, n. 4, p. 332–340, nov. 1998.

HO, Y. S.; MCKAY, G. Pseudo-second order model for sorption processes. **Process Biochemistry**, v. 34, n. 5, p. 451–465, jul. 1999.

HO, Y. S.; WASE, D. A. J.; FORSTER, C. F. Kinetic Studies of Competitive Heavy Metal Adsorption by Sphagnum Moss Peat. **Environmental Technology**, v. 17, n. 1, p. 71–77, jan. 1996.

HOFFMANN, F. et al. Silica-Based Mesoporous Organic–Inorganic Hybrid Materials. **Angewandte Chemie International Edition**, v. 45, n. 20, p. 3216–3251, 12 maio 2006.

HU, L.-X. et al. What is in Nigerian waters? Target and non-target screening analysis for organic chemicals. **Chemosphere**, v. 284, p. 131546, dez. 2021.

HUCKELE, S.; TRACK, T. Risk management of emerging compounds and pathogens in the water cycle (RiSKWa). **Environmental Sciences Europe**, v. 25, n. 1, p. 1, dez. 2013.

IQBAL, A. et al. Recent Advances in Iron Nanoparticles: Preparation, Properties, Biological and Environmental Application. **Journal of Nanoscience and Nanotechnology**, v. 17, n. 7, p. 4386–4409, 1 jul. 2017.

JAIN, M. et al. Development of iron oxide/activated carbon nanoparticle composite for the removal of Cr(VI), Cu(II) and Cd(II) ions from aqueous solution. **Water Resources and Industry**, v. 20, p. 54–74, dez. 2018.

JAMELEDDINE, M. et al. PIN3 Chloroquine and Hydroxychloroquine in COVID-19 with or without Azithromycin: A Systematic Review of in Vitro and Clinical Studies. **Value in Health**, v. 23, p. S545, dez. 2020.

JANUÁRIO, E. F. D. et al. Application of activated carbon functionalized with graphene oxide for efficient removal of COVID-19 treatment-related pharmaceuticals from water. **Chemosphere**, v. 289, p. 133213, fev. 2022.

KABBASHI, N. A. et al. Kinetic adsorption of application of carbon nanotubes for Pb(II) removal from aqueous solution. **Journal of Environmental Sciences**, v. 21, n. 4, p. 539–544, abr. 2009.

KALAISELVI, V. et al. Microwave assisted green synthesis of Hydroxyapatite nanorods using *Moringa oleifera* flower extract and its antimicrobial applications. **International Journal of Veterinary Science and Medicine**, v. 6, n. 2, p. 286–295, dez. 2018.

KANSAL, S. K.; KUMARI, A. Potential of *M. oleifera* for the Treatment of Water and Wastewater. **Chemical Reviews**, v. 114, n. 9, p. 4993–5010, 14 maio 2014.

KHALFAOUI, A. et al. Uptake of Methyl Red dye from aqueous solution using activated carbons prepared from Moringa Oleifera shells. **Cleaner Chemical Engineering**, v. 4, p. 100069, dez. 2022.

KHALID, S. et al. Extraction and Quantification of Moringa oleifera Leaf Powder Extracts by HPLC and FTIR. **Food Analytical Methods**, v. 16, n. 4, p. 787–797, abr. 2023.

KHAWAJA, H. et al. Synthesis and Application of Covalently Grafted Magnetic Graphene Oxide Carboxymethyl Cellulose Nanocomposite for the Removal of Atrazine From an Aqueous Phase. **Journal of Macromolecular Science, Part B**, v. 60, n. 12, p. 1025–1044, 2 dez. 2021.

KINOBE, R. T.; OWENS, L. A systematic review of experimental evidence for antiviral effects of ivermectin and an in silico analysis of ivermectin's possible mode of action against SARS-CoV-2. **Fundamental & Clinical Pharmacology**, v. 35, n. 2, p. 260–276, abr. 2021.

KROGH, K. A. et al. Analysis of the dissipation kinetics of ivermectin at different temperatures and in four different soils. **Chemosphere**, v. 75, n. 8, p. 1097–1104, maio 2009.

KUMAR, K. V. Optimum sorption isotherm by linear and non-linear methods for malachite green onto lemon peel. **Dyes and Pigments**, v. 74, n. 3, p. 595–597, jan. 2007.

KUMARI, M.; KUMAR, A. Can pharmaceutical drugs used to treat Covid-19 infection leads to human health risk? A hypothetical study to identify potential risk. **Science of The Total Environment**, v. 778, p. 146303, jul. 2021.

KURODA, K. et al. Predicted occurrence, ecotoxicological risk and environmentally acquired resistance of antiviral drugs associated with COVID-19 in environmental waters. **Science of The Total Environment**, v. 776, p. 145740, jul. 2021.

KWON, D. H. et al. A point mutation in a glutamate-gated chloride channel confers abamectin resistance in the two-spotted spider mite, *Tetranychus urticae* Koch. **Insect Molecular Biology**, v. 19, n. 4, p. 583–591, ago. 2010.

LANGMUIR, I. THE ADSORPTION OF GASES ON PLANE SURFACES OF GLASS, MICA AND PLATINUM. **Journal of the American Chemical Society**, v. 40, n. 9, p. 1361–1403, set. 1918.

LASOTA, J. A.; DYBAS, R. A. Avermectins, A Novel Class of Compounds: Implications for Use in Arthropod Pest Control. **Annual Review of Entomology**, v. 36, p. 91–117, jan. 1991.

LI, W.-L.; ZHOU, C.-R.; ZHANG, L. Investigation on the decomposition kinetics of Ivermectin. **Journal of Thermal Analysis and Calorimetry**, v. 121, n. 2, p. 797–806, ago. 2015.

LI, Y. et al. Utilizing low-cost natural waste for the removal of pharmaceuticals from water: Mechanisms, isotherms and kinetics at low concentrations. **Journal of Cleaner Production**, v. 227, p. 88–97, ago. 2019.

LIU, J. et al. Adsorption of Congo red dye on FexCo3-xO4 nanoparticles. **Journal of Environmental Management**, v. 238, p. 473–483, maio 2019.

LIU, Y. Is the Free Energy Change of Adsorption Correctly Calculated? **Journal of Chemical & Engineering Data**, v. 54, n. 7, p. 1981–1985, 9 jul. 2009.

LIU, Y.; LIU, Y.-J. Biosorption isotherms, kinetics and thermodynamics. **Separation and Purification Technology**, v. 61, n. 3, p. 229–242, 15 jul. 2008.

LIU, Y.; SHEN, L. A general rate law equation for biosorption. **Biochemical Engineering Journal**, v. 38, n. 3, p. 390–394, mar. 2008.

LOFRANO, G. et al. **Emerging Compounds Removal from Wastewater: Natural and Solar Based Treatments**. Italy: Springer, 2012.

LOU, F. et al. Enhanced kinetics for CO2 sorption in amine-functionalized mesoporous silica nanosphere with inverted cone-shaped pore structure. **Applied Energy**, v. 264, p. 114637, abr. 2020.

LUO, Y. et al. A review on the occurrence of micropollutants in the aquatic environment and their fate and removal during wastewater treatment. **Science of The Total Environment**, v. 473–474, p. 619–641, mar. 2014.

M, R. et al. Modelling and efficiency assessment of the up flow fixed bed process packed with Moringa oleifera for continuous Cd(II) removal from drinking water. **Journal of Molecular Structure**, v. 1236, p. 130328, jul. 2021.

MAGALHÃES-GHIOTTO, G. A. V. et al. Composite hydrogel based on chemically modified gelatin and PVA containing graphene oxide nanoparticles (CHGP-GOn). **Environmental Nanotechnology, Monitoring & Management**, v. 20, p. 100877, dez. 2023.

MAHDAVINIA, G. R.; ETEMADI, H. Surface modification of iron oxide nanoparticles with κ-carrageenan/carboxymethyl chitosan for effective adsorption of bovine serum albumin. **Arabian Journal of Chemistry**, v. 12, n. 8, p. 3692–3703, dez. 2019.

MAMAEVA, V.; SAHLGREN, C.; LINDÉN, M. Mesoporous silica nanoparticles in medicine—Recent advances. **Advanced Drug Delivery Reviews**, v. 65, n. 5, p. 689–702, maio 2013.

MARQUES, S. C. R. et al. Pharmaceuticals removal by activated carbons: Role of morphology on cyclic thermal regeneration. **Chemical Engineering Journal**, v. 321, p. 233–244, ago. 2017.

MARSON, E. O. et al. A review toward contaminants of emerging concern in Brazil: Occurrence, impact and their degradation by advanced oxidation process in aquatic matrices. **Science of The Total Environment**, v. 836, p. 155605, ago. 2022.

MARTIN, R. J.; ROBERTSON, A. P.; CHOUDHARY, S. Ivermectin: An Anthelmintic, an Insecticide, and Much More. **Trends in Parasitology**, v. 37, n. 1, p. 48–64, jan. 2021.

MASALOV, V. M.; SUKHININA, N. S.; EMEL'CHENKO, G. A. Synthesis of Monodisperse Silica Nanoparticles via Heterogeneous Tetraethoxysilane Hydrolysis Using L-Arginine as a Catalyst. **Inorganic Materials**, v. 54, n. 2, p. 156–162, fev. 2018.

MATTHEWS, T.; WILBY, R. L.; MURPHY, C. An emerging tropical cyclone–deadly heat compound hazard. **Nature Climate Change**, v. 9, n. 8, p. 602–606, ago. 2019.

MO, J. et al. A review on agro-industrial waste (AIW) derived adsorbents for water and wastewater treatment. **Journal of Environmental Management**, v. 227, p. 395–405, dez. 2018.

MÓDENES, A. N. et al. Potential of *Salvinia auriculata* biomass as biosorbent of the Cr(III): directed chemical treatment, modeling and sorption mechanism study. **Environmental Technology**, v. 38, n. 12, p. 1474–1488, 18 jun. 2017.

MOODLEY, J. S. et al. Green synthesis of silver nanoparticles from *Moringa oleifera* leaf extracts and its antimicrobial potential. **Advances in Natural Sciences: Nanoscience and Nanotechnology**, v. 9, n. 1, p. 015011, 9 mar. 2018.

MORALES-PAREDES, C. A.; RODRÍGUEZ-DÍAZ, J. M.; BOLUDA-BOTELLA, N. Pharmaceutical compounds used in the COVID-19 pandemic: A review of their presence in water and treatment techniques for their elimination. **Science of The Total Environment**, v. 814, p. 152691, mar. 2022.

MURRAY, S. M. et al. Reduction of Immune Activation with Chloroquine Therapy during Chronic HIV Infection. **Journal of Virology**, v. 84, n. 22, p. 12082–12086, 15 nov. 2010.

NARAYAN, R. et al. Mesoporous Silica Nanoparticles: A Comprehensive Review on Synthesis and Recent Advances. **Pharmaceutics**, v. 10, n. 3, p. 118, 6 ago. 2018.

NASCIMENTO, R. F. et al. **Adsorção: aspectos teóricos e aplicações ambientais**. Fortaleza: Imprensa Universitária, 2014.

NASON, S. L. et al. Changes in Sewage Sludge Chemical Signatures During a COVID-19 Community Lockdown, Part 1: Traffic, Drugs, Mental Health, and Disinfectants. **Environmental Toxicology and Chemistry**, v. 41, n. 5, p. 1179–1192, maio 2022.

NATARAJAN, R. et al. Adsorption performance of magnetic mesoporous silica microsphere support toward the remediation of acetaminophen from aqueous solution. **Journal of Water Process Engineering**, v. 48, p. 102835, ago. 2022.

NAWI, N. S. M. et al. The Impacts of Iron Oxide Nanoparticles on Membrane Properties for Water and Wastewater Applications: a Review. **Arabian Journal for Science and Engineering**, v. 47, n. 5, p. 5443–5464, maio 2022.

NAYAK, P. S.; SINGH, B. K. Instrumental characterization of clay by XRF, XRD and FTIR. **Bulletin of Materials Science**, v. 30, n. 3, p. 235–238, jun. 2007.

NDABIGENGESERE, A.; NARASIAH, K. S.; TALBOT, B. G. Active agents and mechanism of coagulation of turbid waters using Moringa oleifera. **Water Research**, v. 29, n. 2, p. 703–710, fev. 1995.

OLATUNDE, J. O. et al. Determination of pharmaceutical compounds in surface and underground water by solid phase extraction-liquid chromatography. **Journal of Environmental Chemistry and Ecotoxicology**, v. 6, n. 3, p. 20–26, 30 jun. 2014.

OLU-OWOLABI, B. I. et al. Utilizing eco-friendly kaolinite-biochar composite adsorbent for removal of ivermectin in aqueous media. **Journal of Environmental Management**, v. 279, p. 111619, fev. 2021.

PATIDAR, V.; JAIN, P. Green Synthesis of TiO2 Nanoparticle Using Moringa Oleifera Leaf Extract. v. 04, n. 3, mar. 2017.

PETROVIC, M. Analysis and removal of emerging contaminants in wastewater and drinking water. **TrAC Trends in Analytical Chemistry**, v. 22, n. 10, p. 685–696, nov. 2003.

POPP, M. et al. Ivermectin for preventing and treating COVID-19. **Cochrane Database of Systematic Reviews**, v. 2021, n. 10, 28 jul. 2021.

PORTINHO, R.; ZANELLA, O.; FÉRIS, L. A. Grape stalk application for caffeine removal through adsorption. **Journal of Environmental Management**, v. 202, p. 178–187, nov. 2017.

PRAVEENA, S. M. et al. Pharmaceuticals residues in selected tropical surface water bodies from Selangor (Malaysia): Occurrence and potential risk assessments. **Science of The Total Environment**, v. 642, p. 230–240, nov. 2018.

PUBCHEM. **Chloroquine**. **Pub Chem National Center for Biotechnology Information**, 2025. Disponível em: <https://pubchem.ncbi.nlm.nih.gov/>. Acesso em: 7 mar. 2025

QUESADA, H. B. et al. Surface water pollution by pharmaceuticals and an alternative of removal by low-cost adsorbents: A review. **Chemosphere**, v. 222, p. 766–780, maio 2019a.

QUESADA, H. B. et al. Acetaminophen adsorption using a low-cost adsorbent prepared from modified residues of *Moringa oleifera* Lam. seed husks. **Journal of Chemical Technology & Biotechnology**, v. 94, n. 10, p. 3147–3157, out. 2019b.

QUESADA, H. B. et al. Evaluation of novel activated carbons from chichá-do-cerrado (Sterculia striata St. Hil. et Naud) fruit shells on metformin adsorption and treatment of a synthetic mixture. **Journal of Environmental Chemical Engineering**, v. 9, n. 1, p. 104914, fev. 2021.

RĂCUCIU, M.; OANCEA, S. Characterization of the Oxidation of Magnetite Nanoparticles during Their Synthesis by Different Structural Analysis Techniques. **Analytical Letters**, v. 54, n. 1–2, p. 173–183, 22 jan. 2021.

RAMESH, M. et al. Evaluation of acute and sublethal effects of chloroquine (C18H26CIN3) on certain enzymological and histopathological biomarker responses of a freshwater fish Cyprinus carpio. **Toxicology Reports**, v. 5, p. 18–27, 2018.

RAMO, A. et al. Occurrence of Cryptosporidium and Giardia in raw and finished drinking water in north-eastern Spain. **Science of The Total Environment**, v. 580, p. 1007–1013, fev. 2017.

RAVIKUMAR, K.; UDAYAKUMAR, J. *Moringa oleifera* gum composite a novel material for heavy metals removal. **International Journal of Environmental Analytical Chemistry**, v. 101, n. 11, p. 1513–1553, 2 set. 2021.

RECK, I. M. et al. Removal of tartrazine from aqueous solutions using adsorbents based on activated carbon and Moringa oleifera seeds. **Journal of Cleaner Production**, v. 171, p. 85–97, jan. 2018.

RIVERA-UTRILLA, J. et al. Pharmaceuticals as emerging contaminants and their removal from water. A review. **Chemosphere**, v. 93, n. 7, p. 1268–1287, out. 2013.

ROGINSKY, S. Z.; ZELDOVICH, J. **Acta physicochim**. [s.l.] USSR, 1934. v. 1

ROSENBERG, E. S. et al. Association of Treatment With Hydroxychloroquine or Azithromycin With In-Hospital Mortality in Patients With COVID-19 in New York State. **JAMA**, v. 323, n. 24, p. 2493, 23 jun. 2020.

SAHU, D. et al. Applications of different adsorbent materials for the removal of organic and inorganic contaminants from water and wastewater – A review. **Desalination and Water Treatment**, v. 317, p. 100253, jan. 2024.

SANDERS, J. M. et al. Pharmacologic Treatments for Coronavirus Disease 2019 (COVID-19): A Review. **JAMA**, 13 abr. 2020.

SANTOS, R. K. S. et al. Removal of chloroquine from the aqueous solution by adsorption onto açaí-based biochars: Kinetics, thermodynamics, and phytotoxicity. **Journal of Molecular Liquids**, v. 383, p. 122162, ago. 2023.

SAVARINO, A. et al. Effects of chloroquine on viral infections: an old drug against today's diseases. **The Lancet Infectious Diseases**, v. 3, n. 11, p. 722–727, nov. 2003.

SHUKLA, A. et al. Azithromycin and Hydroxychloroquine combination: The future pharmacotherapy of COVID-19. **Journal of Biomedical Sciences**, v. 7, n. 2, p. 54–57, 31 dez. 2020.

SILVESTRE, F. Signaling pathways of oxidative stress in aquatic organisms exposed to xenobiotics. **Journal of Experimental Zoology Part A: Ecological and Integrative Physiology**, v. 333, n. 6, p. 436–448, jul. 2020.

SINDUSFARMA. Indústria farmacêutica projeta crescimento de 12% este ano e 9% no próximo. **Sindicato da Indústria de Produtos Farmacêuticos**, 12 jun. 2024.

SING, K. S. W. et al. Reporting physisorption data for gas/solid systems with special reference to the determination of surface area and porosity. **Pure and Applied Chemistry**, v. 57, n. 4, p. 603–619, 1985.

SIPS, R. On the Structure of a Catalyst Surface. **The Journal of Chemical Physics**, v. 16, n. 5, p. 490–495, maio 1948.

STÖBER, W.; FINK, A.; BOHN, E. Controlled growth of monodisperse silica spheres in the micron size range. **Journal of Colloid and Interface Science**, v. 26, n. 1, p. 62–69, jan. 1968.

TAN, C. G.; BOWEN, B. D.; EPSTEIN, N. Production of monodisperse colloidal silica spheres: Effect of temperature. **Journal of Colloid and Interface Science**, v. 118, n. 1, p. 290–293, jul. 1987.

TOURET, F.; DE LAMBALLERIE, X. Of chloroquine and COVID-19. **Antiviral Research**, v. 177, p. 104762, maio 2020.

TRAN, H. N. et al. Mistakes and inconsistencies regarding adsorption of contaminants from aqueous solutions: A critical review. **Water Research**, v. 120, p. 88–116, set. 2017.

TRAN, H. N.; YOU, S.-J.; CHAO, H.-P. Thermodynamic parameters of cadmium adsorption onto orange peel calculated from various methods: A comparison study. **Journal of Environmental Chemical Engineering**, v. 4, n. 3, p. 2671–2682, set. 2016.

TRIPATHY, J. et al. Advances in Nanoparticles and Nanocomposites for Water and Wastewater Treatment: A Review. **Water**, v. 16, n. 11, p. 1481, 23 maio 2024.

UCHÔA, A. F. J. UNIVERSIDADE FEDERAL DO CEARÁ CENTRO DE CIÊNCIAS DEPARTAMENTO DE QUÍMICA ORGÂNICA E INORGÂNICA PROGRAMA DE PÓS-GRADUAÇÃO EM QUÍMICA. p. 94, 2011.

UEDA YAMAGUCHI, N. et al. A review of Moringa oleifera seeds in water treatment: Trends and future challenges. **Process Safety and Environmental Protection**, v. 147, p. 405–420, mar. 2021.

VERAS, T. B. et al. Analysis of the presence of anti-inflammatories drugs in surface water: A case study in Beberibe river - PE, Brazil. **Chemosphere**, v. 222, p. 961–969, maio 2019.

VIDOVIX, T. B. et al. Evaluation of agro-industrial residue functionalized with iron oxide magnetic nanoparticles for chloroquine removal from contaminated water. **Materials Letters**, v. 326, p. 132915, nov. 2022.

VINCENT, M. J. et al. Chloroquine is a potent inhibitor of SARS coronavirus infection and spread. **Virology Journal**, v. 2, n. 1, p. 69, dez. 2005.

VIOTTI, P. V. et al. Diclofenac removal from water by adsorption on Moringa oleifera pods and activated carbon: Mechanism, kinetic and equilibrium study. **Journal of Cleaner Production**, v. 219, p. 809–817, maio 2019.

WANG, H. et al. A simple room-temperature synthesis of mesoporous silica rods with tunable size and porosity. **Journal of Nanoparticle Research**, v. 15, n. 3, p. 1501, mar. 2013.

WANG, X.-D. et al. Preparation of spherical silica particles by St?ber process with high concentration of tetra-ethyl-orthosilicate. **Journal of Colloid and Interface Science**, v. 341, n. 1, p. 23–29, jan. 2010.

WEBER, W. J.; MORRIS, J. C. Kinetics of Adsorption on Carbon from Solution. **Journal of the Sanitary Engineering Division**, v. 89, n. 2, p. 31–59, 1 abr. 1963.

WERNKE, G. et al. Mathematical modelling applied to the rate-limiting mass transfer step determination of a herbicide biosorption onto fixed-bed columns. **Environmental Technology**, v. 41, n. 5, p. 638–648, 23 fev. 2020.

WORCH, E. **Adsorption technology in water treatment: fundamentals, processes, and modeling**. Berlin ; Boston: De Gruyter, 2012.

ZAMBRI, N. D. S. et al. Utilization of Neem Leaf Extract on Biosynthesis of Iron Oxide Nanoparticles. **Molecules**, v. 24, n. 20, p. 3803, 22 out. 2019.

ZENG, D. et al. Effect of Ammonia Concentration on Silica Spheres Morphology and Solution Hydroxyl Concentration in Stober Process. **Journal of Nanoscience and Nanotechnology**, v. 15, n. 9, p. 7407–7411, 1 set. 2015.

ZHANG, D. et al. Removal of pharmaceuticals and personal care products in aquatic plant-based systems: A review. **Environmental Pollution**, v. 184, p. 620–639, jan. 2014.

ZHAO, D. et al. Triblock Copolymer Syntheses of Mesoporous Silica with Periodic 50 to 300 Angstrom Pores. **Science**, v. 279, n. 5350, p. 548–552, 23 jan. 1998.

ZHU, B.; FAN, T.; ZHANG, D. Adsorption of copper ions from aqueous solution by citric acid modified soybean straw. **Journal of Hazardous Materials**, v. 153, n. 1–2, p. 300–308, maio 2008.

ZOLGHARNEIN, J.; SHAHMORADI, A.; GHASEMI, J. Pesticides Removal Using Conventional and Low-Cost Adsorbents: A Review. **CLEAN – Soil, Air, Water**, v. 39, n. 12, p. 1105–1119, dez. 2011.

CAPÍTULO 3

ARTIGO 2: ENHANCED CHLOROQUINE ADSORPTION USING COBALT-MODIFIED MESOPOROUS SILICAS FOR WATER TREATMENT

De acordo com as normas do Programa de Pós-graduação em Engenharia Química (Resolução nº 142/2023/CTC, Art. 63º), o primeiro artigo foi elaborado e formatado conforme as normas para publicação científica do periódico: *Chemical Engineering and Processing - Process Intensification*.

A revista *Chemical Engineering and Processing - Process Intensification* apresenta uma classificação A1, segundo a plataforma Sucupira-CAPES, possuí fator de impacto de 3.8 e CiteScore 7.8.

DOI: 10.1016/j.cep.2025.110224

ENHANCED CHLOROQUINE ADSORPTION USING COBALT-MODIFIED MESOPOROUS SILICAS FOR WATER TREATMENT

Renata Mariane de Souza[1], Grace Anne Vieira Magalhães-Ghiotto[2], Rosângela Bergamasco[3♣].

[1] State University of Maringa, Department of Chemical Engineering, Graduate Program in Chemical Engineering, Maringa 87020-900, Parana, Brazil. Tel: 55-44-3011-4782, e-mail: renatamarianee@gmail.com. Orcid: 0000-0003-0859-4010.

[2] State University of Maringa, Department of Biotechnology, Genetics and Cell Biology, Graduate Program in Biotechnology, Maringa. State University of Maringa, Department of Biology, Graduate Program in Ecology of Inland Water Ecosystems, Maringa 87020-900, Parana, Brazil. Tel: 55-44-3011-4782, e-mail: gvieiramagalhaes@gmail.com. Orcid: 0000-0002-9750-2853.

[3] State University of Maringa, Department of Chemical Engineering, Graduate Program in Chemical Engineering, Maringa 87020-900, Parana, Brazil. Tel: 55-44-3011-4782, e-mail: rbergamasco@uem.br. Orcid: 0000-0002-2934-6641.

♣ Corresponding author

Rosângela Bergamasco

State University of Maringa, Department of Chemical Engineering, Maringa 87020-900, Parana, Brazil. Tel: 55-44-3011-4782, e-mail: rbergamasco@uem.br.

ABSTRACT

The widespread use of chloroquine (CQ) during the COVID-19 pandemic has led to its accumulation in water bodies due to the inefficiency of wastewater treatment plants (WWTPs). This study synthesized, characterized, and evaluated mesoporous silicas MCM-41 and MCM-48 modified with cobalt oxide nanoparticles for CQ removal. Characterization was conducted to assess the adsorbent properties and their correlation with the adsorption process. The materials exhibited high surface areas (S_{BET} > 369.49 $m^2\ g^{-1}$) and uniform mesoporous structures, confirming their suitability for adsorption and desirable properties for recalcitrant contaminant removal. Adsorption kinetics followed the Elovich model, with equilibrium capacities of 25.3 mg g^{-1} (MCM-41-CoO) and 24.04 mg g^{-1} (MCM-48-CoO), and intraparticle diffusion governed by a multi-step process. Isotherms were best described by the Sips model, with maximum adsorption capacities of 24.78 mg g^{-1} (MCM-41-CoO) and 24.00 mg g^{-1} (MCM-48-CoO) at temperatures ranging from 15 to 45 °C. Thermodynamic parameters indicated a spontaneous, endothermic process with low randomness, suggesting chemical interaction in a monolayer followed by electrostatic interactions. These findings highlight the efficiency of modified mesoporous silicas as adsorbents for CQ, a critical pharmaceutical contaminant, and contribute to developing sustainable water treatment technologies essential for environmental protection and public health.

Keywords: Sustainable water treatment; Adsorption; Pharmaceutical contaminants; Emerging contaminants; Mesoporous silica; Cobalt Oxide Nanoparticles.

10. INTRODUCTION

With advances in medicine, the rapid development of pharmaceutical compounds, and the widespread misuse of self-medication, global pharmaceutical consumption has significantly increased (GHASEMYANI et al., 2022). After consumption, these substances and their metabolites reach rivers and lakes through various pathways, primarily via the discharge of domestic sewage following inefficient treatment in WWTPs (QUESADA et al., 2019a), leading to a major environmental challenge for the decontamination of water bodies.

Although chloroquine (CQ) is a drug indicated for the treatment of autoimmune diseases such as systemic lupus erythematosus, rheumatoid arthritis, and malaria, it was extensively used by the population, particularly in Brazil and the United States, for the treatment of COVID-19 (FOOD AND DRUG ADMINISTRATION, 2020; TOURET; DE LAMBALLERIE, 2020). Studies have reported a significant increase in chloroquine and hydroxychloroquine levels in water sources (KUMARI; KUMAR, 2021; KURODA et al., 2021). For instance, during the pandemic, hydroxychloroquine concentrations reached nearly 50 μg L^{-1} in primary sludge at a U.S. wastewater treatment plant just weeks after the Emergency Use Authorization (NASON et al., 2022).

Wastewater-based epidemiology also revealed a surge in chloroquine usage from 12 g/day to 57 g/day in Greece during the same period (GALANI et al., 2021). Other reports include concentrations of 1.7 μg L^{-1} in Lombardy, Italy (CAPPELLI et al., 2022), 0.071 μg L^{-1} in Vitoria-Gasteiz, Spain (DOMINGO-ECHABURU et al., 2022), and 32 ng L^{-1} in surface waters during the pandemic (KURODA et al., 2021). Pre-pandemic data from Nigeria reported 110 ng L^{-1} in surface waters and up to 5,000 ng L^{-1} in groundwater, with concentrations linked to malaria incidence (HU et al., 2021; OLATUNDE et al., 2014). These findings highlight the transport of chloroquine through domestic sewage, raising concerns about its ecological impact. Despite these observations, comprehensive studies on chloroquine contamination remain limited.

To remove this contaminant from aqueous matrices, various methods, techniques, and technologies have been developed for treating pharmaceutical-

contaminated water (RIVERA-UTRILLA et al., 2013a; WANG; WANG, 2016). Among these treatment methods, adsorption is one of the most widely employed due to its high efficiency in pollutant removal, low implementation cost, and operational simplicity (ALI; ALOTHMAN; AL-WARTHAN, 2016; RIVERA-UTRILLA et al., 2013a). Furthermore, the adsorption process is recognized as an economically viable water treatment technology, with costs varying between US$ 10 and US$ 200 per million liters, compared to other technologies that can reach US$ 450 and generate hazardous byproducts. In addition, adsorption offers advantages such as low energy consumption, favorable operating conditions and the absence of byproducts, highlighting its economic and environmental viability (GRELA; KUC; BAJDA, 2021).

Among the various types of adsorbent materials that have been developed, there are those made from silica. These materials can provide large surface areas (greater than 1,000 $m^2\ g^{-1}$), high pore volume, and a heterogeneous surface (EL-YAZEED et al., 2022; SALAMA; EL-BAHY; MANNAA, 2021). Additionally, some materials are regenerative and possess an ordered and uniform internal structure (BUI; CHOI, 2009; NATARAJAN et al., 2022). Furthermore, the synthesis process allows for the modification and adjustment of pore size, morphology, and surface chemistry, making them more selective and efficient in removing specific contaminants (A. MANNAA; ALTASS; SALAMA, 2021; CASHIN et al., 2018; DOU et al., 2011; IBRAHIM et al., 2021b).

According to (GRELA; KUC; BAJDA, 2021), the channels developed in mesoporous silicas, such as MCM-41, are composed mainly of amorphous SiO_2, which gives the pure material a neutral character that limits or reduces its applications in catalysis or adsorption processes. In this context, incorporating functionalizers emerges as an effective solution to confer properties that enable a more selective and efficient removal of desired compounds. Metallic nanoparticles possess structural and textural characteristics that facilitate the effective removal of organic pollutants (ANDRADE et al., 2022; LIU et al., 2019). Moreover, cobalt oxide nanoparticles are widely utilized in catalysis due to their high oxidative potential (ASPROMONTE et al., 2012; JIAO; FREI, 2009; KARSE; FITE, 2024) In this study, their application focuses on the evaluation of adsorption efficiency while also opening pathways for future research on their potential for catalyst reuse, emphasizing their applicability in sustainable processes.

The versatility of mesoporous silicas, both functionalized and non-functionalized, has led to their synthesis for various applications, such as catalysis (IBRAHIM et al., 2021a; JIAO; FREI, 2009), photocatalysis (EL-HAKAM et al., 2022), gas drying and purification (DOU et al., 2011), biomedicine (CHEN et al., 2020), and contaminated water treatment (CASHIN et al., 2018), among others. Although some studies demonstrate the application of certain types of mesoporous silicas, such as SBA-15 and MCM-41, in the removal of drugs such as diclofenac, carbamazepine, ibuprofen, and tetracycline (AL-SHEHRI et al., 2019; BUI; CHOI, 2009; GRELA; KUC; BAJDA, 2021), there are still few reports in the scientific literature on the use of different types of silicas for removing various drugs from water.

In addition, with the growth of the pharmaceutical market and the constant development of new drugs, this research, aimed at treating contaminated water, presents an innovative nature, making it essential for scientific advancements. In this context, the use of mesoporous silicas for removing chloroquine from contaminated water becomes particularly relevant due to its potential environmental impact, highlighting the originality and importance of this study.

Therefore, the objective of this research was to develop a mesoporous silica-based adsorbent, functionalize it with cobalt oxide, and evaluate its application in the removal of chloroquine from contaminated water, thus making the use of this material novel in the field of contaminant removal.

11. MATERIALS AND METHODS

All experiments conducted in this research took place at the Environmental Management, Control, and Preservation Laboratory (LGCPA), Adsorption and Ion Exchange Laboratory (LATI), and the Research Support Center Complex (COMCAP) at the State University of Maringá (UEM) main campus, in the city of Maringá, PR.

11.1. CHEMICALS AND REAGENTS

Tetraethyl orthosilicate ($C_8H_{20}O_4Si$) (TEOS, Sigma Aldrich, 97.5% purity), Cetyltrimethylammonium bromide ($C_{19}H_{42}BrN$) (CTAB, Inlab, 98%), Ammonium Hydroxide (NH_4OH, Anidrol, 28%) and Ethyl alcohol (C_2H_6O, Synth, 99.5%). The synthesis of cobalt oxide nanoparticles used the following reagents: Vinyl polyalcohol $(CH_2CHOH)_n$ (PVA, Sigma Aldrich, 99.8%), hydrated cobalt nitrate ($Co(NO_3)2.6H_2O$, Sigma Aldrich, 99.9%). For the adsorption studies, Chloroquine diphosphate ($C_{18}H_{32}ClN_3O_8P_2$) (CQN, São Paulo Pharma, Purity > 95%) was diluted in deionized water and the concentration readings were performed on a UV–VIS spectrophotometer (Metash UV-5100, Shangai, CN) with a wavelength of λ=343 nm and standard calibration curve ranging from 1 to 100 mg L^{-1} (R^2 = 0.999). The properties of all reagents used are described in supplementary materials S1.

11.2. SYNTHESIS OF MESOPOROUS SILICA

The synthesis of adsorbents consists of a production method based on the Stöber process, which involves mixing the following reagents: tetraethyl orthosilicate, cetyltrimethylammonium bromide, ammonium hydroxide, and deionized water.

The preparation of the adsorbents was based on the methods proposed by (ZOLA et al., 2016) for the synthesis of MCM-41 and by (SCHUMACHER; GRÜN; UNGER, 1999) for MCM-48. Presenting a molar composition of MCM-41 gel of 1 TEOS: 0.3 CTAB: 11 NH_3: 144 H_2O: 58 EtOH, while MCM-48 was synthesized with a composition of 1 TEOS: 0.4 CTAB: 12.5 NH_3: 174 H_2O: 54 EtOH.

To obtain such molar composition values in the synthesis of MCM-41, 3.67 g of CTAB was initially diluted in 66.9 mL of deionized water. Then, 112.30 mL of the ethanol co-solvent and 25 mL of the 0.5 M ammonium hydroxide solution were added to the becker, after which the mixture was stirred for 15 minutes until the solution became clear in appearance.

Then, while the mixture remained under stirring, 7.5 mL of TEOS was added dropwise, which instantly changed the reaction to a milky white color due to the action of silica. The reaction was maintained under stirring at 300 rpm for 2 hours at room temperature. After that, the mixture was left to rest for 16 hours, allowing for the sedimentation of the gel formed by the reaction.

At the end of the time interval, the resulting precipitate was separated by filtration using a vacuum pump. The precipitate was then washed with deionized water until a neutral pH was reached. The material was subsequently placed in an air circulation oven at 80ºC, where it remained for 24 hours.

Finally, after the material was cleaned and dried, it was calcined in a muffle furnace at 550 ºC for 5 hours with a heating rate of 3 ºC min^{-1}, removing the surfactant molecules present on the surface of the adsorbent and obtaining MCM-41.

The synthesis of MCM-48 followed a preparation methodology similar to that of MCM-41; however, it involved different reagent proportions, using 2.4 g of CTAB dissolved in 50 mL of deionized water, followed by the addition of 50 mL of ethanol and 12 mL of ammonium hydroxide solution, and finally, 3.6 mL of TEOS was added to the reaction.

11.3. SYNTHESIS OF COBALT NANOPARTICLES

The cobalt oxide nanoparticles used for the functionalization of mesoporous silicas were previously prepared by (ANDRADE et al., 2022). Cobalt oxide nanoparticles were synthesized using a modified sol-gel methodology. Initially, 10 g of polyvinyl alcohol (PVA) was dissolved in 100 mL of deionized water and stirred for 2 hours at room temperature. Subsequently, a solution containing 3.67 g of cobalt nitrate, previously dissolved in approximately 20 mL of deionized water, was added to the PVA solution. This resulted in a molar ratio of cobalt nitrate ions to the PVA monomeric unit of 1:18.

The mixture was stirred for an additional 2 hours at room temperature. Then, the temperature was increased to 250ºC and maintained for approximately 5 hours, or until the water had completely evaporated and the PVA had burned. The resulting powder was then calcined in a muffle furnace at 400ºC for 4 hours.

After cooling to room temperature in a desiccator, cobalt oxide (CoO) nanoparticles were obtained.

11.4. FUNCTIONALIZATION OF MESOPOROUS SILICA WITH COBALT NANOPARTICLES

The functionalization occurred from the mixture in a mass proportion % (w/w) of cobalt oxide nanoparticles in each mesoporous silica, varying from 0 to 100%, where 0 represents the absence of cobalt oxide and 100% represents complete presence. Thus, the functionalization occurred by physical mixing the mass proportions and adding deionized water to the mixture. To improve homogenization, the beaker containing the materials was placed in an ultrasound bath (Ultracleaner Unique 1400 A, São Paulo, BR) (KRUATIM; JANTASEE; JONGSOMJIT, 2017) for approximately one hour or until complete homogenization of the solution. The resulting material was then dried in an air circulation oven at 80 ºC, resulting in MCM-41-CoO or MCM-48-CoO.

11.5. ADSORBENTS CHARACTERIZATIONS

For the morphological and textural characterization of the functionalized mesoporous silica adsorbents, the following analyses were used: scanning electron microscopy (SEM) in a FEI Quanta 200 microscope (Eindhoven, Netherlands) operated at 10 kV; Transmission electron microscopy (TEM), was carried out using a JEOL JEM-1250 microscope (CF200-Cu, EMS), operated at 120 kV. The analysis of zeta potential was determined using a Delsa™ NanoC particle analyzer (Beckman Coulter, Brea, CA, USA), immersing 10 mg of each adsorbent, before and after adsorption, in 20 mL of deionized water.

The structural characterization of the samples was performed using X-ray diffraction (XRD) with a Shimadzu LabX 6000 X-ray diffractometer, aiming to identify the crystalline phases and evaluate the crystallinity of the materials. The analysis was conducted using Cu Kα radiation, with a wavelength of λ = 1.5406 Å (40 mA, 40 kV). The diffraction scan was performed in two distinct analyses: one in the 2θ range of 0° to 10°, characterized as low-angle, and the other in the range of 10° to 80°, classified as high-angle. Both analyses were conducted at a

scanning speed of 1°/min. To estimate the average crystallite size, the data obtained in the high-angle XRD analysis were applied to the Scherrer Equation (Equation 1), using data from three peaks of greatest intensity.

$$D = \frac{K.\lambda}{\beta.\cos(\theta)} \quad (1)$$

Where D represents the crystallite size (nm), K is the Scherrer constant, the value of 0.89 being applied related to the spherical approach, λ is the radiation wavelength (nm), **β** is the peak width at half height (rad), and θ corresponds to the Bragg diffraction angle (rad) (ANDRADE et al., 2022). The final result for the average crystallite size was obtained by averaging the data for the three peaks with the highest intensity.

The textural properties were evaluated with physisorption analysis (Linde, > 99.999 % purity) at 77 K and pressures ranging from 1.2×10^{-3} to 0.092 using Micromeritics ASAP 2020 (Norcross, GA, United States of America). Before analysis, the sample was degassed at 1.3×10^{-4} MPa and 200 °C, with a temperature ramp rate of 5 °C min^{-1}, for 6 hours. The specific surface area was determined using the BET equation (BRUNAUER; EMMETT; TELLER, 1938), and the pore volume was calculated using single-point adsorption at $P/P_0 = 1$.

The chemical composition of the materials synthesized as mesoporous silicas of the MCM-41 and MCM-48 type functionalized with cobalt oxide was characterized using an Energy Dispersive X-ray Fluorescence Spectrometer (EDX-720, Shimadzu). Furthermore, to characterize the functional groups present in the adsorbents before and after CQ adsorption, Fourier transform infrared spectroscopy (FT-IR) analysis was performed using a Bruker Vertex 70v spectrometer (Germany) from 4000 to 400 cm^{-1}, with a nominal resolution of 4 cm^{-1} and 128 scans. The adsorbents were mixed with KBr in a 1:100 (w/w) proportion.

11.6. BATCH ADSORPTION STUDIES

All batch adsorption tests were performed in a shaker with temperature control and a fixed rotation speed of 150 rpm (TECNAL, TE-424, Piracicaba, SP, BR). The adsorption studies were conducted in duplicate using airtight flasks containing 25 mL of the CQ solution at a concentration of 50 mg L^{-1}. The CQ

solution was prepared by diluting the stock solution, which was previously obtained by dissolving a specific amount of CQ powder in deionized water to achieve a concentration of 500 mg L^{-1}. The stock solution was then stored in an amber bottle in a dark environment at room temperature (approximately 23 °C).

The adsorption experiments were followed by effect studies, evaluating the impact of mass and pH. The first effect study varied the adsorbent dosage from 1 to 4 g L^{-1}, while the second study adjusted the pH of the CQ solution from pH 2 to pH 8. Both effect studies were conducted at 25°C with a contact time of 24 hours.

Based on the experimental data from the effect studies, the ideal conditions for the maximum adsorption capacity of CQ were determined, allowing the continuation of the adsorption kinetics study. In this study, the contact time between the adsorbent and adsorbate was varied from 0 to 15 hours at 25°C. The equilibrium isotherms were evaluated by changing the initial concentration of CQ from 0 to 300 mg L^{-1} at temperatures ranging from 15°C to 45°C, with a contact time of 24 hours to ensure adsorption equilibrium.

To evaluate the reuse process, each adsorbent material impregnated with CQ was subjected to a new contact with 25 mL of CQ solution at 50 mg L^{-1} and kept under agitation for 24 hours at 25°C. Afterward, the material underwent filtration and was dried in an oven at 80°C for 24 hours. Subsequently, the material was again subjected to experimental adsorption tests, with the adsorption cycles being repeated.

The calculation of the adsorption capacity of each sample and the estimation of the adsorption percentage were obtained using equations 2 and 3, respectively.

$$q_e = \frac{(C_0 - C_e).V}{m} \tag{2}$$

$$\% \text{ removal} = \frac{(C_0 - C_e) \,.\, 100}{C_0} \tag{3}$$

Where qe is the adsorption capacity at equilibrium (mg g^{-1}), C_0 and C_e are the initial and final concentrations, respectively (mg L^{-1}), V is the volume of the solution (L), and m is the mass of the adsorbent (g).

Thus, the experimental kinetic data were fitted to the pseudo-first order, pseudo-second order, and Elovich models. The experimental equilibrium

isotherm data were fitted to the Langmuir, Freundlich, and Sips models. From the fitting to the most appropriate isothermal model, the equilibrium constant (K_c) was extracted, which was subsequently used to obtain the thermodynamic parameters related to the adsorption process, such as the Gibbs free energy (Equation 4).

$$\Delta G° = -R.T.ln(K_c) \quad (4)$$

Where ∆Gº is the Gibbs free energy (kJ mol^{-1}), R is the ideal gas constant (0.008314 kJ mol^{-1} K^{-1}), T is the temperature (K), and K_c is the equilibrium constant, obtained from the best fit to the equilibrium isotherm model.

Finally, the thermodynamic parameters of enthalpy (∆Hº) and entropy (∆Sº) were obtained through the graph of ln (K_c) versus 1/T (Equation 5). From the equation of the line, the slope and intercept correspond to the enthalpy and entropy, respectively.

$$\ln(K_c) = \frac{\Delta S}{R} - \frac{\Delta H}{RT} \quad (5)$$

Where ∆Hº represents the enthalpy (kJ mol^{-1}), ∆Sº represents the entropy (kJ mol K^{-1}), T is the temperature (K), and K_c is the equilibrium constant.

12. RESULTS AND DISCUSSION

12.1. OPTIMAL ADSORBENT FUNCTIONALIZATION RATIO

To enhance the adsorption of chloroquine, cobalt oxide nanoparticles were incorporated into MCM-41 and MCM-48 to functionalize the adsorbent surface. Based on the methodology presented in section 2.3, the proportion of cobalt oxide in the synthesized mesoporous silicas was varied. The proportions tested were 5 %, 10 %, 15 %, 20 %, 25 %, 50 %, and 75 %. Additionally, samples with 0 % cobalt oxide (representing only mesoporous silica) and 100 % cobalt oxide (representing only the nanoparticles) were also tested.

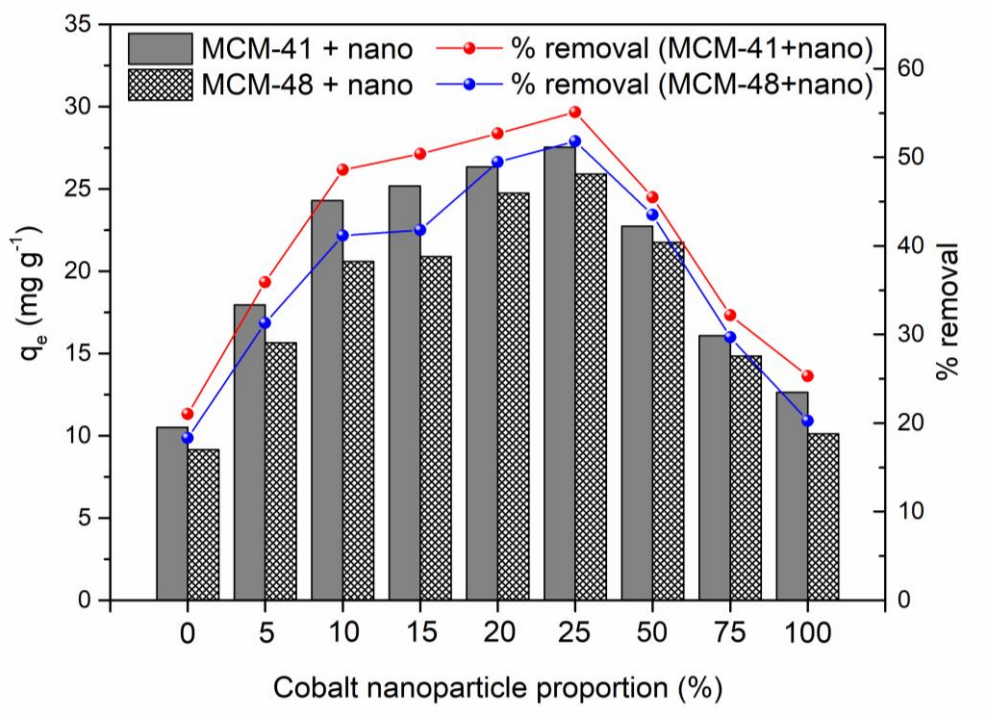

Figure. 1. Influence of cobalt oxide nanoparticle proportion in mesoporous silicas (MCM-41 and MCM-48) on chloroquine removal. The bar graph shows adsorption capacity (q_e), and the line plot represents removal percentage. The 25% proportion achieved the highest adsorption capacity (q_e > 25 mg g^{-1}) and removal efficiency (%removal > 50%).

After the adsorption test of the materials with CQ, Figure 1 shows that the best adsorption capacity was observed in both mesoporous silicas functionalized with 25 % cobalt oxide. The graph also indicates that the presence of only mesoporous silicas, such as MCM-41 and MCM-48, as well as their complete absence, resulted in lower adsorption capacity compared to other adsorbents containing both cobalt oxide and mesoporous silica, highlighting a positive chemical interaction between the materials in the CQ adsorption process. Therefore, the 25 % cobalt oxide ratio was selected for further adsorbent synthesis.

Although the application of MCM-41-CoO and MCM-48-CoO in the adsorption process is innovative, other studies have also demonstrated the chemical interaction of these materials. For instance, (ASPROMONTE et al., 2012) produced cobalt oxide nanoparticles deposited on MCM-41 using the reactive supercritical CO_2 deposition method. While this method allows material synthesis in a single container, it requires impregnation under supercritical CO_2 conditions, which involve high temperature and pressure. In contrast, the functionalization methodology used in the present work differs from that of

(ASPROMONTE et al., 2012), as the preparations were carried out in a simplified manner using beakers and without the application of pressure.

(SALAM; ABUKHADRA; MOHAMED, 2020) also highlight the interaction between cobalt oxide and mesoporous silica, synthesized using glass waste as a precursor for MCM-41 and cobalt oxide nanoparticles obtained through green synthesis from green tea leaf extract. The resulting green nanocomposite was successfully applied in the catalytic oxidation of the pesticide methyl parathion, demonstrating effective contaminant degradation.

Therefore, the incorporation of 25% cobalt oxide increased the available adsorption sites, thereby enhancing the adsorption efficiency of CQ onto the newly synthesized materials, MCM-41-CoO and MCM-48-CoO.

12.2. CHARACTERIZATION OF ADSORBENTS

The synthesized materials were characterized by several analyses, including Scanning Electron Microscopy (SEM) images, as shown in Figure 2.

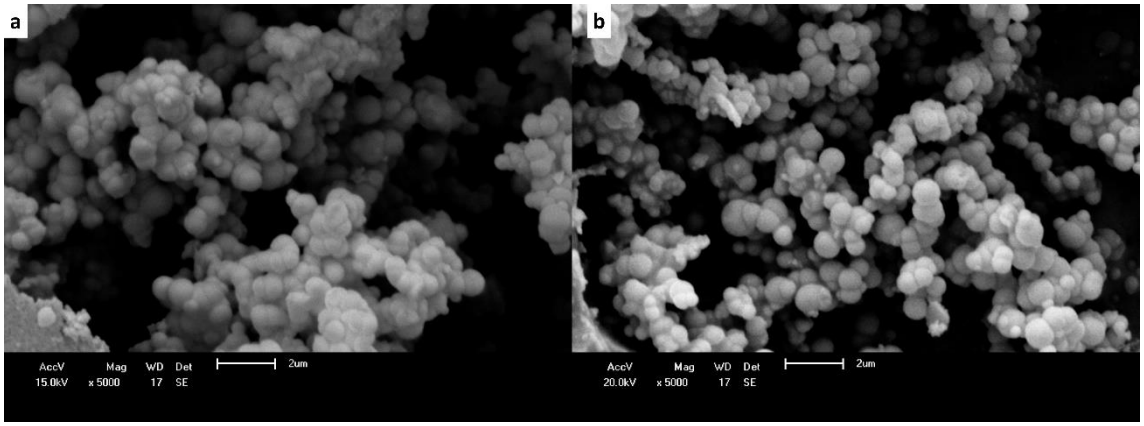

Figure. 2. SEM images of synthesized mesoporous silica spheres: (a) MCM-41-CoO and (b) MCM-48-CoO. Both materials exhibit spherical morphology with particle agglomeration, showing a uniform size around 0.8 µm.

From the images presented in Figure 2, it can be observed that the mesostructure of the materials reveals the formation of silica spheres in both synthesized samples, exhibiting a uniform appearance with minimal variations in diameter. As a result, the average particle sizes were determined to be 0.78 µm for MCM-41-CoO and 0.81 µm for MCM-48-CoO, confirming the low variation in particle size and shape, which aligns with the expected characteristics of the Stöber method used for material synthesis. According to (WU; MOU; LIN, 2013),

this method enables the production of uniform mesoporous silicas with particle sizes that can vary depending on the proportion of the silica precursor (TEOS) and the pH of the reaction.

In addition to the SEM images, Transmission Electron Microscopy (TEM) images were obtained to evaluate the structural organization of the nanoparticles, as shown in Figure 3.

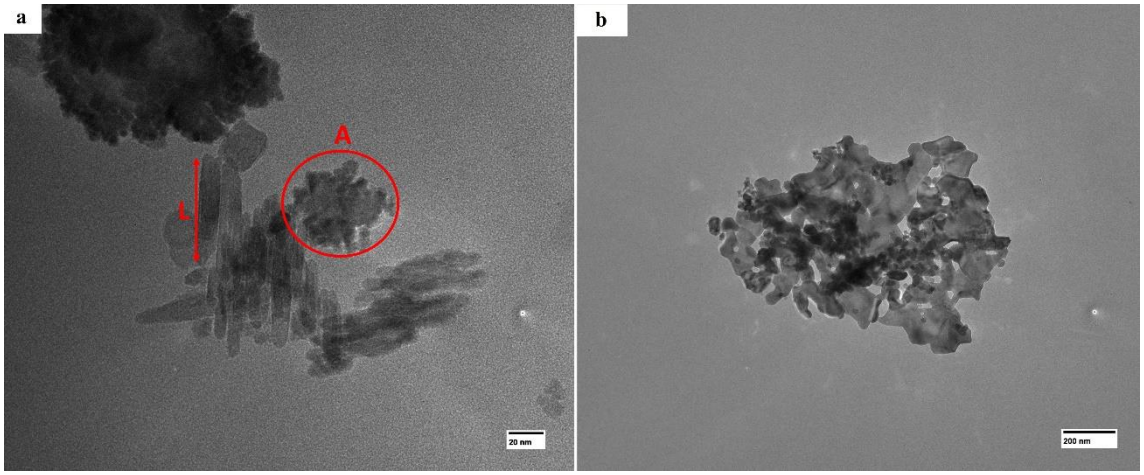

Figure. 3. TEM images of synthesized mesoporous silica spheres: (a) MCM-41-CoO at 20 nm, showing a tubular structure (L) and a honeycomb-like hexagonal arrangement (A), indicating the axial view of mesoporous channels; (b) MCM-48-CoO at 200 nm, revealing an interconnected mesoporous network without apparent cubic symmetry. Dark regions suggest the presence of cobalt oxide.

(CAI et al., 2001) synthesized and characterized MCM-41 mesoporous silica with a hexagonal structure, distinguished by ordered cylindrical channels. In the TEM image, specifically in the central part of Figure 3a, MCM-41-CoO exhibits the typical hexagonal structure of MCM-41, visible from both a side view (L) and a top view of the nanotubes (A).

The functionalization of the material with cobalt oxide (CoO) is confirmed by the presence of dark particles dispersed throughout the silica matrix. These CoO particles indicate a homogeneous distribution within the pores of MCM-41, which is crucial for maximizing contaminant adsorption efficiency, as evidenced by the cobalt oxide ratio results presented in Figure 1.

In a study conducted by (ASPROMONTE et al., 2012), cobalt oxide particles were dispersed in mesoporous silicas, specifically MCM-41 and Al-MCM-41, using the supercritical deposition technique. The authors also reported results regarding the dispersion of cobalt oxide on the silica support. Additionally, they found that the cobalt oxide particles ranged in size from 15 to 20 nm.

However, these data could not be verified in the TEM images of this study, as the cobalt oxide particles were completely dispersed within the MCM-41 and MCM-48 silicas, making it impossible to visually measure the particle size. MCM-48 features a three-dimensional cubic structure with interconnected channels (AKPOTU; MOODLEY, 2018; BORCĂNESCU et al., 2023; SCHUMACHER; GRÜN; UNGER, 1999). As shown in Figure 3b, several interconnected channels form a complex mesoporous network. However, it is also evident that there is no clear cubic organization or symmetry in the TEM image of MCM-48-CoO.

Similar to the MCM-41-CoO images, the darker particles in the MCM-48-CoO image represent the distribution of cobalt oxide within the mesoporous silica matrix. Therefore, the presence of these dark particles makes it more difficult to observe the cubic symmetry in the image.

X-ray diffraction (XRD) analysis was conducted to characterize the crystallinity of the CoO, MCM-41-CoO, and MCM-48-CoO samples and to compare the diffraction profiles of the modified samples with those of the precursor materials (Figure 4).

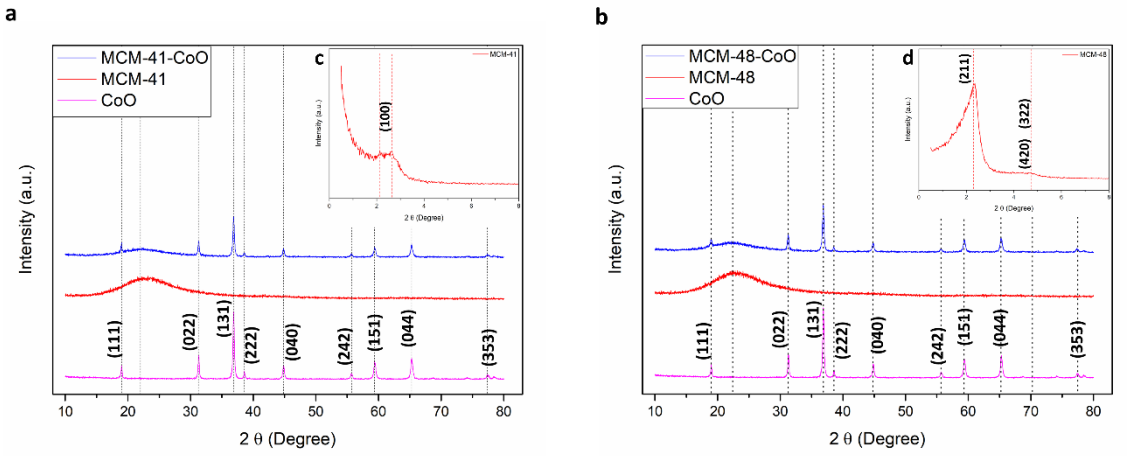

Figure. 4. Comparison of XRD patterns of mesoporous silica spheres. (a) The high-angle spectra of MCM-41, MCM-41-CoO, and CoO, and (b) MCM-48, MCM-48-CoO, and CoO show the combined spectral profiles, confirming cobalt oxide deposition. The insets display low-angle XRD: (c) MCM-41, showing a low-intensity band in the (100) region, possibly influenced by pH during synthesis, and (d) MCM-48, exhibiting a (211) peak but without a complete reflection pattern.

As illustrated in Figure 4, both MCM-41-CoO and MCM-48-CoO exhibit predominant crystallinity, maintaining the characteristic structural pattern of cobalt oxide (CoO) in the synthesized materials. This suggests that the deposition of CoO on the mesoporous materials did not compromise their original crystalline structure but merely incorporated the cobalt oxide nanoparticles.

Figures 4a and b show that the high-angle XRD spectra for MCM-41 and MCM-48 exhibit a broad reflection between 2θ angles of 15° to 31° for both materials without CoO deposition. According to (SARMA; KUMAR; GUPTA, 2024), the XRD pattern observed in the angular range of 2θ from 20° to 35° is characteristic of SiO_2 nanoparticle materials. Consistent with the MCM-41 and MCM-48 samples, which were synthesized using TEOS, a silica precursor reagent, the presence of these reflections confirms their silica composition.

The low-angle XRD patterns of the unfunctionalized mesoporous materials, MCM-41 and MCM-48, presented in Figures 4c and d, respectively, reveal distinct structural characteristics.

As shown in Figure 4c, the diffraction patterns obtained for the MCM-41 sample exhibit a band reflection in the region between $2.14º < 2\theta < 2.64º$, with a low-intensity (100) peak and the absence of the expected peaks in the regions of $3.5º < 2\theta < 4.8º$ and $5.6º < 2\theta < 6.7º$, which are attributed to the (110), (200), and (210) reflections, indicative of a well-ordered hexagonal structure (ABU-ZIED; HUSSEIN; ASIRI, 2014). Therefore, it is suggested that the synthesis of the mesoporous MCM-41 material resulted in poor formation of hexagonal channels.

According to research by (ABU-ZIED; HUSSEIN; ASIRI, 2014), increasing the pH to values above 10.5 during the synthesis of mesoporous materials, such as MCM-41, can significantly reduce the intensity of the (100) peak, indicating a reduction in the structural order of the material.

In this sense, adding a high amount of ammonia solution during the material synthesis may have increased the pH of the mixture to values above 10, which would explain the results observed in Figure 4c. Despite the less ordered structure, the synthesized and functionalized adsorbent demonstrated promising results in chloroquine removal from contaminated water. Thus, the introduction of cobalt oxide likely contributed to the formation of active sites, offsetting the reduction in structural order.

The diffraction pattern obtained for the MCM-48 material (Figure 4d) differs from that of MCM-41, exhibiting a more intense and well-defined diffraction peak at $2\theta = 2.3°$, attributed to the (211) reflection. Additionally, a low-intensity band around $2\theta \approx 4.7°$ is observed, associated with slight reflections of (420) and (322), characteristic of a cubic mesoporous structure (MOREY et al., 2000; SCHUMACHER; GRÜN; UNGER, 1999). However, the peak corresponding to

the (220) reflection, which is typically located near the end of the (211) peak, was not identified in the material synthesized in this study. This absence can be attributed to the surfactant removal method used, as, according to (SCHUMACHER et al., 2000), thermal treatment by calcination may result in lower-quality materials compared to those obtained through hydrothermal treatment.

Although the diffraction patterns of both MCM-41 and MCM-48 indicate limitations in structural purity, ordering, and synthesis quality, both materials exhibited significant adsorption capacities.

For high-angle XRD analysis, well-defined diffraction peaks in the CoO spectrum appear at 2θ angles of 18.99° (111), 31.27° (022), 36.84° (131), 38.55° (222), 44.81° (040), 55.66° (242), 59.36° (151), and 65.24° (044), confirming the identification of the compound as cobalt oxide. This result corroborates previous studies indicating the high crystallinity of cobalt oxide nanoparticles, with pronounced peaks at similar angles, such as 18.99°, 36.84°, 38.55°, 44.81°, 59.36°, and 65.24° (AL-SENANI; DERAZ; ABD-ELKADER, 2020; KARSE; FITE, 2024). The persistence of these peaks in the spectra of the synthesized materials confirms the structural stability of CoO after incorporation into the mesoporous supports.

Furthermore, the most intense peaks, corresponding to the planes (131), (040), (022), and (151), suggest that the crystallites of the CoO sample are preferentially oriented along these indicated planes, as shown in Table 1.

Table. 1. Position 2θ, d-spacing values, full width at half maximum (FWHM), and prominent peak intensities of pure CoO.

CoO						
2θ	**Indices**			**d-spacing (A)**	**FWHM (2thº)**	**Intensity (%)**
	h	**k**	**l**			
18.98	1	1	1	4.67348	0.13780	16.7
31.26	0	2	2	2.86075	0.19680	32.7
36.86	1	3	1	2.43798	0.17710	100.0
38.56	2	2	2	2.33440	0.11810	8.2
44.83	0	4	0	2.02148	0.27550	18.4
55.67	2	4	2	1.65104	0.19680	7.6
59.38	1	5	1	1.55644	0.27550	25.8
65.24	0	4	4	1.42996	0.23620	29.1
74.17	3	5	3	1.27847	0.31490	1.7

77.43	3	5	3	1.23258	0.39360	5.0
78.42	2	6	2	1.21945	0.47230	3.1

Using the three most intense peaks at 36.86º, 31.26º, and 65.24º, the Scherrer Equation was applied to estimate the crystallite size of CoO, as described in the methodology. The results are presented in Table 2.

Table. 2. Estimation of average crystallite size based on the Scherrer Equation.

2θ (º)	Peak θ (º)	Peak (rad)	FWHM (º)	FWHM (rad)	Diameter (Å)	Diameter (nm)
36.86	18.43	0.3216	0.1771	0.003091	467.3917	46.73
31.26	15.63	0.2727	0.1968	0.003435	414.3546	41.43
65.24	32.62	0.5693	0.2362	0.004122	394.7344	39.47
					Average diameter	**42.54**

The average crystallite size of the cobalt oxide nanoparticles was 42.54 nm. This result is consistent with other studies, such as (GUL et al., 2020), which reported an average size of 30.6 nm, and (ATHAR et al., 2012), which obtained approximately 50 nm for CoO. Variations in the crystallite size are expected due to differences in the synthesis conditions of the materials being compared.

Figure 5 shows the nitrogen sorption isotherms of the samples, both with and without the deposition of cobalt oxide nanoparticles.

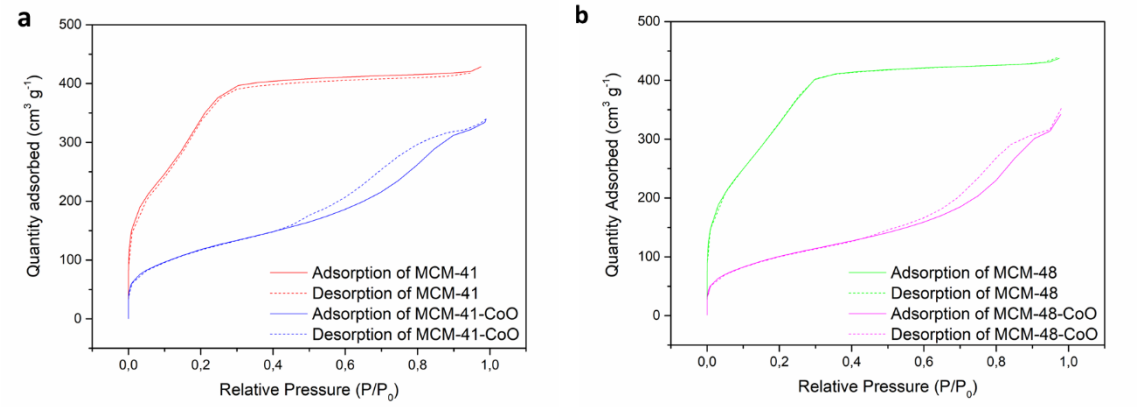

Figure. 5. N_2 sorption isotherms: (a) MCM-41 and MCM-41-CoO, and (b) MCM-48 and MCM-48-CoO, displaying both adsorption and desorption curves. The modified materials exhibit a type IV isotherm with a well-defined H1-type hysteresis loop, indicating a uniform mesoporous structure, whereas the unmodified mesoporous silica samples do not show any evident hysteresis.

It is observed that the isotherms for the MCM-41-CoO and MCM-48-CoO materials correspond to type IV in the classification by the International Union of Pure and Applied Chemistry (IUPAC), which is characterized by typical

adsorption behavior in mesoporous solids (ROUQUEROL; ROUQUEROL; SING, 1999). The formation of hysteresis in the N_2 adsorption and desorption isotherms is attributed to capillary condensation in mesoporous materials, which is crucial for determining both the pore size distribution and the pore structure of the material (HORIKAWA; DO; NICHOLSON, 2011).

The isotherm curves for the modified materials, such as MCM-41-CoO and MCM-48-CoO, exhibit a well-defined hysteresis loop, similar to the H1-type loop in the IUPAC classification. In contrast, the original mesoporous silicas do not display a well-defined hysteresis loop. According to (HORIKAWA; DO; NICHOLSON, 2011) and (OLIVEIRA; ANDRADA, 2019), the H1-type hysteresis loop is characterized by symmetrical curves and similar, parallel adsorption and desorption curves. Additionally, these curves exhibit gradual convergence at the lower limit of the hysteresis loop. The authors also note that this type of hysteresis is typical for adsorbent materials with regular, uniform pore distribution and open ends, such as cylindrical and regular polyhedral pores, which are commonly found in solids like the MCM-41 and SBA-15 types.

When comparing the isotherm curves of the unmodified adsorbents with those modified by the deposition of cobalt oxide nanoparticles, a widening of the hysteresis is observed. This suggests that the deposition has altered the material's pore diameter, a change that is further supported by the data presented in Table 3.

Table. 3. Textural parameters of the original mesoporous silicas (MCM-41 and MCM-48) and those modified by the deposition of cobalt oxide nanoparticles (MCM-41-CoO and MCM-48-CoO).

Materials	S_{BET} (m^2g^{-1})	V (cm^3g^{-1})	Pore size (nm)	Average Particle Size (nm)
MCM-41	1356.70	10.3733	30.58	4.42
MCM-41-CoO	431.27	0.5258	4.87	13.91
MCM-48	1291.52	0.9005	2.78	4.64
MCM-48-CoO	369.49	9.2991	100.66	16.23

It can be seen from the data presented in Table 3 that the deposition of cobalt oxide nanoparticles onto mesoporous silicas caused a decrease in the specific surface area (S_{BET}) of the adsorbents. The modified materials, MCM-41-CoO and MCM-48-CoO, showed a reduction of approximately 68 % and 71 % in surface area, respectively, compared to the original forms (MCM-41 and MCM-

48). (ASPROMONTE et al., 2012) observed a reduction of about 20 % in the surface area of mesoporous silica MCM-41 after the addition of cobalt oxide via supercritical deposition. However, the smaller decrease in this study could be attributed to the lower amount of cobalt oxide used by the authors (4.3 wt.%). Similarly, (WANG et al., 2021) reported a 40 % and 75 % reduction in the surface area of MCM-48 after incorporating different concentrations of cobalt into the material.

This decrease can be attributed to the partial blocking of the pores by the deposition of cobalt oxide nanoparticles. This also explains the reduction in pore volume observed in the MCM-41-CoO material, particularly due to its cylindrical structure, which facilitates the filling and/or obstruction of the adsorbent pores. However, for MCM-48-CoO, the increase in pore volume can be explained by its three-dimensional cubic structure, which allows for better distribution of the nanoparticles. Additionally, the fusion or agglomeration of materials, as observed in the TEM analysis in Figure 3, could create additional spaces, thus increasing the effective pore volume.

Characterization was carried out using Fourier transform infrared spectroscopy (FTIR) to identify the structural characteristics and functional groups present in the materials. These functional groups are crucial for understanding the mechanisms involved in the adsorption processes.

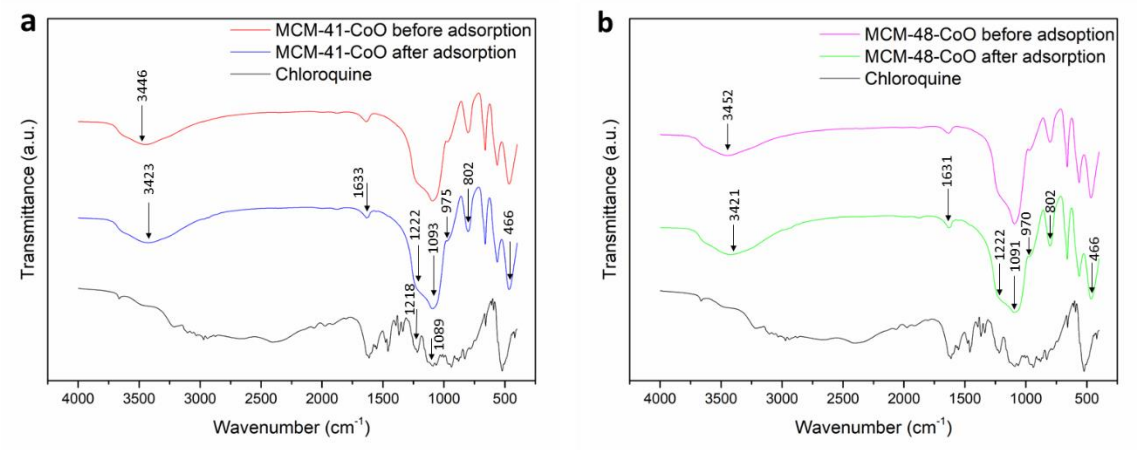

Figure. 6. FTIR spectra: (a) MCM-41-CoO and (b) MCM-48-CoO, showing surface functional groups before and after adsorption. Characteristic peaks confirm the deposition of CoO and its interactions with chloroquine, as evidenced by shifts and changes in intensity, particularly in the silanol groups (Si−OH), suggesting hydrogen bonding as the mechanism of interaction between the adsorbent and the adsorbate.

In the images presented by means of the spectrogram of the materials MCM-41-CoO and MCM-48-CoO before adsorption, characteristic peaks can be observed at 3411, 1585, 1222, 1093, 979, 804 and 466 cm^{-1}, as well as at 3421, 1631, 1222, 1091, 973, 802, 659, 565 and 465 cm^{-1} for the two materials, respectively. These peaks may be associated with the OH stretching and bending vibrations in the silanol group, seen at 3411 and 1585 cm^{-1} in MCM-41-CoO, and at 3421 cm^{-1} and 1631 cm^{-1} in MCM-48-CoO, respectively, associated with the presence of adsorbed water on the materials (CHOONG et al., 2024). The presence of compacted silica can be attributed to the signals represented by the shoulder of the band at 1222 cm^{-1}, as well as the peaks at 802 and 466 cm^{-1}, due to the Si−O−Si bond (siloxane bonds) in MCM-41-CoO and in the MCM-48-CoO sample (KALITA; TALUKDAR, 2024). Additionally, the internal vibrations of the Si−O bond are represented by the signals at 1093 and 1091 cm^{-1} in MCM-41-CoO and MCM-48-CoO, respectively (ZHOLOBENKO et al., 1997). The presence of cobalt oxide nanoparticles is confirmed by the signals at 975 cm^{-1} for MCM-41-CoO and 970 cm^{-1} for MCM-48-CoO, which correspond to the Co−O−Si bonds, verifying the successful deposition of CoO on the adsorbents (MOREY et al., 2000). According to (CHOONG et al., 2024), the shoulder presented around the signals at 965 cm^{-1} may suggest the anchoring site of Co in the MCM-41 materials.

The interaction between the contaminant and the functional groups present in the adsorbent can be demonstrated by slight shifts and changes in intensity in the signals (MAGALHÃES-GHIOTTO et al., 2023). After adsorption, a slight shift of the peaks from 3452 to 3421 cm^{-1} and from 1095 to 1091 cm^{-1} is observed in the MCM-48-CoO samples, which also presented peak-to-band changes, with signal broadening and an increase in transmittance intensity (VIDOVIX et al., 2022).

The interactions of MCM-41-CoO with the contaminant can be evidenced by the intensification, attenuation, and shift of peaks in the spectra before and after the adsorption process. As with MCM-48-CoO, MCM-41-CoO also showed a slight shift of the peak from 3446 cm^{-1} to 3423 cm^{-1}, demonstrating that the silanol group (Si−OH), present in both materials, interacts with the chloroquine molecules, possibly through hydrogen bonding. In Figure 6, it can be observed

that there was an intensification of the peaks at 1222, 1093, 975, 802, and 466 cm^{-1}, especially the shoulder of the band at 1222 and 1093 cm^{-1}, which became more defined and elongated. This modification can be attributed to interactions with the peaks near 1218 and 1089 cm^{-1}, present in the chloroquine spectrum, which, according to (DODDAGA; PEDDAKONDA, 2013), correspond to the bonds between C−N and C−Cl molecules, respectively.

In addition to these interactions identified by FTIR, X-ray fluorescence (XRF) analysis was performed to determine the chemical composition of the synthesized adsorbents, as shown in Figure 7.

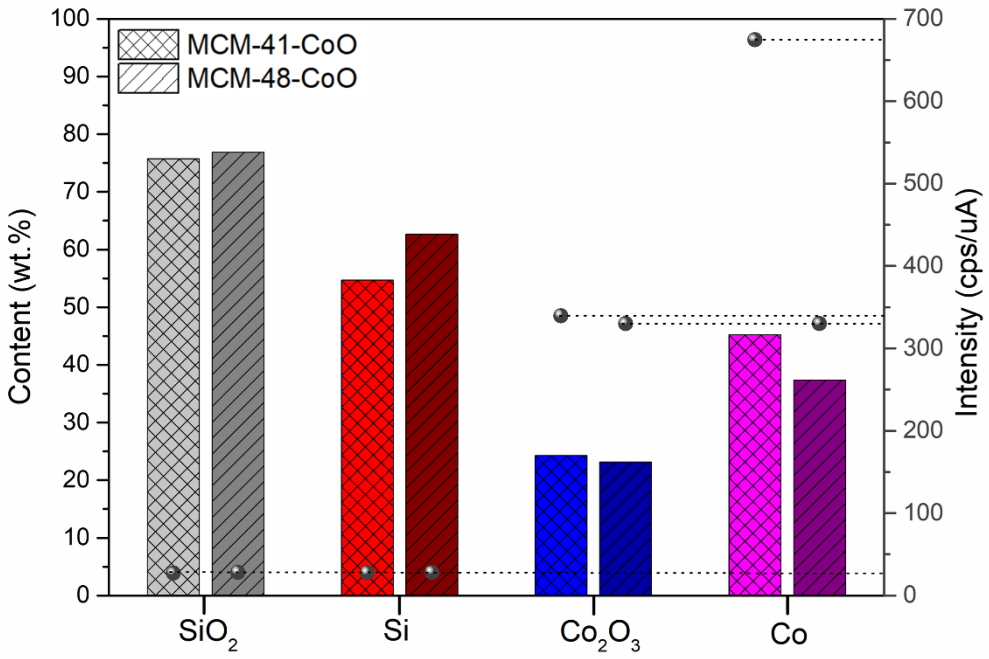

Figure. 7. Chemical composition of MCM-41-CoO and MCM-48-CoO materials obtained from XRF analysis. The bars represent the number of identified elements (left Y-axis), while the dots indicate detection intensity (right Y-axis). The figure shows a predominant silicon dioxide (SiO_2) content of 75.73 % and 76.84 %, respectively, along with cobalt oxide (Co_2O_3) at 24.28 % and 23.15 %, confirming successful functionalization.

X-ray fluorescence analysis revealed the predominant presence of silicon dioxide (SiO_2) in both materials, with approximately 75.73 % in MCM-41-CoO and 76.84 % in MCM-48-CoO. Additionally, cobalt oxide (Co_2O_3) was detected in amounts of 24.28 % and 23.15 % in MCM-41-CoO and MCM-48-CoO, respectively, confirming the functionalization proportion of the synthesized adsorbents.

Furthermore, in elemental proportion, the XRF analysis demonstrated a quantitative detection of Si of approximately 55 % in both materials, correlating with the presence of TEOS as a silica precursor reagent. The elemental quantitative detection of Co was 45.19 % in MCM-41-CoO and 42.58 % in MCM-48-CoO, confirming the successful incorporation of cobalt oxide into the synthesized mesoporous structure.

In addition to the chemical composition of the adsorbent materials, colloidal stability and electrostatic interactions are also important factors in evaluating the adsorption potential of modified mesoporous silicas for CQ removal. To assess these properties, zeta potential analysis was performed for both MCM-41-CoO and MCM-48-CoO, as shown in Figure 8.

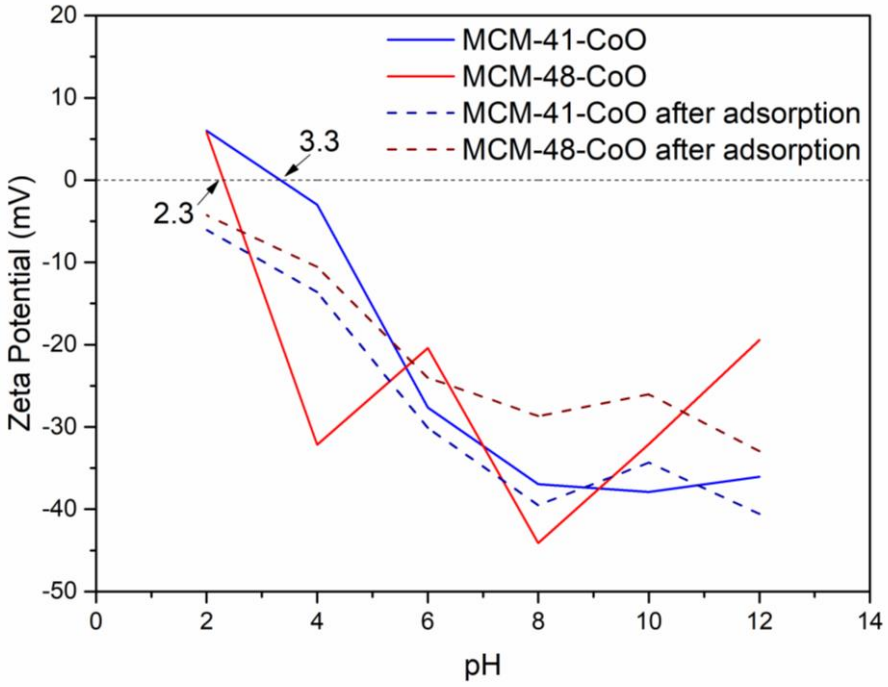

Figure. 8. Zeta potential of MCM-41-CoO and MCM-48-CoO before and after adsorption, illustrating surface charge behavior. The isoelectric points are 3.3 for MCM-41-CoO and 2.3 for MCM-48-CoO, with a negative charge above these pH values, indicating potential electrostatic interactions during the adsorption process.

As shown in Figure 8, both synthesized solids exhibited a wide pH range with a negative surface charge, indicating low pH values for the isoelectric point (Pie), 3.3 for MCM-41-CoO and 2.3 for MCM-48-CoO. According to (LIU et al., 2014), the isoelectric point corresponds to the pH at which the number of positive and negative charges on the material's surface are balanced, resulting in an electrically neutral surface. Therefore, in solutions with a pH lower than the

isoelectric point, the adsorbent surface carries a positive charge, whereas at pH values above the isoelectric point, the surface becomes negatively charged. Still, Figure 8 shows that the adsorbent's isoelectric profile presents similar characteristics before and after adsorption, exhibiting a negative surface charge.

Several previously published studies on mesoporous silicas have demonstrated that these solids typically have low isoelectric points (Pie ≈ 2.5 to 3.0) and, in most cases, exhibit a negatively charged surface (LI et al., 2025; MIN et al., 2024; TIAN et al., 2025), aligning with the results obtained in this research.

According to (MAGALHÃES-GHIOTTO et al., 2023), chloroquine has three pKa values—4, 8.4, and 10.2—which directly influence its protonation state. The authors explain that in solutions with pH < 7, chloroquine exists in a di-protonated form; when the pH is close to 8, it loses one proton, remaining in its mono-protonated form; and at pH > 10, the molecule loses all protons, presenting an anionic form with negative charges.

Based on the pKa values of chloroquine and the isoelectric points of the adsorbent materials, it can be inferred that electrostatic interactions play a crucial role in the adsorption process. At pH values below the isoelectric points, the surface of the adsorbents is positively charged, which may result in electrostatic repulsion with the tri-protonated form of chloroquine (pH < 4), reducing the adsorption efficiency in physisorption processes. However, at pH values higher than the isoelectric point (pH > Pie), the surface of the adsorbents becomes negatively charged, favoring interactions with chloroquine in its di-protonated and mono-protonated forms (4 < pH < 10.2) through electrostatic attraction.

In Brazil, water treatment legislation (BRASIL, 2021) mandates that pH levels be maintained between 5 and 9. Within this range, the removal of contaminants is likely minimally impacted, as the adsorbent surface remains predominantly negatively charged while the contaminant molecules are in their protonated forms. Adhering to these regulations ensures the effectiveness of treatment processes.

12.3. SUMMARY ABOUT CHARACTERIZATION OF THE MCM-41-COO AND MCM-48-COO

The characterization analyses of the MCM-41-CoO and MCM-48-CoO adsorbents provided crucial insights into their structural and compositional

properties. SEM and TEM images revealed a uniform particle distribution, with CoO nanoparticles effectively incorporated into the silica matrix. XRD analysis confirmed the high crystallinity of the materials and the retention of CoO's characteristic structural patterns. FTIR analysis identified key functional groups, including Si-OH, Si-O-Si, and Co-O-Si bonds, which are important for chloroquine adsorption. XRF analysis showed the predominant presence of SiO_2 in both materials (75.73 % in MCM-41-CoO and 76.84 % in MCM-48-CoO) and confirmed the successful incorporation of CoO in proportions of 24.28 % and 23.15 %, respectively. These characterization results collectively prove the successful functionalization of the synthesized materials.

12.4. STUDIES OF EFFECTS ON ADSORPTION CAPACITY

The amount of adsorbent material used in the adsorption process plays a crucial role in determining the contaminant removal efficiency in aqueous media (NATARAJAN et al., 2022). To evaluate this effect, the concentrations of MCM-41-CoO and MCM-48-CoO adsorbents were varied from 1 to 4 g L^{-1} in individual experiments, as shown in Figure 9.

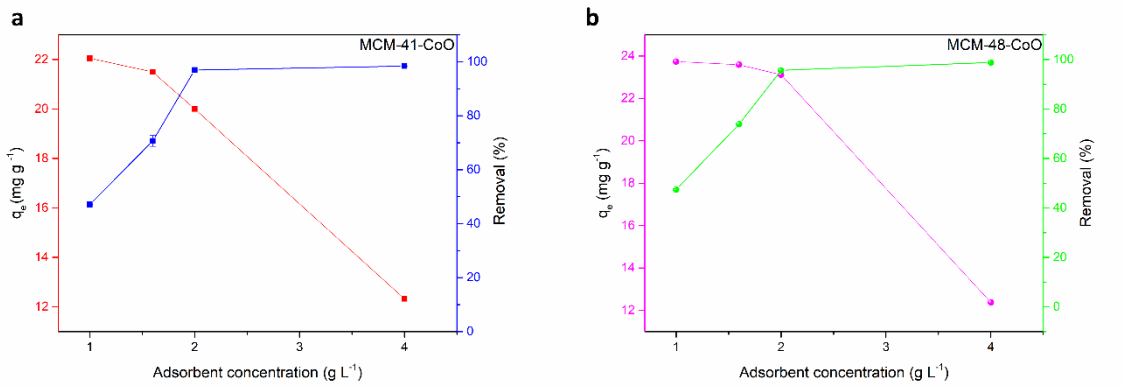

Figure. 9. The effect of adsorbent dose on the adsorption capacity and removal percentage of CQ for MCM-41-CoO (a) and MCM-48-CoO (b). Higher adsorbent doses increased the removal efficiency but significantly reduced the adsorption capacity. Therefore, 1.0 g L^{-1} was determined to be the optimal dose.

It was observed that increasing the concentration of both adsorbent materials led to a higher percentage of contaminant removal, reaching 100 % at 4 g L^{-1}. This can be attributed to the greater number of active sites available for the adsorption of CQ molecules. However, despite achieving complete removal,

the increase in adsorbent concentration resulted in a reduction of approximately 50 % in adsorption capacity, decreasing from ≈ 24 mg g^{-1} to 12 mg g^{-1} due to the increased mass of the solids. A similar effect has been reported in other studies (CUSIOLI et al., 2021a; DE SOUZA et al., 2021; QUESADA et al., 2021).

According to (CUSIOLI et al., 2021a), the high availability of binding sites makes it difficult to determine the maximum adsorption capacity, as material saturation is not reached. Therefore, to ensure the maximum adsorption capacity, the adsorbent concentration that yielded the highest adsorption capacity value, 1.0 g L^{-1}, was selected for all adsorption experiments.

Similar to the effect of adsorbent concentration, the pH of the solution plays a crucial role in the adsorption capacity of contaminants. To evaluate this influence, the pH of the CQ solution was varied from 2 to 8 during the adsorption process, as illustrated in Figure 10.

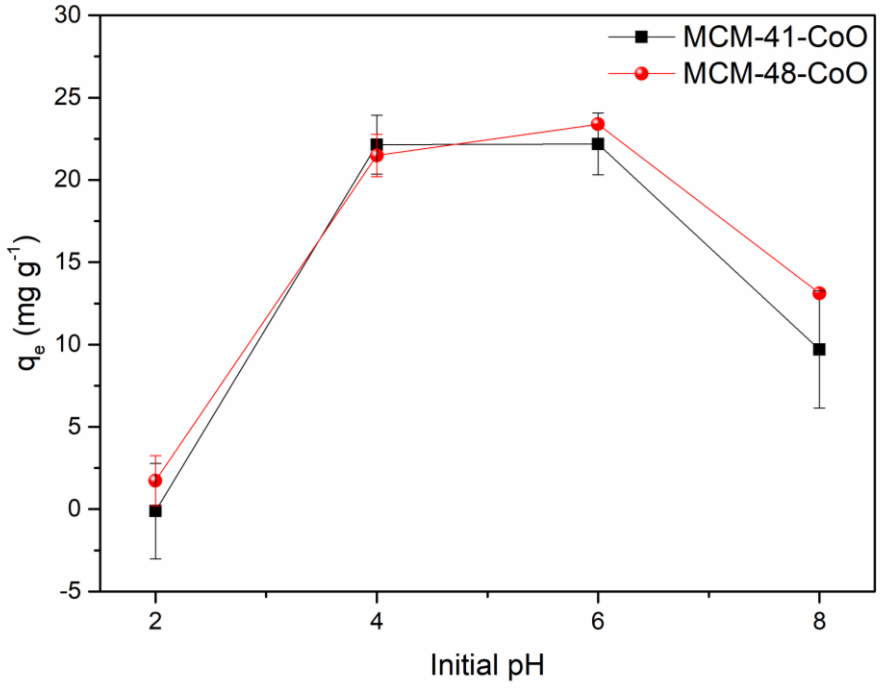

Figure. 10. Effect of pH on CQ adsorption by MCM-41-CoO and MCM-48-CoO. Adsorption was highest at pH 4–6, likely due to favorable electrostatic interactions, while both lower and higher pH values reduced the adsorption capacity (qe). Therefore, the optimum pH for adsorption experiments was the natural pH of CQ, which is 5.5.

The graph in Figure 10 indicates that in low pH solutions (pH < 4) and at high pH values (pH > 6), there is a significant reduction in adsorption capacity. This result was expected due to the electrostatic interactions between the

adsorbent materials and the pKa of the contaminant, as discussed previously in the zeta potential section.

The highest adsorption capacity value was observed in the neutral pH range (4 < pH < 6), with adsorption capacities of 22.14 and 22.18 mg g^{-1} for the MCM-41-CoO adsorbent, and 21.48 and 23.38 mg g^{-1} for the MCM-48-CoO adsorbent, at pH 4 and pH 6, respectively. This behavior is likely due to more significant electrostatic interactions. In this pH range, the surface of the adsorbents is predominantly negatively charged, while the pKa of the contaminant indicates the presence of free di-protonated ions, which favor adsorption. Therefore, the pH used in all adsorption experiments was the natural pH of the CQ solution, approximately 5.5.

12.5. KINETIC STUDY OF ADSORPTION

The analysis of adsorption kinetics is fundamental in evaluating an adsorbent-adsorbate system, as it helps us understand the mechanisms that govern the interaction between the adsorbent material and the contaminant over time (ABU RUMMAN et al., 2021; DE SOUZA et al., 2021). Thus, the adsorption kinetics study was conducted by varying the contact time from 0 to 15 hours to evaluate the removal of CQ using mesoporous silicas MCM-41-CoO and MCM-48-CoO, as shown in Figure 11.

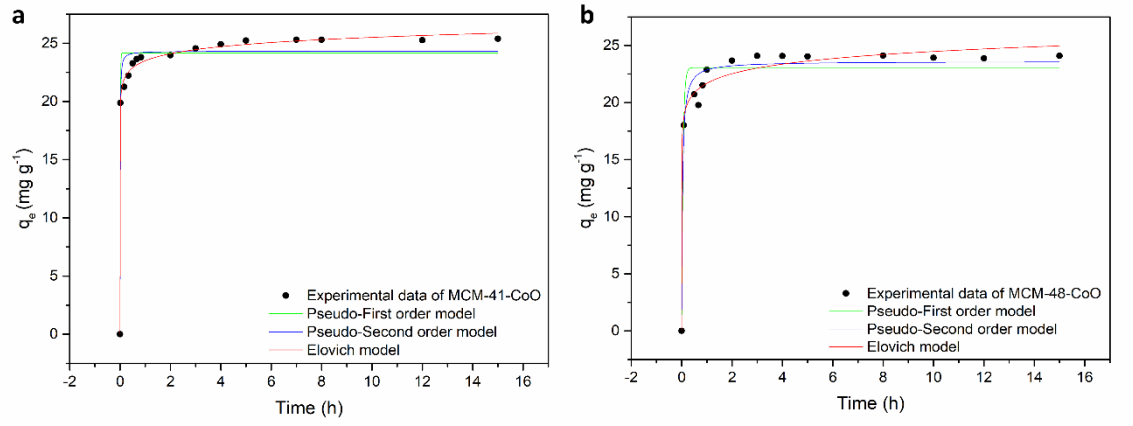

Figure. 11. The kinetic study of CQ adsorption by MCM-41-CoO (a) and MCM-48-CoO (b) shows the adsorption capacity over time. Adsorption was rapid during the first 2 hours, reaching equilibrium at 7 hours for MCM-41-CoO and at 4 hours for MCM-48-CoO. The Elovich model provided the best fit, indicating that chemisorption is the controlling mechanism.

Figure 11 illustrates that during the initial stages of the adsorption process, there was a rapid uptake of the adsorbate on the surface of both materials. This behavior can be attributed to the high availability of accessible pores and the electrostatic attraction between the adsorbents and the CQ solution, as previously discussed in the pH study. In just 2 hours, adsorption capacities of 23.97 mg g^{-1} for MCM-41-CoO and 23.67 mg g^{-1} for MCM-48-CoO were achieved. Equilibrium was reached after 7 hours for MCM-41-CoO and 4 hours for MCM-48-CoO, with equilibrium adsorption capacities of 25.30 mg g^{-1} and 24.04 mg g^{-1}, respectively.

Compared with other adsorbent materials used for chloroquine removal (Table 4), MCM-41-CoO and MCM-48-CoO demonstrate competitive and, in some cases, superior performance. For example, (JANUÁRIO et al., 2022), reported an equilibrium adsorption capacity of 19.83 mg g^{-1} using babassu coconut activated carbon combined with graphene oxide (GAC-GO) for the removal of drugs, including chloroquine and dipyrone. This capacity is approximately 22 % lower than the one achieved in this study. Additionally, the mesoporous silicas exhibited significantly shorter equilibrium times, with MCM-41-CoO reaching equilibrium approximately 2.5 times faster and MCM-48-CoO 4.5 times faster than GAC-GO.

Table. 4. Comparison of adsorbent materials used in the removal of chloroquine in contaminated water.

Adsorbent	Inicial concentration of CQ (mg L^{-1})	Adsorbent mass (g)	Kinetic Model	Isotherm Model	Equilibrium time (h)	q_e (mg g^{-1})	Reference
SBH-Fe3O4	20	0.01	PFO	Langmuir	2	55.88	(VIDOVIX et al., 2022)
GAC-GO	30	0.03	PSO	Langmuir	18	19.83	(JANUÁRIO et al., 2022)
CHGP-GOn	36.19	0.037	Elovich	Sips	4	13.31	(MAGALHÃES-GHIOTTO et al., 2023)
Açaí-based biochar (CAA)	20	0.02	PSO	Freundlich	2	39.07	(SANTOS et al., 2023)
Animal Bone (AC)	20	0.02	PSO	Langmuir	5	28.85	(CUSIOLI et al., 2022)
MCM-41-CoO	50	0.025	Elovich	Sips	7	25.3	This research
MCM-48-CoO	50	0.025	Elovich	Sips	4	24.04	This research

Furthermore, adjusting the mathematical models provides a better understanding of the adsorption mechanisms (QUESADA et al., 2019b). As shown in Table 5, the Elovich model best fit the adsorption process on MCM-41-CoO and MCM-48-CoO, yielding the highest correlation coefficients (R^2 = 0.996 and 0.988) and the lowest relative errors (χ^2 = 0.135 and 0.556), compared to the pseudo-first order and pseudo-second order models. This model is particularly suited for describing adsorption on heterogeneous surfaces and suggests that chemisorption is likely the dominant mechanism controlling the adsorption rate (CRINI; BADOT, 2008b; TURNER, 1975).

Table. 5. Kinetic model parameters applied to experimental data on CQ adsorption on MCM-41-CoO and MCM-48-CoO.

Models	Equation	Parameters	MCM-41-CoO	MCM-48-CoO
Pseudo-first order	$q_t = q_e(1 - e^{-k_1 t})$	$q_{e,exp}$ (mg g^{-1})	25.30	24.03
		$q_{e,calc}$ (mg g^{-1})	24.167	23.311
		k_1 (min^{-1})	103.753	17.796
		R^2	0.960	0.971
		χ^2	1.587	1.355
Pseudo-second order	$q_t = \frac{k_2 q_e^2 t}{1 + k_2 q_e t}$	$q_{e,calc}$ (mg g^{-1})	24.332	23.777
		k_2 (g mg^{-1} min^{-1})	9.483	1.371
		R^2	0.969	0.986
		χ^2	1.239	0.64
Elovich Model	$\frac{dq_t}{dt} = ae^{-bq_t}$	a (mg g^{-1} min)	$4.51*10^{11}$	$1.04*10^{8}$
		b (mg g^{-1})	1.147	0.834
		R^2	0.996	0.988
		χ^2	0.135	0.556

To further understand the mass transport steps within the pores of the adsorbents and the impact of diffusion resistance on the adsorption process, the Weber and Morris intraparticle diffusion model was applied to the kinetic data (Figure 12 and Table 6). According to this model, if the qt vs. $t^{0.5}$ plot intersects the origin, it indicates that intraparticle diffusion is the sole limiting step controlling the adsorption rate (WEBER; MORRIS, 1963b).

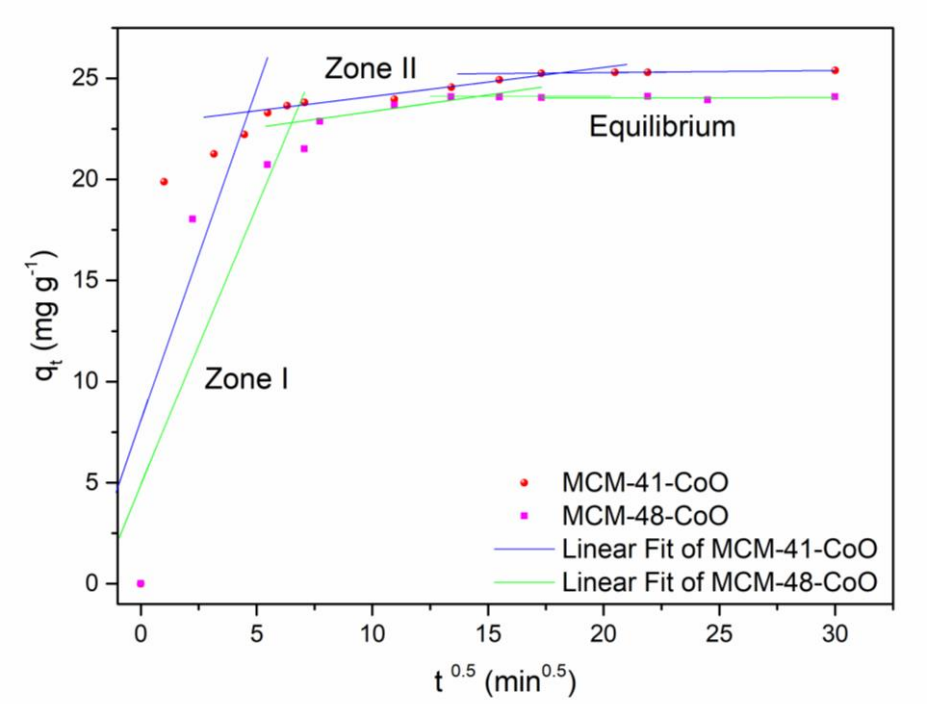

Figure. 12. Intraparticle diffusion model applied to CQ adsorption on MCM-41-CoO and MCM-48-CoO, illustrating the mass transport steps. The adsorption process follows a multi-stage mechanism, which includes film diffusion, intraparticle diffusion, and surface interactions.

Based on Figure 12, it can be observed that the linear adjustments for both adsorbents do not pass through the origin, indicating that the mass transfer process is governed by a multi-stage system. This system involves three distinct stages: film diffusion, intraparticle diffusion, and surface reaction.

The parameters of the intraparticle diffusion model presented in Table 6 provide information on the transport velocity (K_{dif}) and the diffusion resistance (C) (DE SOUZA et al., 2021). Thus, in Zone I, the adsorption process, controlled by film diffusion, shows low transport resistance and high diffusion speed. In Zone II, a significant increase in C (22.687 mg g^{-1} for MCM-41-CoO and 21.743 mg g^{-1} for MCM-48-CoO) was observed, indicating greater transport resistance. This reflects the transition to the intraparticle diffusion stage, as evidenced by the decrease in K_{dif} values, which represents a slower rate at which particles enter the contaminant into the pores of the adsorbents. Upon reaching the third and final stage, the system reaches equilibrium, with the CQ molecule fully deposited inside the adsorbent material. Similar results were observed in other studies of CQ removal from contaminated water, where a multi-stage adsorption system

was also identified (JANUÁRIO et al., 2022; MAGALHÃES-GHIOTTO et al., 2023; VIDOVIX et al., 2022).

Table. 6. Parameters of the intraparticle diffusion model.

Zone	Equation	Parameters	MCM-41-CoO	MCM-48-CoO
I	$q_e = K_{dif}\, t^{0.5} + c$	K_{dif} (g mg^{-1} min$^{0.5}$)	3.282	2.74
		C (mg g^{-1})	8.065	4.936
		R^2	0.597	0.605
		$\chi 2$	1.555	1.157
II		K_{dif} (g mg^{-1} min$^{0.5}$)	0.142	0.162
		C (mg g^{-1})	22.687	21.743
		R^2	0.940	0.845
		$\chi 2$	0.015	0.038
Equilibrium		q_e (mg g^{-1})	25.29	24.03

According to (EJHED et al., 2018), some sewage treatment plants can retain effluent for 2 to 6 days, depending on factors such as flow rate and treatment efficiency. Therefore, the adsorption kinetics in this study align with the CQ removal equilibrium, which was reached after 7 hours for MCM-41-CoO and 4 hours for MCM-48-CoO.

12.6. ADSORPTION ISOTHERM EQUILIBRIUM

Equilibrium isotherm studies were conducted to better understand the adsorbent capacity of the material. For these studies, 25 mL of contaminant solution with concentrations ranging from 0 to 300 mg L^{-1} of CQ were performed. To each solution, 0.025 g of MCM-41-CoO (Figure 13 and Table 7) or MCM-48-CoO (Figure 14) was added, and the mixtures were kept under stirring for 24 hours. The experiments were conducted at varying temperatures: 15 ºC, 25 ºC, 35 ºC, and 45 ºC, following the previously described methodology. To investigate the adsorption process and evaluate the adsorption equilibrium of CQ on the adsorbent materials, the Langmuir (6), Freundlich (7), and Sips (8) mathematical models were applied, as represented by the following equations:

$$q_e = \frac{q_{max}\, K_L\, C_e}{1 + K_L\, C_e} \quad (6)$$

$$q_e = K_F C_e^{\,1/n_F} \quad (7)$$

$$q_e = \frac{Q_{max}(K_S C)^{1/n_S}}{1+(K_S C)^{1/n_S}} \quad (8)$$

Where q_e represents the equilibrium adsorption capacity (mg g^{-1}), C_e is the equilibrium adsorbate concentration (mg L^{-1}), Q_{max} is the maximum adsorption capacity (mg g^{-1}), and the constants K_L (L mg^{-1}), K_F ((mg g^{-1})/(mg L^{-1})^n), and K_s (mg L^{-1}) correspond to the adsorbate/adsorbent interactions in the Langmuir, Freundlich, and Sips models, respectively. Additionally, n_F and ns represent the adsorption intensity or surface heterogeneity in the Freundlich and Sips models.

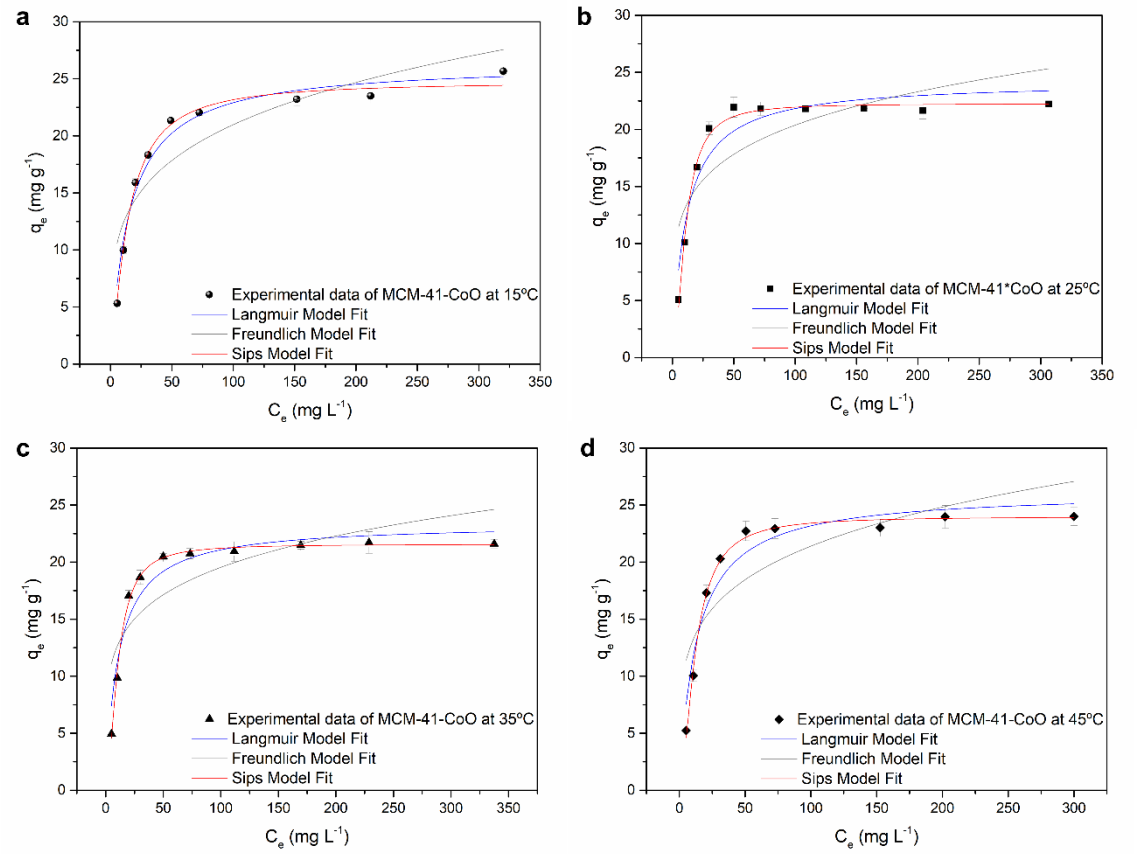

Figure. 13. Equilibrium isotherm curves for CQ adsorption on MCM-41-CoO at different temperatures (15–45 ºC), applying Langmuir, Freundlich, and Sips models. The Sips model provided the best fit ($R^2 > 0.99$, $\chi^2 < 0.5$), indicating adsorption on a heterogeneous surface. The maximum adsorption capacity reached 24.78 mg g^{-1} at 15 °C.

Table. 7. Parameters of isothermal fitting of CQ adsorption using MCM-41-CoO.

MCM-41-CoO					
Isotherm	**Parameters**	**15 ºC**	**25 ºC**	**35 ºC**	**45 ºC**
Langmuir	q_m (mg g^{-1})	26.39	24.222	23.391	26.199
	K_L (L mg^{-1})	0.065	0.091	0.091	0.076
	R^2	0.976	0.915	0.933	0.937

Freundlich	$\chi 2$	1.089	3.039	2.223	2.89
	K_F (mg g^{-1})/(mg $L^{-1})^{n_F}$	7.129	8.345	8.154	7.993
	n_F	4.266	5.158	5.268	4.675
	R^2	0.795	0.632	0.658	0.682
Sips	$\chi 2$	9.492	13.286	11.319	14.645
	Qmax (mg g^{-1})	24.784	22.267	21.572	24.003
	K_S (L mg^{-1})	0.072	0.094	0.095	0.082
	n_S	1.343	1.887	1.818	1.74
	R^2	0.99	0.991	0.995	0.993
	$\chi 2$	0.465	0.319	0.151	0.279

As shown in Figure 13 and Table 7, the Sips model provided the best fit for all isotherm curves at different temperatures, exhibiting the highest correlation coefficient ($R^2 > 0.99$) and the lowest relative error ($\chi^2 < 0.5$).

Similarly to MCM-41-CoO, the MCM-48-CoO adsorbent also demonstrated equilibrium isotherm data (Figure 14) and corresponding parameters (Table 8), confirming that the Sips model was the most suitable. This conclusion is supported by the highest correlation coefficient (R^2) and the lowest chi-square (χ^2) values across all evaluated temperatures.

The Sips model, which combines the mathematical principles of the Langmuir and Freundlich models, predicts that an adsorbate molecule can occupy one or more active adsorption sites (RIBEIRO et al., 2024) through adsorption on a heterogeneous surface (FANG et al., 2017), relating to the deposition of the contaminant within the mesoporous adsorbent capillaries (LEE; SHIM; MOON, 2004). Therefore, the present results align with the kinetic investigation findings, which indicate the diffusion movement of the contaminant through the adsorbent pores in a multi-stage process.

According to (MEHRVARZ; GHOREYSHI; JAHANSHAHI, 2017), the Sips exponent (n_s) value indicates heterogeneity. In a homogeneous system, the Sips exponent is equal to one, therefore, the higher the n_s values are, the more heterogeneous the system is. At all evaluated temperatures, the mesoporous adsorbents exhibited ns values greater than one, confirming the heterogeneity of the adsorbent surfaces. Although MCM-41-CoO and MCM-48-CoO have distinct internal structures (hexagonal and cubic, respectively, as evidenced by the TEM results), they display similar surface heterogeneity.

Consistent with these findings, previous studies have also reported contaminant removal via heterogeneous surface adsorption, with the adsorption process governed by the Sips model on adsorbents with comparable structures (HUA et al., 2022). This suggests that the Sips model effectively represents adsorption on heterogeneous surfaces, regardless of internal structural differences.

Based on the best-fitting mathematical model, the adsorbents exhibited a maximum calculated adsorption capacity of 24.78 mg g^{-1} for MCM-41-CoO at 15°C and 24.00 mg g^{-1} for MCM-48-CoO at 45 °C, with experimental values closely matching the calculated ones. When comparing these adsorbents with other materials used for chloroquine removal, mesoporous silicas demonstrated a slightly higher capacity than that reported by (ATUNWA et al., 2022), who used palm kernel shell activated carbon doped with AgNPs (PKSAC@AgNPs) and achieved a qe of 15.51 mg g^{-1}. In contrast, studies such as (JANUÁRIO et al., 2022), which utilized activated carbon with graphene oxide, reported higher maximum adsorption capacities, reaching a qe of 37.65 mg g^{-1}.

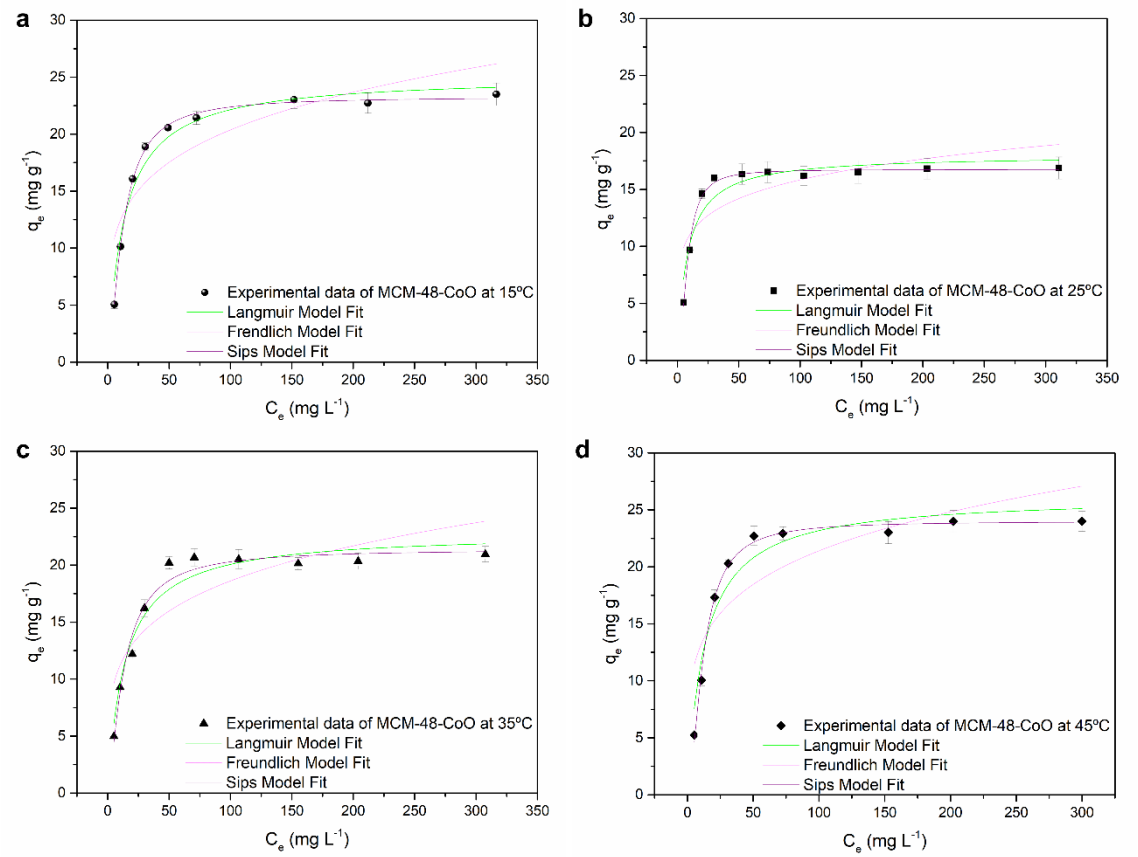

Figure. 14. Equilibrium isotherm curves for CQ adsorption on MCM-48-CoO at different temperatures (15–45 ºC), applying the Langmuir, Freundlich, and Sips models. The Sips model provided the best fit ($R^2 > 0.96$, $\chi^2 < 1.0$), confirming adsorption on a heterogeneous surface. The maximum adsorption capacity reached 24.00 mg g^{-1} at 45 °C.

Table. 8. Parameters of isothermal fitting of CQ adsorption using MCM-48-CoO.

		MCM-48-CoO			
Isotherm	**Parameters**	**15 ºC**	**25 ºC**	**35 ºC**	**45 ºC**
Langmuir	q_m (mg g^{-1})	25.134	18.007	22.861	26.199
	K_L (L mg^{-1})	0.074	0.128	0.071	0.076
	R^2	0.965	0.903	0.947	0.937
	$\chi 2$	1.429	1.492	1.75	2.89
Freundlich	K_F (mg g^{-1})/(mg L^{-1})^{nF}	7.487	7.642	6.731	7.993
	n_F	4.601	6.322	4.528	4.675
	R^2	0.737	0.594	0.724	0.682
	$\chi 2$	10.82	6.296	9.136	14.645
Sips	Qmax (mg g^{-1})	23.286	16.747	21.422	24.003
	K_S (L mg^{-1})	0.081	0.123	0.076	0.082
	n_S	1.527	1.981	1.414	1.74
	R^2	0.997	0.992	0.966	0.993
	$\chi 2$	0.093	0.123	1.099	0.279

The monitoring of contaminants in water resources has revealed hydroxychloroquine concentrations up to 50 μg L^{-1} in primary sludge from water treatment plants in the USA during the pandemic (NASON et al., 2022). Our study indicates that the adsorbents MCM-41-CoO and MCM-48-CoO demonstrate maximum adsorption capacities of 24.78 mg g^{-1} and 24 mg g^{-1}, respectively, during the isotherm studies, highlighting their potential for real-world applications. These adsorbents effectively remove CQ at relevant concentrations, offering efficiency, simplicity, and cost-effectiveness.

Finally, both materials, MCM-41-CoO and MCM-48-CoO, exhibited better performance at extreme temperatures of 15 ºC and 45 ºC. However, at intermediate temperatures (25 ºC and 35 ºC), a slight reduction in the maximum adsorption capacity of MCM-41-CoO was noted (approximately 10 % of Q_{max} between 15 ºC and 25 ºC). In contrast, a more pronounced reduction was observed for MCM-48-CoO, with a decrease of approximately 28 % for the same temperature variation. This behavior suggests that the materials perform better under more extreme temperature conditions, making them promising for applications in regions with fluctuating temperatures or significant thermal variations.

12.7. THERMODYNAMIC STUDY

Thermodynamic analysis of adsorption processes enables the evaluation of the spontaneity and the nature of interactions between the adsorbent and the adsorbate (DE SOUZA et al., 2021). Through the parameters of Gibbs free energy (ΔG°), enthalpy (ΔH°), and entropy (ΔS°), presented in Table 9, it is possible to infer essential information about the adsorption process.

Table. 9. Parameters for the thermodynamic study of CQ adsorption onto modified mesoporous silicas.

	Temperature (K)	**∆G° (KJ mol^{-1})**	**∆H° (KJ mol^{-1})**	**∆S° (KJ mol^{-1} K^{-1})**
MCM-41-CoO	288	-24.0511	3.257758	0.095678
	298	-25.5468		
	308	-26.4311		
	318	-26.9002		
MCM-48-CoO	288	-24.3331	3.204465	0.074661
	298	-26.2130		

308	-25.8597
318	-26.9002

According to (TIAN et al., 2025), negative values of Gibbs free energy ($\Delta G° < 0$) indicate the spontaneity of the reaction. In this regard, the process is spontaneous and favorable at all evaluated temperatures for both MCM-41-CoO and MCM-48-CoO adsorbents. For MCM-41-CoO, there is a slight increase in spontaneity with rising temperature, suggesting a greater affinity between the adsorbent and adsorbate under varying thermal conditions. In contrast, MCM-48-CoO exhibits less temperature sensitivity, indicating that spontaneity remains stable as temperature increases.

The analysis of enthalpy data ($\Delta H°$) indicates whether the process is endothermic ($\Delta H° > 0$) or exothermic ($\Delta H° < 0$) based on heat variation ($\Delta H°$) (DE SOUZA et al., 2021). As shown in Table 9, the enthalpy change ($\Delta H°$) for CQ adsorption by mesoporous silicas is positive, indicating that heat is absorbed during the adsorption process. Therefore, this suggests that the process is endothermic for both adsorbent materials. Furthermore, according to (HAYWARD; TRAPNELL, 1964), enthalpy values provide insights into the adsorption mechanism, distinguishing between physisorption ($2.1 < \Delta H° < 20.9$ kJ mol^{-1}) and chemisorption ($80 < \Delta H° < 200$ kJ mol^{-1}).

The enthalpy variation values obtained for MCM-41-CoO and MCM-48-CoO were 3.25 and 3.20 kJ mol^{-1}, respectively, indicating that both processes are governed by physisorption mechanisms. Although enthalpy results suggest a predominance of physisorption, FTIR analysis - which indicates interactions between the adsorbent and adsorbate via electrostatic forces and hydrogen bonds, along with adsorption kinetics data, where R^2 values for pseudo-first order, pseudo-second order, and the Elovich models exhibit minimal variation ($0.960 < R^2 < 0.996$) - suggests that CQ adsorption by MCM-41-CoO and MCM-48-CoO may occur through a combination of physisorption and chemisorption processes.

Considered a measure of disorder, entropy provides insight into the randomness of the adsorption reaction (NATARAJAN et al., 2022). Based on the obtained entropy values (0.095 and 0.074 kJ mol^{-1} K^{-1}), the adsorption process is characterized by low randomness at the solid/liquid interface.

Regarding molecular interactions, increasing the temperature can weaken the interactions between contaminant molecules and the material surface. This process requires energy to break these interactions, leading to weaker adsorption bonds. Endothermic adsorption occurs as these interactions weaken, which increases entropy and promotes desorption, allowing the molecules greater freedom of movement (EBELEGI; AYAWEI; WANKASI, 2020; TERZYK, 2004). This may explain the decrease in adsorption capacity observed at 25 °C and 35 °C.

In this context, previous studies on CQ adsorption have reported similar results to the present study, showing a spontaneous, endothermic process with low randomness during CQ adsorption onto stone mango with iron oxide (RIBEIRO et al., 2024). Likewise, (VIDOVIX et al., 2022) reported CQ removal via a spontaneous, endothermic process, with low and positive entropy values, indicating a tendency for adsorbate behavior.

12.8. REUSE STUDY AND PROPOSAL OF ADSORPTION MECHANISM

Reusing adsorbent materials is closely associated with sustainable waste treatment practices and aligns with the principles of the circular economy (FOUDA-MBANGA; ONOTU; TYWABI-NGEVA, 2024). To evaluate the reusability of the material, a reuse study was conducted.

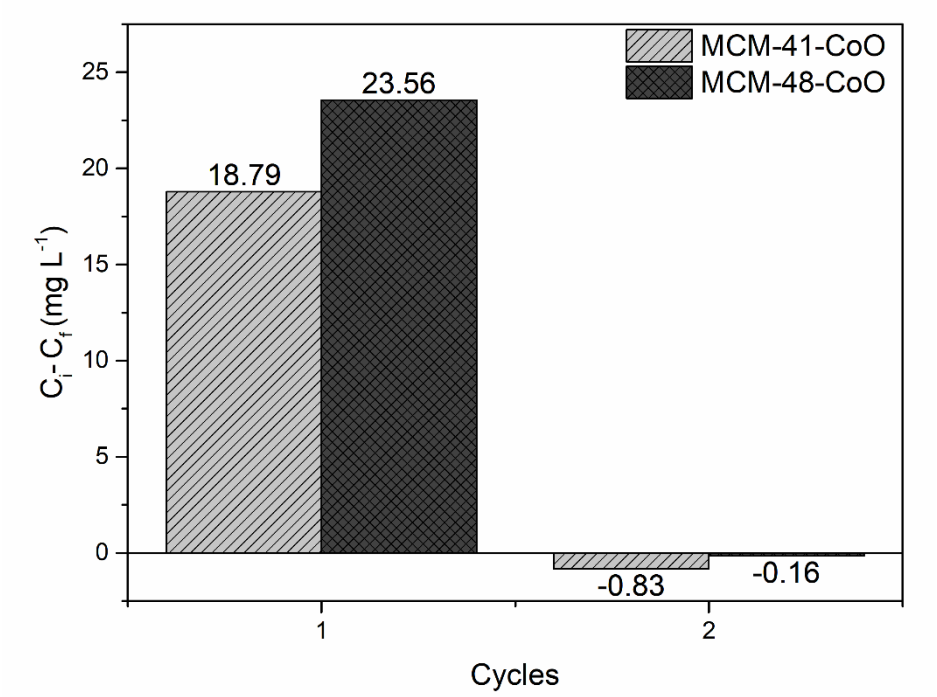

Figure. 15. Reuse study of mesoporous silicas for CQ adsorption from water. The bar graph shows CQ retention by MCM-41-CoO and MCM-48-CoO over two cycles. The first cycle retained 18.79 mg L^{-1} and 23.56 mg L^{-1}, respectively, while negative values in the second cycle indicate partial desorption.

As shown in Figure 15, during the first adsorption cycle, 18.79 mg L^{-1} of CQ was retained by the MCM-41-CoO adsorbent. However, in the second cycle, a value of -0.83 mg L^{-1} was observed. For MCM-48-CoO, the first cycle removed 23.56 mg L^{-1}, followed by -0.16 mg L^{-1} in the second cycle. The negative values in the second adsorption cycle indicate the desorption of some CQ molecules from the adsorbents, leading to an increase in CQ concentration in the aqueous solution the adsorption cycle.

According to (GIL, 2023), physical adsorption is governed by Van der Waals forces and is characterized by weak adsorbent-adsorbate interactions, a multilayer adsorption process, and an exothermic nature. The opposite occurs in chemical adsorption, where the chemisorption mechanism is driven by the formation of chemical bonds, resulting in a strong bond between the adsorbent and adsorbate. This makes it difficult for the adsorbate to detach, resulting in the formation of a single monolayer. Although overlapping of the contaminant on the solid may occur, it is governed by physical adsorption.

Based on the literature and the results obtained in this research, it is assumed that the adsorption mechanisms are governed by both physisorption

and chemisorption. The reuse data show minimal release of contaminant molecules during the adsorption cycles, which may be attributed to the weak interactions between CQ and mesoporous silicas.

The presence of physical interactions can be supported by the possible electrostatic interactions identified through the zeta potential analysis. This analysis demonstrates that the surface of the adsorbent, at the pH of the natural CQ solution, tends to carry negative charges, while the contaminant in the same pH range exists in its di-protonated form. Therefore, electrostatic interactions may occur between the adsorbent and adsorbate.

The reuse study also supports the presence of interactions driven by the chemisorption process, as the release of chloroquine molecules in the second cycle was insignificant, indicating a strong bond between CQ and the surface of mesoporous silicas. Additionally, the lack of adsorption in the subsequent cycle suggests that all possible chemical bonds and the occupation of the available active sites on the adsorbents were completed in the first adsorption cycle, resulting in the formation of a monolayer, characteristic of a chemical adsorption process.

Along with the reuse results, the FTIR analysis further corroborates the existence of potential chemical bonds, primarily driven by hydrogen band bonds interactions between the oxygen molecules in the silanol and siloxane groups of the MCM-41-CoO and MCM-48-CoO materials and the hydrogen molecules in CQ. There may also be bonds between the hydrogen molecules of the solid formations and the nitrogen and chlorine molecules in the contaminant, as shown in Figure 16.

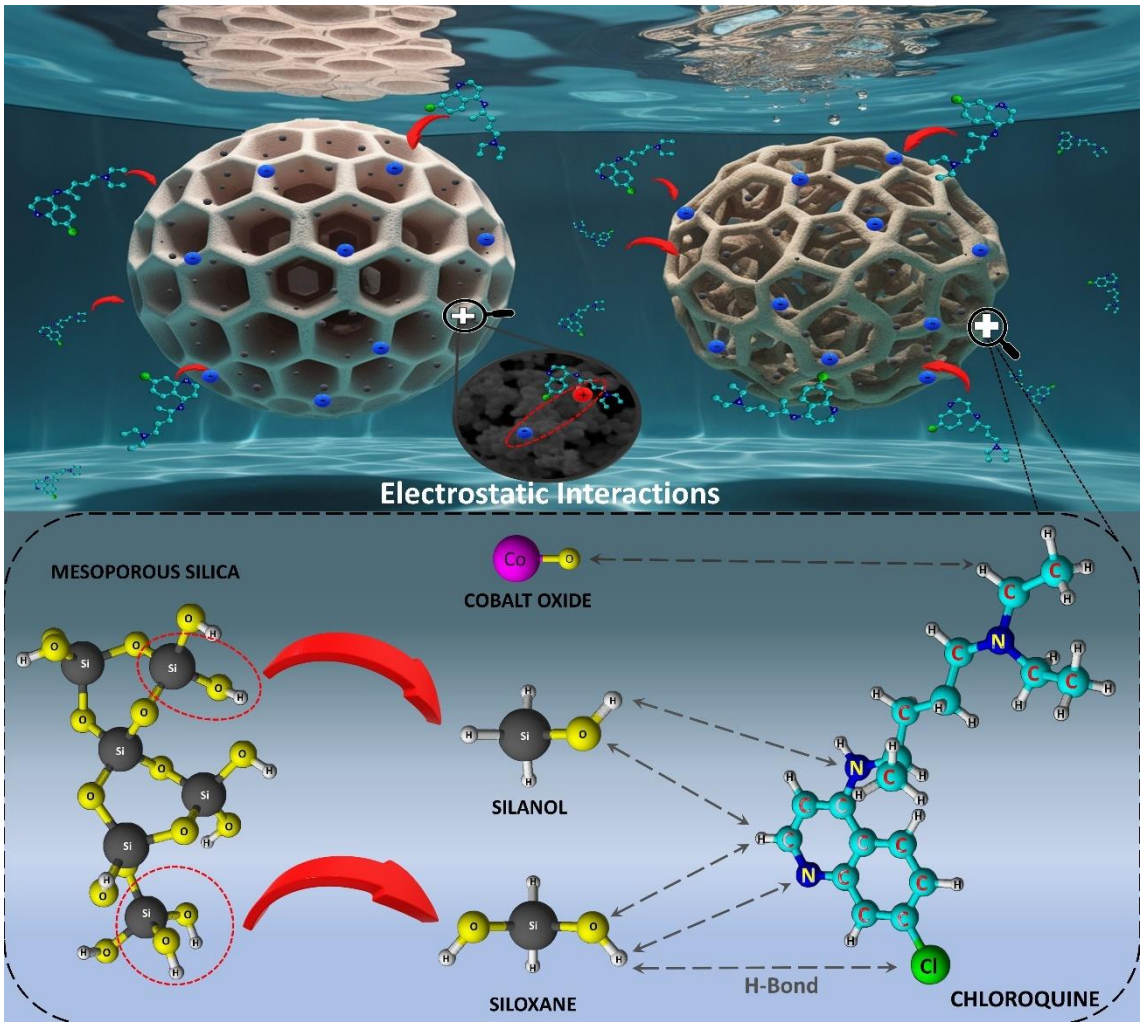

Figure. 16. Supposed mechanism of interaction between the mesoporous silicas and the CQ molecule in the adsorption process. The figure illustrates both physical (physisorption) and chemical (chemisorption) adsorption mechanisms, with weak electrostatic interactions and stronger chemical bonds.

The proposed results of physical and chemical adsorption may prove to be both interesting and attractive for the treatment of water contaminated by CQ. They demonstrate the attraction of the contaminant to the adsorbent solid, with complete adhesion to the adsorbent surface, resulting in robust and stable interactions. This minimizes the risk of detachment and contributes to the efficient and selective removal of the contaminant.

Similarly, the isotherm studies support the proposed mechanisms, indicating that CQ adsorption follows the Langmuir model, which suggests monolayer formation with limited adsorption sites. This was further corroborated by the material reuse studies. However, the presence of a heterogeneity coefficient in the Sips isotherm suggests variability in the adsorption process, a

behavior characteristic of the Freundlich model. In this context, the observed monolayer formation and surface heterogeneity explain the effective removal of the contaminant.

Therefore, the proposed adsorption mechanism integrates strong and stable interactions between the adsorbent and the contaminant, supported by experimental evidence from adsorption studies.

13. CONCLUSION

In this study, the synthesis, characterization, and evaluation of mesoporous silicas of the MCM-41 and MCM-48 types were carried out. These materials were modified by the deposition of cobalt oxide nanoparticles, forming new adsorbents, MCM-41-CoO and MCM-48-CoO, which were used in the removal of chloroquine from contaminated water.

The newly synthesized materials exhibited characteristic structures of mesoporous silicas, with high surface areas (S_{BET} > 369.49 mg g^{-1}), featuring a uniform and spherical mesostructure, with differences in their internal porous formations for each type of silica. Furthermore, the adsorbents demonstrated high crystallinity, primarily from the cobalt oxide nanoparticles, confirming the success of their deposition. It was also observed in the evaluation of the effects that, in the pH range of the natural chloroquine solution (pH ≈ 5.5), the surface of the adsorbents is negatively charged. In contrast, the contaminant solution has positive charges, making electrostatic attraction a favorable mechanism for adsorption.

The kinetic study demonstrated an equilibrium adsorption capacity of 25.3 and 24.04 mg g^{-1} for the MCM-41-CoO and MCM-48-CoO adsorbents, with equilibrium times of 7 hours and 4 hours, respectively. The kinetic results best fit the Elovich model for both adsorbents (R^2 = 0.996 e 0.988), describing a process governed by chemisorption. In the analysis of intraparticle diffusion, a mass transfer process controlled by multiple stages was observed, including the stages of film diffusion, intraparticle diffusion, and surface reaction. Regarding the equilibrium isotherm study, the best fit was observed with the Sips model at all evaluated temperatures (15 to 45 ºC), presenting a maximum adsorption capacity

of 24.78 mg g^{-1} at 15 ºC for MCM-41-CoO and 24.00 mg g^{-1} at 45 ºC for MCM-48-CoO.

The thermodynamic parameters studied for the two adsorbents indicate a spontaneous and favorable adsorption process at all temperatures analyzed, presenting stable behavior with temperature variation. Furthermore, the enthalpy results suggest an endothermic reaction and low randomness in the adsorptive system. Although the thermodynamic study indicates contaminant removal through physisorption, other evidence suggests that CQ adsorption may also have occurred through chemisorption processes. These processes could involve a chemical interaction in a monolayer, filling the active sites of the adsorbent, followed by stacking through physical interactions.

These findings are further supported by the reuse study, which was limited to a single removal cycle and showed only slight release of adsorbate molecules in the subsequent cycle. Based on these results, it is evident that mesoporous silicas modified with cobalt oxide nanoparticles are highly efficient and selective adsorbent materials, with a low risk of secondary pollution from the release of contaminating compounds. Therefore, they represent promising materials for treating pharmaceutical effluents. In real-world systems, these materials can be integrated into the final stage of wastewater treatment, serving as an advanced process to effectively remove recalcitrant contaminants.

Acknowledgments

This study was partially funded by the Higher Education Personnel Improvement – Brazil (CAPES) – Finance Code 001, and the National Council for Scientific and Technological Development (CNPq) – Finance Code 001. The authors also thank the Laboratory of Adsorption and Ion Exchange for conducting the N_2 physisorption analysis and the Complex for Research Support Center (COMCAP) of the State University of Maringá for additional characterizations.

Declaration of Competing Interest

The authors declare that they have no known competing financial interests or personal relationships that could have appeared to influence the work reported in this paper.

14. REFERENCES

A. MANNAA, M.; ALTASS, H. M.; SALAMA, R. S. MCM-41 grafted with citric acid: The role of carboxylic groups in enhancing the synthesis of xanthenes and removal of heavy metal ions. **Environmental Nanotechnology, Monitoring & Management**, v. 15, p. 100410, maio 2021.

ABU RUMMAN, G. et al. Adsorption performance of an amine-functionalized MCM–41 mesoporous silica nanoparticle system for ciprofloxacin removal. **Environmental Nanotechnology, Monitoring & Management**, v. 16, p. 100536, dez. 2021.

ABU-ZIED, B. M.; HUSSEIN, M. A.; ASIRI, A. M. Development and characterization of the composites based on mesoporous MCM-41 and polyethylene glycol and their properties. **Composites Part B: Engineering**, v. 58, p. 185–192, mar. 2014.

AKPOTU, S. O.; MOODLEY, B. MCM-48 encapsulated with reduced graphene oxide/graphene oxide and as-synthesised MCM-48 application in remediation of pharmaceuticals from aqueous system. **Journal of Molecular Liquids**, v. 261, p. 540–549, jul. 2018.

ALI, I.; ALOTHMAN, Z. A.; AL-WARTHAN, A. Sorption, kinetics and thermodynamics studies of atrazine herbicide removal from water using iron nano-composite material. **International Journal of Environmental Science and Technology**, v. 13, n. 2, p. 733–742, fev. 2016.

AL-SENANI, G. M.; DERAZ, N. M.; ABD-ELKADER, O. H. Magnetic and Characterization Studies of CoO/Co3O4 Nanocomposite. **Processes**, v. 8, n. 7, p. 844, 15 jul. 2020.

AL-SHEHRI, B. M. et al. A review: the utilization of mesoporous materials in wastewater treatment. **Materials Research Express**, v. 6, n. 12, p. 122002, 12 nov. 2019.

ANDRADE, M. B. et al. Evaluation of magnetic nano adsorbent produced from graphene oxide with iron and cobalt nanoparticles for caffeine removal from aqueous medium. **Chemical Engineering and Processing - Process Intensification**, v. 170, p. 108694, jan. 2022.

ASPROMONTE, S. G. et al. Cobalt oxide nanoparticles on mesoporous MCM-41 and Al-MCM-41 by supercritical CO2 deposition. **Microporous and Mesoporous Materials**, v. 148, n. 1, p. 53–61, jan. 2012.

ATHAR, T. et al. Wet Synthesis of Monodisperse Cobalt Oxide Nanoparticles. **ISRN Materials Science**, v. 2012, p. 1–5, 7 maio 2012.

ATUNWA, B. T. et al. Synthesis, physiochemical and spectroscopic characterization of palm kernel shell activated carbon doped AgNPs

(PKSAC@AgNPs) for adsorption of chloroquine pharmaceutical waste. **Materials Today: Proceedings**, v. 65, p. 3538–3546, 2022.

BORCĂNESCU, S. et al. Functionalized Ordered Mesoporous MCM-48 Silica: Synthesis, Characterization and Adsorbent for CO2 Capture. **International Journal of Molecular Sciences**, v. 24, n. 12, p. 10345, 19 jun. 2023.

BRASIL. GM/MS Nº 888. PORTARIA GM/MS Nº 888, DE 4 DE MAIO DE 2021. . 2021.

BRUNAUER, S.; EMMETT, P. H.; TELLER, E. Adsorption of Gases in Multimolecular Layers. **Journal of the American Chemical Society**, v. 60, n. 2, p. 309–319, fev. 1938.

BUI, T. X.; CHOI, H. Adsorptive removal of selected pharmaceuticals by mesoporous silica SBA-15. **Journal of Hazardous Materials**, v. 168, n. 2–3, p. 602–608, set. 2009.

CAI, Q. et al. Dilute Solution Routes to Various Controllable Morphologies of MCM-41 Silica with a Basic Medium. **Chemistry of Materials**, v. 13, n. 2, p. 258–263, 1 fev. 2001.

CAPPELLI, F. et al. Suspect screening of wastewaters to trace anti-COVID-19 drugs: Potential adverse effects on aquatic environment. **Science of The Total Environment**, v. 824, p. 153756, jun. 2022.

CASHIN, V. B. et al. Surface functionalization and manipulation of mesoporous silica adsorbents for improved removal of pollutants: a review. **Environmental Science: Water Research & Technology**, v. 4, n. 2, p. 110–128, 2018.

CHEN, L. et al. Recent developments of mesoporous silica nanoparticles in biomedicine. **Emergent Materials**, v. 3, n. 3, p. 381–405, 1 jun. 2020.

CHOONG, Z.-Y. et al. Waste-derived MCM-41 as dual-functional support for cobalt ferrite: Performance as peroxymonosulfate activator for ciprofloxacin decontamination. **Applied Surface Science**, v. 645, p. 158861, fev. 2024.

CRINI, G.; BADOT, P.-M. Application of chitosan, a natural aminopolysaccharide, for dye removal from aqueous solutions by adsorption processes using batch studies: A review of recent literature. **Progress in Polymer Science**, v. 33, n. 4, p. 399–447, abr. 2008.

CUSIOLI, L. F. et al. Modified *Moringa oleifera* Lam. Seed husks as low-cost biosorbent for atrazine removal. **Environmental Technology**, v. 42, n. 7, p. 1092–1103, 21 mar. 2021.

CUSIOLI, L. F. et al. Adsorption of Covid-19-related drug from contaminated water using activated carbon. **Desalination and Water Treatment**, v. 277, p. 85–89, nov. 2022.

DE SOUZA, R. M. et al. Adsorption of non-steroidal anti-inflammatory drug (NSAID) by agro-industrial by-product with chemical and thermal modification:

Adsorption studies and mechanism. **Industrial Crops and Products**, v. 161, p. 113200, mar. 2021.

DODDAGA, S.; PEDDAKONDA, R. Chloroquine-N-oxide, a major oxidative degradation product of chloroquine: Identification, synthesis and characterization. **Journal of Pharmaceutical and Biomedical Analysis**, v. 81–82, p. 118–125, jul. 2013.

DOMINGO-ECHABURU, S. et al. Drugs used during the COVID-19 first wave in Vitoria-Gasteiz (Spain) and their presence in the environment. **Science of The Total Environment**, v. 820, p. 153122, maio 2022.

DOU, B. et al. Adsorption performance of VOCs in ordered mesoporous silicas with different pore structures and surface chemistry. **Journal of Hazardous Materials**, v. 186, n. 2–3, p. 1615–1624, fev. 2011.

EBELEGI, A. N.; AYAWEI, N.; WANKASI, D. Interpretation of Adsorption Thermodynamics and Kinetics. **Open Journal of Physical Chemistry**, v. 10, n. 03, p. 166–182, 2020.

EJHED, H. et al. The effect of hydraulic retention time in onsite wastewater treatment and removal of pharmaceuticals, hormones and phenolic utility substances. **Science of The Total Environment**, v. 618, p. 250–261, mar. 2018.

EL-HAKAM, S. A. et al. Application of nanostructured mesoporous silica/ bismuth vanadate composite catalysts for the degradation of methylene blue and brilliant green. **Journal of Materials Research and Technology**, v. 18, p. 1963–1976, maio 2022.

EL-YAZEED, W. S. A. et al. Ag-PMA supported on MCM-41: Surface Acidity and Catalytic Activity. **Journal of Sol-Gel Science and Technology**, v. 102, n. 2, p. 387–399, maio 2022.

FANG, H. et al. Phosphorus adsorption onto clay minerals and iron oxide with consideration of heterogeneous particle morphology. **Science of The Total Environment**, v. 605–606, p. 357–367, dez. 2017.

FOOD AND DRUG ADMINISTRATION. **EUA Chloroquine Phosphate Health Care Provider Fact Sheet**. FDA, , 27 abr. 2020. Disponível em: <https://www.fda.gov/media/136535/download>. Acesso em: 6 nov. 2023

FOUDA-MBANGA, B. G.; ONOTU, O.; TYWABI-NGEVA, Z. Advantages of the reuse of spent adsorbents and potential applications in environmental remediation: A review. **Green Analytical Chemistry**, v. 11, p. 100156, dez. 2024.

GALANI, A. et al. Patterns of pharmaceuticals use during the first wave of COVID-19 pandemic in Athens, Greece as revealed by wastewater-based epidemiology. **Science of The Total Environment**, v. 798, p. 149014, dez. 2021.

GHASEMYANI, S. et al. Global, WHO Regional, and Continental Prevalence of Self-medication from 2000 to 2018: A Systematic Review and Meta-analysis. **Annals of Public Health**, v. 1, 2022.

GIL, A. Classical and new insights into the methodology for characterizing adsorbents and metal catalysts by chemical adsorption. **Catalysis Today**, v. 423, p. 114016, nov. 2023.

GRELA, A.; KUC, J.; BAJDA, T. A Review on the Application of Zeolites and Mesoporous Silica Materials in the Removal of Non-Steroidal Anti-Inflammatory Drugs and Antibiotics from Water. **Materials**, v. 14, n. 17, p. 4994, 1 set. 2021.

GUL, I. et al. Characterization of Cobalt Oxide and CALCIUM-ALUMINUM Oxide nano-catalyst through Scanning Electron Microscopy, X-RAY diffraction, and Energy Dispersive X-RAY Spectroscopy. **Microscopy Research and Technique**, v. 83, n. 9, p. 1124–1131, set. 2020.

HAYWARD, D. O.; TRAPNELL, B. M. W. **Chemisorption**. Londres: Butterworth, 1964.

HORIKAWA, T.; DO, D. D.; NICHOLSON, D. Capillary condensation of adsorbates in porous materials. **Advances in Colloid and Interface Science**, v. 169, n. 1, p. 40–58, nov. 2011.

HU, L.-X. et al. What is in Nigerian waters? Target and non-target screening analysis for organic chemicals. **Chemosphere**, v. 284, p. 131546, dez. 2021.

HUA, T. et al. Synthesis of mesoporous-structured MIL-68(Al)/MCM-41-NH2 for methyl orange adsorption: Optimization and Selectivity. **Environmental Research**, v. 215, p. 114433, dez. 2022.

IBRAHIM, A. A. et al. Synthesis of sulfated zirconium supported MCM-41 composite with high-rate adsorption of methylene blue and excellent heterogeneous catalyst. **Colloids and Surfaces A: Physicochemical and Engineering Aspects**, v. 616, p. 126361, maio 2021a.

IBRAHIM, A. A. et al. Synthesis of 12-tungestophosphoric acid supported on Zr/MCM-41 composite with excellent heterogeneous catalyst and promising adsorbent of methylene blue. **Colloids and Surfaces A: Physicochemical and Engineering Aspects**, v. 631, p. 127753, dez. 2021b.

JANUÁRIO, E. F. D. et al. Application of activated carbon functionalized with graphene oxide for efficient removal of COVID-19 treatment-related pharmaceuticals from water. **Chemosphere**, v. 289, p. 133213, fev. 2022.

JIAO, F.; FREI, H. Nanostructured Cobalt Oxide Clusters in Mesoporous Silica as Efficient Oxygen-Evolving Catalysts. **Angewandte Chemie**, v. 121, n. 10, p. 1873–1876, 23 fev. 2009.

KALITA, A.; TALUKDAR, A. K. Streamlined synthesis of iron and cobalt loaded MCM-48: High-performance heterogeneous catalysts for selective liquid-phase oxidation of toluene to benzaldehyde. **Heliyon**, v. 10, n. 6, p. e27296, mar. 2024.

KARSE, S. D.; FITE, M. C. Studies on structural and optical properties of cobalt oxide nanoparticles using co-precipitation. **Physica B: Condensed Matter**, v. 689, p. 416181, set. 2024.

KRUATIM, J.; JANTASEE, S.; JONGSOMJIT, B. Improvement of Cobalt Dispersion on Co/SBA-15 and Co/SBA-16 Catalysts by Ultrasound and Vacuum Treatments during Post-Impregnation Step. **Engineering Journal**, v. 21, n. 1, p. 17–28, 31 jan. 2017.

KUMARI, M.; KUMAR, A. Can pharmaceutical drugs used to treat Covid-19 infection leads to human health risk? A hypothetical study to identify potential risk. **Science of The Total Environment**, v. 778, p. 146303, jul. 2021.

KURODA, K. et al. Predicted occurrence, ecotoxicological risk and environmentally acquired resistance of antiviral drugs associated with COVID-19 in environmental waters. **Science of The Total Environment**, v. 776, p. 145740, jul. 2021.

LEE, J. W.; SHIM, W. G.; MOON, H. Adsorption equilibrium and kinetics for capillary condensation of trichloroethylene on MCM-41 and MCM-48. **Microporous and Mesoporous Materials**, v. 73, n. 3, p. 109–119, set. 2004.

LI, S. et al. Nanoconfined polyethyleneimine in mesoporous MCM-41 silica for heavy metal ions removal. **Separation and Purification Technology**, v. 353, p. 128421, jan. 2025.

LIU, H. et al. Magnetic mesoporous clay adsorbent: Preparation, characterization and adsorption capacity for atrazine. **Microporous and Mesoporous Materials**, v. 194, p. 72–78, ago. 2014.

LIU, J. et al. Adsorption of Congo red dye on FexCo3-xO4 nanoparticles. **Journal of Environmental Management**, v. 238, p. 473–483, maio 2019.

MAGALHÃES-GHIOTTO, G. A. V. et al. Composite hydrogel based on chemically modified gelatin and PVA containing graphene oxide nanoparticles (CHGP-GOn). **Environmental Nanotechnology, Monitoring & Management**, v. 20, p. 100877, dez. 2023.

MEHRVARZ, E.; GHOREYSHI, A. A.; JAHANSHAHI, M. Adsorptive separation of CO2 and CH4 by the broom sorghum based activated carbon functionalized by diethanolamine. **Korean Journal of Chemical Engineering**, v. 34, n. 2, p. 413–424, fev. 2017.

MIN, C. H. et al. Engineered MCM-48 nanoparticles as potential carriers for oral vaccine delivery. **Journal of Industrial and Engineering Chemistry**, v. 129, p. 193–201, jan. 2024.

MOREY, M. S. et al. Hydrothermal and Postsynthesis Surface Modification of Cubic, MCM-48, and Ultralarge Pore SBA-15 Mesoporous Silica with Titanium. **Chemistry of Materials**, v. 12, n. 4, p. 898–911, 1 abr. 2000.

NASON, S. L. et al. Changes in Sewage Sludge Chemical Signatures During a COVID-19 Community Lockdown, Part 1: Traffic, Drugs, Mental Health, and Disinfectants. **Environmental Toxicology and Chemistry**, v. 41, n. 5, p. 1179–1192, maio 2022.

NATARAJAN, R. et al. Adsorption performance of magnetic mesoporous silica microsphere support toward the remediation of acetaminophen from aqueous solution. **Journal of Water Process Engineering**, v. 48, p. 102835, ago. 2022.

OLATUNDE, J. O. et al. Determination of pharmaceutical compounds in surface and underground water by solid phase extraction-liquid chromatography. **Journal of Environmental Chemistry and Ecotoxicology**, v. 6, n. 3, p. 20–26, 30 jun. 2014.

OLIVEIRA, D. M.; ANDRADA, A. S. Synthesis of ordered mesoporous silica MCM-41 with controlled morphology for potential application in controlled drug delivery systems. **Cerâmica**, v. 65, n. 374, p. 170–179, jun. 2019.

QUESADA, H. B. et al. Surface water pollution by pharmaceuticals and an alternative of removal by low-cost adsorbents: A review. **Chemosphere**, v. 222, p. 766–780, maio 2019.

QUESADA, H. B. et al. Evaluation of novel activated carbons from chichá-do-cerrado (Sterculia striata St. Hil. et Naud) fruit shells on metformin adsorption and treatment of a synthetic mixture. **Journal of Environmental Chemical Engineering**, v. 9, n. 1, p. 104914, fev. 2021.

RIBEIRO, A. C. et al. Synthesis of a novel functionalized biosorbent from mango stone and its application in the pharmaceutical's removal from water and a synthetic mixture. **Chemosphere**, v. 346, p. 140520, jan. 2024.

RIVERA-UTRILLA, J. et al. Pharmaceuticals as emerging contaminants and their removal from water. A review. **Chemosphere**, v. 93, n. 7, p. 1268–1287, out. 2013.

ROUQUEROL, J.; ROUQUEROL, F.; SING, K. **Adsorption by Powders and Porous Solids: Principles, Methodology and Applications**. London: Academic Press, 1999.

SALAM, M. A.; ABUKHADRA, M. R.; MOHAMED, A. S. Effective oxidation of methyl parathion pesticide in water over recycled glass based-MCM-41 decorated by green Co3O4 nanoparticles. **Environmental Pollution**, v. 259, p. 113874, abr. 2020.

SALAMA, R. S.; EL-BAHY, S. M.; MANNAA, M. A. Sulfamic acid supported on mesoporous MCM-41 as a novel, efficient and reusable heterogenous solid acid catalyst for synthesis of xanthene, dihydropyrimidinone and coumarin derivatives. **Colloids and Surfaces A: Physicochemical and Engineering Aspects**, v. 628, p. 127261, nov. 2021.

SANTOS, R. K. S. et al. Removal of chloroquine from the aqueous solution by adsorption onto açaí-based biochars: Kinetics, thermodynamics, and phytotoxicity. **Journal of Molecular Liquids**, v. 383, p. 122162, ago. 2023.

SARMA, B.; KUMAR, R.; GUPTA, D. N. Nitrogen plasma treated cotton fabrics coated with SiO2 followed by RGO deposition for water purification process. **Chemical Physics Impact**, v. 8, p. 100612, jun. 2024.

SCHUMACHER, K. et al. Characterization of MCM-48 Materials. **Langmuir**, v. 16, n. 10, p. 4648–4654, 1 maio 2000.

SCHUMACHER, K.; GRÜN, M.; UNGER, K. K. Novel synthesis of spherical MCM-48. **Microporous and Mesoporous Materials**, v. 27, n. 2–3, p. 201–206, fev. 1999.

TERZYK, A. P. Molecular properties and intermolecular forces—factors balancing the effect of carbon surface chemistry in adsorption of organics from dilute aqueous solutions. **Journal of Colloid and Interface Science**, v. 275, n. 1, p. 9–29, jul. 2004.

TIAN, K. et al. Adsorption performance of 1,4-dioxane by MCM-22 and Beta zeolites and their bio-zeolite composite system in the presence of co-contaminants. **Separation and Purification Technology**, v. 354, p. 128752, fev. 2025.

TOURET, F.; DE LAMBALLERIE, X. Of chloroquine and COVID-19. **Antiviral Research**, v. 177, p. 104762, maio 2020.

TURNER, N. Kinetics of chemisorption: An examination of the Elovich equation. **Journal of Catalysis**, v. 36, n. 3, p. 262–265, mar. 1975.

VIDOVIX, T. B. et al. Evaluation of agro-industrial residue functionalized with iron oxide magnetic nanoparticles for chloroquine removal from contaminated water. **Materials Letters**, v. 326, p. 132915, nov. 2022.

WANG, J.; WANG, S. Removal of pharmaceuticals and personal care products (PPCPs) from wastewater: A review. **Journal of Environmental Management**, v. 182, p. 620–640, nov. 2016.

WANG, L. et al. Construction of lattice-confined Co-MCM-48 for boosting sulfite oxidation in wet desulfuration. **Chemical Engineering Journal**, v. 407, p. 127210, mar. 2021.

WEBER, W. J.; MORRIS, J. C. Kinetics of Adsorption on Carbon from Solution. **Journal of the Sanitary Engineering Division**, v. 89, n. 2, p. 31–59, 1 abr. 1963.

WU, S.-H.; MOU, C.-Y.; LIN, H.-P. Synthesis of mesoporous silica nanoparticles. **Chemical Society Reviews**, v. 42, n. 9, p. 3862, 2013.

ZHOLOBENKO, V. L. et al. Synthesis of MCM-41 materials: an in situ FTIR study. **Microporous Materials**, v. 11, n. 1–2, p. 83–86, ago. 1997.

ZOLA, A. S. et al. Effect of Silylation and Support Porosity of Co/MCM-41 and Co/SiO2 Catalysts in Fischer–Tropsch Synthesis. **Topics in Catalysis**, v. 59, n. 2–4, p. 219–229, fev. 2016.

CAPÍTULO 4

15. CONCLUSÃO GERAL DA TESE

A presente tese abordou o desenvolvimento e a aplicação de materiais adsorventes de origem natural e sintética para a remoção de fármacos em meio aquoso, contribuindo para a mitigação da contaminação ambiental. O primeiro estudo demonstrou o potencial da casca da semente de *Moringa oleifera Lam*. funcionalizada com óxido de ferro para a remoção de ivermectina. Os resultados indicaram características texturais favoráveis, como alta porosidade, além de desempenho adsortivo eficiente em diferentes condições de pH e força iônica. A cinética indicou um processo rápido, com equilíbrio em 400 min e capacidade de 89,41 mg g^{-1}, ajustando-se ao modelo de pseudo-primeira ordem. A isoterma de equilíbrio, demonstrou uma boa correlação ao modelo de Langmuir, com capacidade máxima de 143,76 mg g^{-1}. O processo foi espontâneo, exotérmico e reversível, e o reuso em múltiplos ciclos reforçou o potencial do material como alternativa viável para a remoção de contaminantes emergentes.

O segundo estudo focou na síntese e caracterização das sílicas mesoporosas MCM-41 e MCM-48 funcionalizadas com nanopartículas de óxido de cobalto para a remoção de cloroquina. Os materiais apresentaram alta cristalinidade, ampla área superficial e estrutura mesoporosa definida. A adsorção ocorreu principalmente por interação eletrostática, complementada por interações químicas em monocamada. A cinética seguiu o modelo de Elovich, indicando quimissorção como mecanismo dominante. A análise termodinâmica apontou um processo espontâneo, favorável e estável em diferentes temperaturas. A reutilização limitada dos materiais indica a necessidade de estudos adicionais para aprimorar sua performance em múltiplos ciclos.

Dessa forma, os resultados obtidos demonstram que tanto a casca da semente de *Moringa oleifera Lam.* quanto as sílicas mesoporosas funcionalizadas são alternativas promissoras para a remoção de fármacos da água. O uso de adsorventes naturais representa uma abordagem sustentável e de baixo custo, enquanto os materiais sintéticos oferecem maior seletividade e eficiência na remoção de contaminantes específicos. As descobertas desta tese ampliam o conhecimento sobre a adsorção de fármacos e oferecem bases para novas estratégias de tratamento de água e efluentes, contribuindo para a mitigação do impacto ambiental dos contaminantes emergentes.